2019

Site Effects Study in the Mississippi Embayment and Uncertainties Evaluation in Site Response Analysis

Arash Yarahmadi

Site Effects Study in the Mississippi Embayment and Uncertainties Evaluation in Site Response Analysis

by

Arash Yarahmadi

A Dissertation

Submitted in Partial Fulfillment of the

Requirements for the Degree of

Doctor of Philosophy

Major: Engineering

The University of Memphis

June 2019

In memory of my father the source of inspiration. To my mother the symbol of true love, and my sweet sister the source of rationality and kindness.

ACKNOWLEDGMENTS

I would like to thank Dr. Shahram Pezeshk, my advisor, for providing me a great opportunity to pursue my doctoral studies at the University of Memphis. His outstanding knowledge, support and encouragement helped me a lot during this chapter of my life. I will always appreciate your dedication to provide a remarkable environment in the Civil Engineering department for students like me to accomplish their goals and dreams. I also would like to thank my committee members, Drs. Chris Cramer, Charles Camp, Roger Meier, and Scott Stovall, for all their help and comments that improved the quality of this study.

Abstract

The local site conditions have paramount influence on the characteristics of seismic ground shaking. There are several methods of investigating seismic site effects and they can be classified into two major categories: common site-specific response analysis, and procedures that use solely earthquake time series like the Standard Spectral Ratio (SSR) and Horizontal to Vertical Ratio (HVSR) methods. In the SSR method, the spectral ratios of earthquake records at a certain target station can be evaluated with respect to a reference station located on a nearby outcrop rock.

In the first part of the dissertation, we use earthquake records to find a suitable reference station and use that reference station to find the site amplifications at six target stations inside the Mississippi Embayment (ME). Thirty-five local and regional earthquakes in the New Madrid and Arkansas seismic zones are used to perform the necessary data inversion. The results show that the fundamental frequencies of these stations are as low as 0.2 HZ to 1 HZ, which corresponds to the soft features of their local conditions.

In the second part of this dissertation, we investigate uncertainties in the 1-D equivalent-linear site response analysis (SRA). In SRA these uncertainties are accounted for by generating random cases of soil parameters. Choosing suitable randomization bounds can decrease the effects of the uncertainties in soil parameters on SRA results like predicted spectral accelerations. These bounds are quantified by the coefficient of variation (COV), which can be defined for different soil parameters. Using vertical seismometer arrays, we can compare predicted and observed surface ground motions. Using different COVs for the various soil parameters that are the main input parameters of the equivalent-linear SRA. Coefficients of variation that generate minimum

root means square errors between the observed and predicted response spectra are obtained for different site classes.

Table of Contents

List of Figures

List of Tables

1. Site Effect Studies in the Mississippi Embayment

Abstract

There are several methods for obtaining seismic site effects; the standard spectral ratio (SSR) method is one of them. The critical assumption in this method is that the record of a surface reference rock site is equivalent to the input motion at the base of the soil layer. Performing SSR depends on the availability of a proper reference site for which the site amplification is negligible. In this study, we investigate a series of stations near the New Madrid seismic zone (NMSZ) to find stations adjacent to the Mississippi embayment (ME) that have the characteristics of a reference station. Furthermore, we use the most suitable reference station to find the site amplification inside the ME. To find reference stations, we categorize the considered stations by their fundamental frequencies and their average shear-wave velocities. We use the horizontal-to-vertical spectrum ratio (HVSR) method to find the amplification factors of 10 stations located mostly on the west side of the ME. A total of 62 local and regional earthquakes with magnitudes between 3 and 4.8 have been selected to obtain three-component waveform data. HVSRs are computed for the frequency range of 0.1 to 20 Hz using Fourier spectra of the shear waves. Most of the stations that have been studied in this paper have similar characteristics of a reference station. Among these stations, three of them (WHAR, W41B, and UALR) in the west of the ME show acceptable characteristics of a reference station. The location of these three stations is reasonably close to most of the stations located inside the ME region. These stations can be used as reference for other target stations, but depending on their distances to the reference stations, the frequency dependent Q factor and the geometrical spreading must be accounted for. The rock stations with the

characteristics of reference stations are suitable for further studies of probabilistic seismic hazard analysis (PSHA) since their site effects are low. Amplification factors are obtained for six target stations inside the ME using an inversion method and the WHAR seismic station as the reference station. Thirty-five local and regional earthquakes in the New Madrid and Arkansas seismic zones are used to perform this study. The results show the fundamental frequencies of these stations are as low as 0.2 HZ to 1 HZ, which corresponds to the soft features of their local conditions.

1.1. Finding Reference Stations in the Vicinity of the Mississippi Embayment

1.1.1. Introduction

Several algorithms have been used to estimate site effects using just earthquake data in different regions. Among them, the horizontal to vertical spectral ratio (HVSR) and standard spectral ratio (SSR) methods are the most popular. The SSR procedure uses amplification factor ratios of three-component records from different earthquakes at various stations. This technique takes into account the ratio between the spectrum at the site of interest and the spectrum at a reference site, which is usually a nearby rock site. If the two sites have similar source and path effects, then the resulting spectral ratio creates an estimate of the site amplification.

The most non-induced seismically active region in the United States east of the Rocky Mountains is the New Madrid seismic zone (NMSZ) located in the north of the Mississippi Embayment. The absence of a large earthquake in the NMSZ since the 1811 and 1812 intraplate earthquakes, in combination with the high seismic activity, increase the probability of an occurrence of a large magnitude earthquake in this region. Occurrence of a large magnitude event in the NMSZ can affect the thick deposits of the Mississippi Embayment (ME) and can have far-reaching consequences if not prepared for properly and accurately. The ME starts in Southern Illinois and extends south following the Mississippi river until it reaches the Gulf of Mexico. The embayment is composed of several layers which consist of clay and sand in the shallow parts and become stiffer with depth until it reaches the Paleozoic rock. The depth of Paleozoic rock varies in different parts of the embayment and reaches 1 km in the center. The behavior of such thick deposits against large earthquakes have large uncertainties that vary by the geology and deposit thicknesses.

The HVSR technique was first developed by Nakamura (1989). Later Lemo and Chavez-Garcia (1993) used this technique to evaluate site effects using the S-wave part of seismograms. Since then, the HVSR has been used by numerous researchers to estimate site amplification. A major assumption in this method is that local site conditions and geology features have very low effects on the vertical component of the ground motions. By dividing the horizontal spectrum at each frequency to the vertical spectrum at the same frequency, we can obtain the site response at the location of the station. Zandieh and Pezeshk (2011) investigated the HVSR ratios of the recorded ground motions at 11 stations in the NMSZ, and they found that the soft deposits amplify the ground motions at low frequencies at different parts of the ME.

The SSR method was first developed by Borcherdt (1970), and since its introduction the methodology has been utilized by numerous researchers. In this procedure, the spectral ratios of the earthquake records at certain stations can be evaluated with respect to a reference station located on a nearby outcrop rock. The major assumption in this method is that the earthquake record on a surface rock station is equivalent to the input motion at the base of the soil layers; hence, to calculate the site amplification we can divide the specified station spectrum by the reference rock station spectrum.

A seismogram can be represented as the convolution of the source, path, site effect, and instrument response. By transferring this convolution to a frequency domain, the Fourier amplitude spectrum (FAS) can be represented as:

$$A_{ij}(f) = S_i(f) P_{ij}(f) G_j(f) I_j(f), \tag{1-1}$$

where f is frequency, $A_{ij}(f)$ is the Fourier spectrum of the ground motion of the ith event at the jth station at the frequency f. $S_i(f)$ is the source term of the ith event, $P_{ij}(f)$ is the effect of the wave

travelling a path from the *i*th event to the *j*th station. $G_j(f)$ is the site effect and $I_j(f)$ is the instrument response of the *j*th station.

To evaluate the site amplification at a station, we can divide the Fourier amplitude of the ground motion at the recording station by the Fourier amplitude of the ground motion recorded at a rock site (reference station):

$$\frac{A_{ij}(f)}{A_{ik}(f)} = \frac{S_i(f)P_{ij}(f)G_j(f)I_j(f)}{S_i(f)P_{ik}(f)G_k(f)I_k(f)}, \tag{1-2}$$

If both the soil-target station and the rock-reference station record the same event, then the source terms are the same at both stations. Furthermore, the instrument response is going to be removed by a transform function. The path term can be the same for both records if the distance between the stations is smaller than their hypocentral distances to the mutual event, so that the only remaining term is the site effect:

$$\frac{A_{ij}(f)}{A_{ik}(f)} = \frac{G_j(f)}{G_k(f)}. \tag{1-3}$$

Borcherdt (1970) investigated site spectral amplification in the San Fernando Valley area with respect to rock stations located on the Black Mountains adjacent to the valley. The target stations were located close enough to the reference station to qualify them for use in the direct SSR method. If the stations are not close enough, a path correction is needed (Steidl et al., 1996). There are different methods to implement path corrections. The first procedure is to correct for the geometrical spreading by multiplying the data by its hypocentral distance or S-P time (Steidl, 1996). An alternate method is to use an inversion to solve the path and site effects simultaneously. The Northridge earthquake with magnitude 6.7 led to a series of studies such as Bonilla et al.

(1997) for investigating site effects in the San Fernando basin. Bonilla et al. (1997) used different methods similar to the SSR and inversion to estimate the site response at stations located on soil considering 6 rock stations within the same area as their reference stations. They used S-wave and coda waves to conclude that these methods are good assumptions to obtain spectrum amplifications, and that they are compatible with the trends of other methods such as the HVSR method. One of the biggest problems that researchers encounter in these studies is how to choose the reference station. This was the motivation of several studies about reference stations and their response characteristics, which is also the main objective of this study.

A reference rock site should not exhibit resonances due to local site conditions. suitable sites are usually found in flat topographic areas and should be located on unweathered rock. Steidl et al. (1996) suggested using a bedrock borehole station as a reference station because even sites located in what appears to be hard rock show amplification in high frequency when compared to the bedrock in a borehole. The problem is that the borehole bedrock data is rare to find in some areas, such as in the ME, making it hard to find suitable reference stations in these areas.

The average shear-wave velocity of the top 30 meters (V_{S30}) of a soil column reveals the characteristics of the site under study. In building codes and recent ground motion predictions (GMPEs), the V_{S30} is widely used as a suitable parameter to consider site classifications.

Boore and Campbell (2017) proposed shear-wave velocity profiles for generic rock and very hard rock sites. In their study, V_{S30} of rock and very hard rock sites are 620 m/s and 2000 m/s respectively. They suggested that the amplification factors for rock and hard rock sites are normally less than 2, and in high frequencies the amplification factors are larger in rock sites as compared to the sites with softer conditions.

To study site or basin effects in the ME, choosing a reference station with the characteristics of a standard rock station located near the ME is of great importance. The main purpose of this study is to find seismic stations near the ME that can be considered as reference stations. For this purpose, we considered the V_{S30} of all the stations around the ME and chose stations with V_{S30} greater than 760 m/s, which are sites that are considered to be rock by the National Earthquake Hazard Program (NEHRP) soil classifications.

We used the Pacific Earthquake Engineering Research Center (PEER) Next Generation of Attenuations (NGA-East) database (Goulet et al., 2014) to find stations around the ME with V_{S30} larger than 760 m/s. These values of V_{S30} are measured geotechnically for only 6 percent of all the stations (1379 stations) available in the NGA-East database. This means that the majority of the V_{S30} values are estimated using proxy-based methods such as: estimation based on ground slope, surface geology, terrain proxy, P-wave seismogram estimation, and hybrid slope-geology proxy (Goulet et al., 2014).

The NEHRP suggests that sites with V_{S30} higher than 760 m/s should be considered as rock sites; however, studies such as Cadet et al. (2010) show that such an assumption is not sufficient for reference rock stations. In addition to V_{S30} as a site classification, the fundamental frequency, f_0, reveals more evidence about the site conditions, particularly about the whole shear-wave profile. Cadet et al. (2010) investigated numerous shear-wave profiles in the KiK-Net seismograph network and defined two criteria for V_{S30} and f_0 of a rock-references site. They suggested that rock sites with f_0 greater than 8 Hz and V_{S30} higher than 750 m/s have a better characterization as a reference station. The rock sites with these criteria have higher shear-wave velocities in the shallow depths of their profiles, and f_0 is more strongly correlated with the whole velocity profile of a site than with the mean shear-wave profile of the top 30 meters.

Despite the fact that an ideal reference station should have a flat transfer function almost equal to one (Steidl et al., 1996), we can identify a standard rock station using the criteria proposed by Cadet et al. (2010). Van Houtte et al. (2012) used these criteria to find a standard rock station in Canterbury, New Zealand, in order to investigate soil amplifications in the Christchurch area. They used the HVSR method to obtain site responses at 10 rock stations. They found the fundamental frequencies and their associated amplification factors for all the sites, and only one site in their study matched the Cadet et al. (2010) criteria.

The f_0 of a soil column can reveal valuable information for a study site. A high value of f_0 shows that the site of interest is located on a thin, stiff layer of soil or on a weathered rock, and a low f_0 corresponds to a soft soil. Therefore, in this study we are going to find the f_0 of each site by obtaining their site amplification factors.

In this study, we obtain the frequency dependent site amplification using HVSR. By having these ratios, we determine which selected stations have the characteristics of a reference station.

1.1.2. Study Area

The purpose of this part of the study is to find the best reference station(s) in the ME to be used in methods such as SSR. For this goal, we perform a survey to find stations in the vicinity of the embayment but not on soft deposits of the ME. Therefore, we need to have a good understanding of the geology of the ME and its surrounding regions. Earthquakes used in this study were located in southern Illinois, southeastern Missouri, Arkansas and northwestern Tennessee (regions within NMSZ), and also the intraplate earthquakes swarm of central Arkansas.

The active faults in the NMSZ are hidden beneath sediments of the ME and located in the northern part of the ME. However, the location of these faults is determined by studying seismograph recordings of small earthquakes, paleo seismic data, and historical seismicity patterns (Petersen et al., 2014). The zigzag fault system, which consists of three segments and forms the main part of the NMSZ, are the Reelfoot thrust fault and two strike-slip ruptures. These faults are associated with three large events that occurred during 1811 and 1812. The swarm of earthquakes that occurred in the central Arkansas region is associated with the Guy-Greenbrier fault, which is located to the northwest of Little Rock, and they appear to be induced events (Majenu, 2014).

Arkansas is divided into a highland area in the northwest and a lowland region in the south and east (Figure 1-1). The lowlands of Arkansas are mostly the same as the lowlands of the ME. They consist of unconsolidated clay, sand, gravel, limited consolidated deposits of clay, sand, gravel and also Cretaceous marl, chalk, and limestones. The highlands mostly consist of rock with thin layers of alluvium which is found in sediments produced by different kinds of surface water (General Geology of Arkansas, www.geology.ar.gov/geology/general_geology.htm, accessed 30 Sept. 2017).

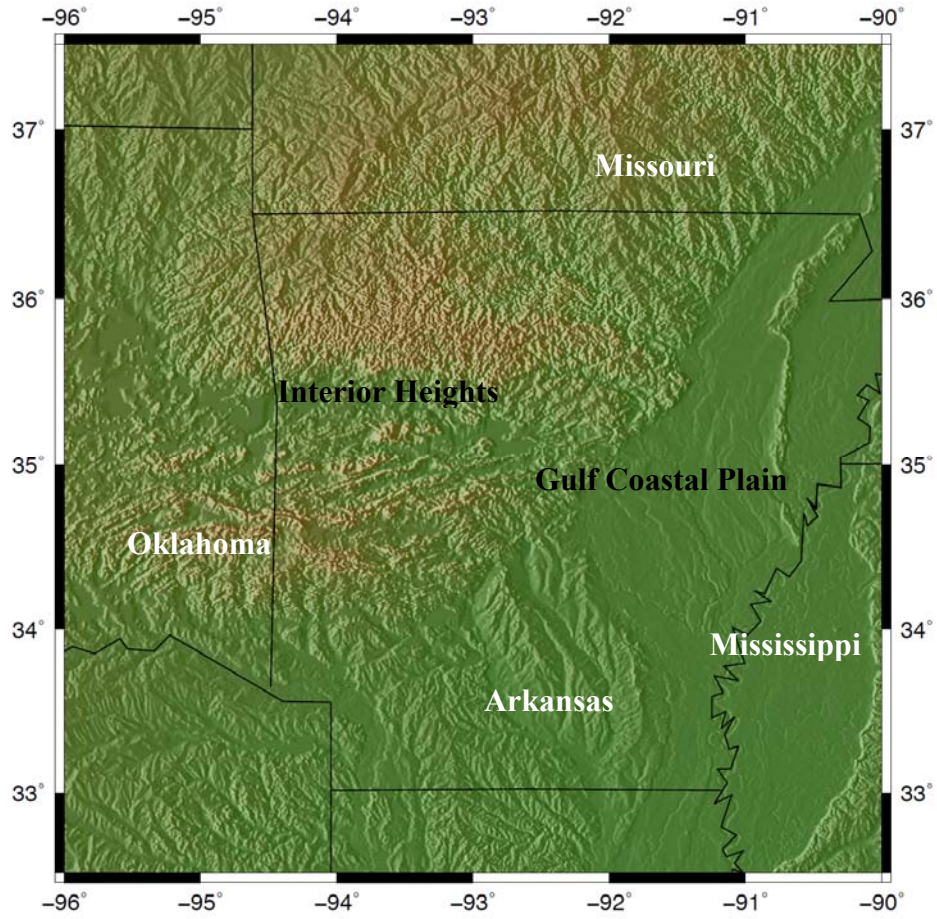

Figure 1-1. Arkansas Topographic Map.

The ME is a wedge-shaped region that extends from its apex in southern Illinois to the south along the Mississippi river. It covers 70,000 square miles and eight states (Hart et al., 2008). It becomes wider and deeper as it extends south; the depth of the post Paleozoic layers of the ME reaches almost 18,000 ft in the extreme southern parts of the region (Cushing et al., 1964). This region is filled with different sedimentary rocks that belong to different geological periods such as the Paleozoic, Mesozoic, and Cenozoic (Van Arsdale and TenBrink, 2000). Each geologic period consists of different layers of rock, sand, and clay corresponding to its depth.

Dhar and Cramer (2017) developed an improved 3D geological model of the ME and used surface geological maps to perform site response analysis and prepare liquefaction hazard maps for this region using studies like Van Arsdale and TenBrink (2000), Hart et al. (2008), Csontos (2007) and Arsdale and Cupples (2013).

Hart et al. (2008) used more than 26,000 geophysical logs to study and to develop nine digital surfaces to show the hydrologic framework for the Mississippi Embayment Regional Aquifer Study (MERAS). They used geographic information systems to produce the digital surfaces of the tops of the nine different layers in the ME. Having the top elevation of each layer, we can find the thickness of different layers from the Midway Confining Unit of the Upper Paleocene age to the land surface. Hart et al. (2008) did not provide information about the Paleozoic rocks in the ME. The Paleozoic rocks, which have characteristics close to a reference rock, have a shear-wave velocity of 2500 m/s (Toro et al., 1992) and shape the base of the embayment. The depth of Paleozoic rocks varies in the different parts of the embayment. Van Arsdale and TenBrink (2000) found tops of post-Paleozoic sediments in the north ME using well, outcrop and seismic reflection data. Figure 1-2 illustrates the Midway Confining Unit from MERAS, and Paleozoic rock of the northern ME from the Van Arsdale and TenBrink (2000) data. Having the elevation of different layers, we can find layer thicknesses in the northern ME.

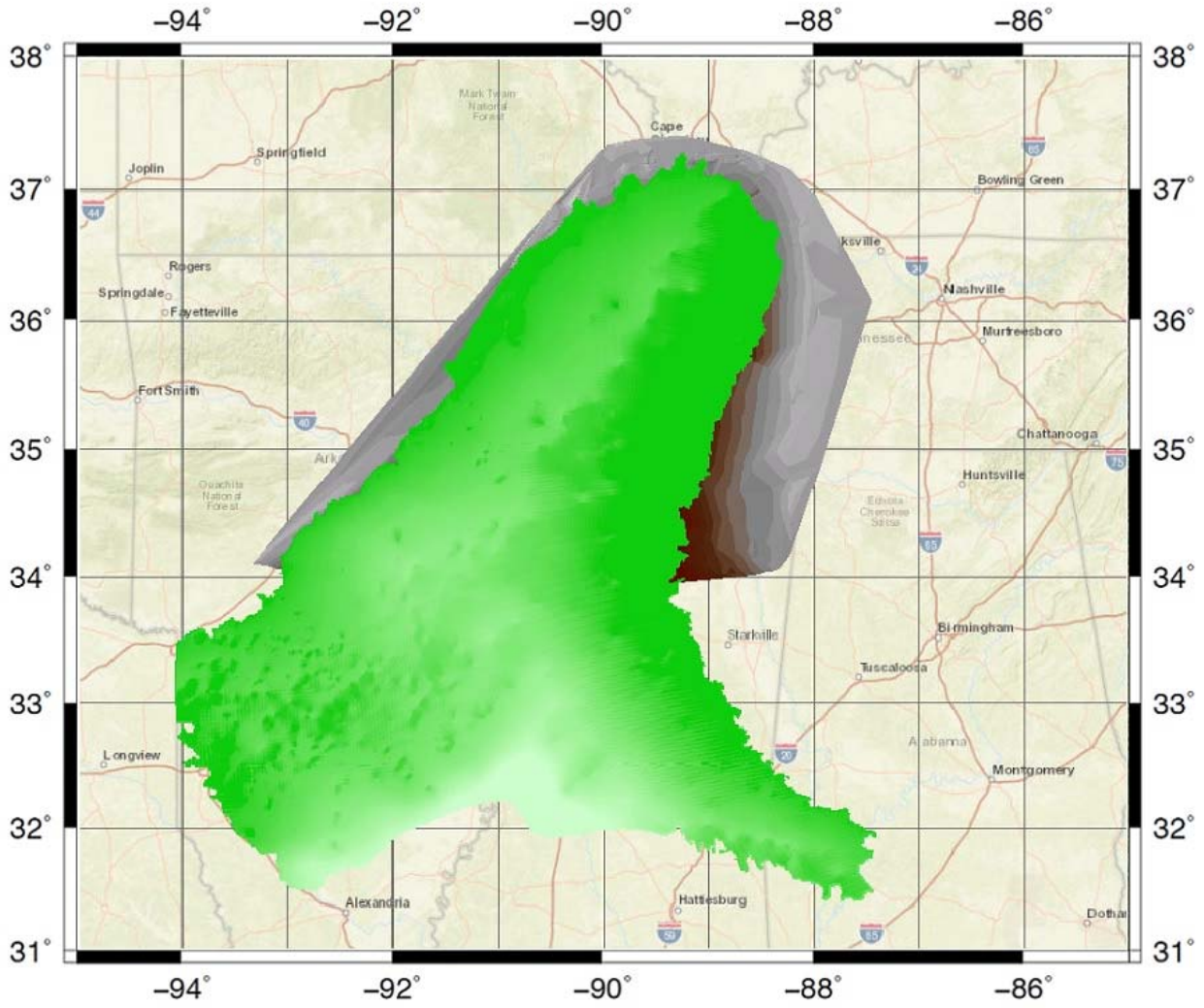

Figure 1-2. Paleozoic rock (gray layer) using Van Arsdale and TenBrink (2000) data and Midway Confining Unit (green layer) using MERAS data.

1.1.3. Purpose of The Study

The initial goal of this part of the research is measuring site amplification in the New Madrid seismic zone (NMSZ) using the standard spectral ratio (SSR) method for local and regional earthquakes. In this method, it is difficult to separate the attenuation factor from the site effect. Hence, we use a joint inversion method to determine the attenuation coefficient and site response from spectral ratios. On the other hand, finding a suitable rock station to use as a reference station

is important in these kinds of studies, and we have to make sure they have the characteristics of a reference rock station. For this purpose, we take advantage of the HVSR method to find suitable reference stations near the NMSZ.

This part of the study consists of two major sections. First, we study stations near the ME by implementing the HVSR method to find reference stations; then, we use the most suitable rock stations to estimate site amplification factors for the stations in the ME.

1.1.4. Finding Reference Stations Adjacent to The Mississippi Embayment

We perform a survey to find stations in the vicinity of the embayment but not on soft deposits of the ME. A good way to select reference stations is to find stations on the Paleozoic rock outcrop or close to it. Figure 1-3 shows the location of the stations within and in the vicinity of the northern part of the ME.

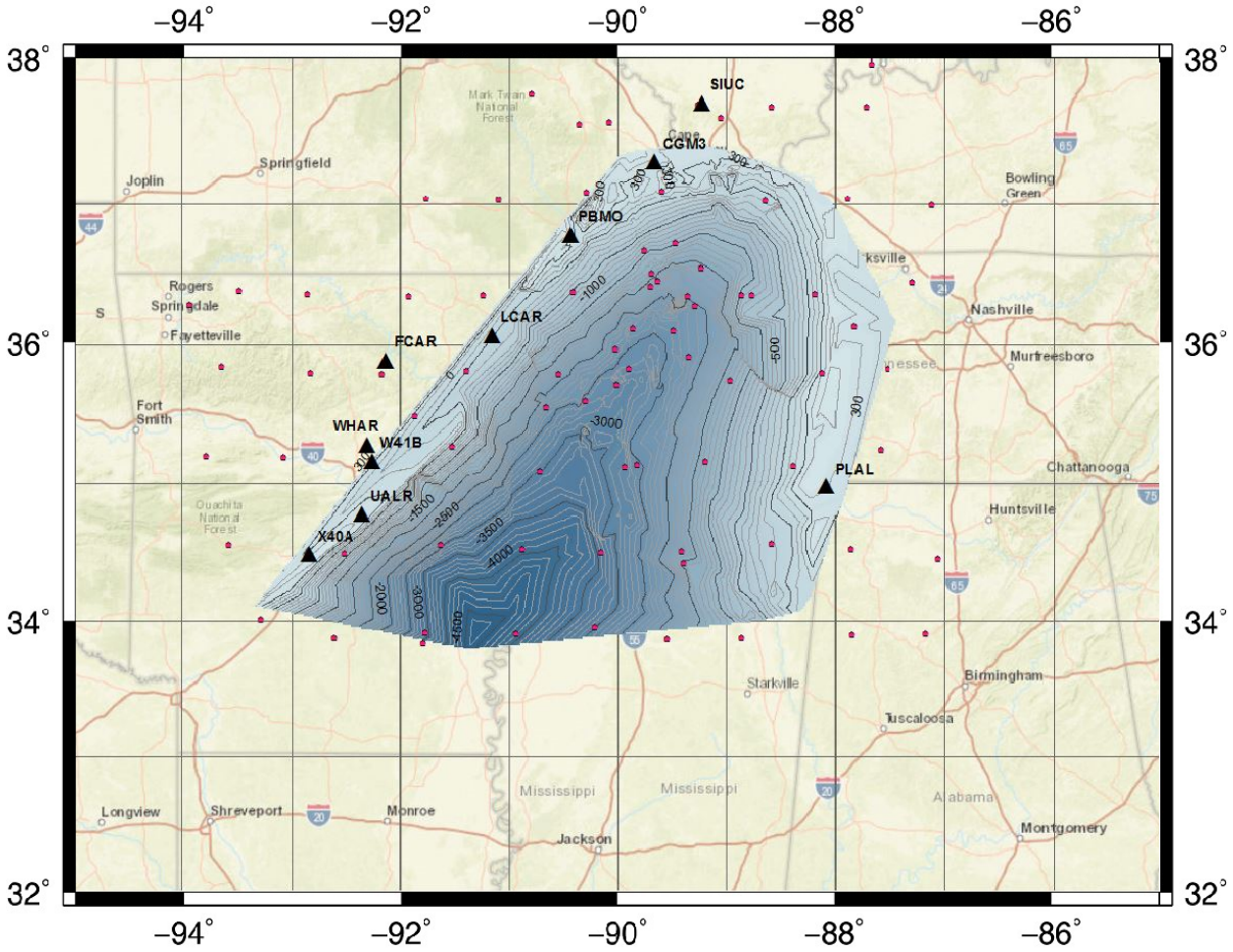

Figure 1-3. Contour map of the top of the Paleozoic strata of the northern Mississippi Embayment after Van Arsdale and TenBrink (2000) varying between -4500 feet to -300 feet. Solid triangles represent considered rock stations on the edge of the ME. Solid dots represent all the other stations available in the Incorporated Research Institutions for Seismology (IRIS) database for the ME and its vicinity.

Considering the stations near the embayment, we used the PEER NGA-East flatfile to get the V_{S30} for each station. A list of stations and their corresponding information is presented in Table 1-1. Column 6 of Table 1-1 provides the method that was used to estimate the V_{S30}. Code "0" means V_{S30} in the table is obtained through field measurement. Code "2" means V_{S30} is estimated by the P-wave seismogram method. Code "3" indicates the V_{S30} is estimated by the hybrid slope-

geology. Code "5" represents the weighted average of V_{S30} estimated from all available proxies where the P-wave estimates are not available. Details of V_{S30} estimates and how their standard deviations have been calculated are available in the PEER NGA-East database (Goulet et al., 2014). There are around 20 stations in the west, north, and east of the ME that can be considered as reference stations. Among these stations, there are a few stations (such as V41A, T43A, and W46A) that are temporary seismic stations, and there some other stations (such as MIAR and HHAR) which are far from the ME. We chose 10 stations which are suitable for this study. Figure 1-3 shows the location of these stations relative to the Paleozoic rock layer and the depth of the layer.

Table 1-1. Considered rock stations close to the ME and their corresponding information.

Station ID	Station Name	Latitude	Longitude	Elevation (m)	V_{S30} code	V_{S30} (m/s)	Standard Deviation	NEHRP
AG. FCAR	Ozark Folk Center	35.8898	-92.1242	190	5	592.9	0.5697	C
AG. LCAR	Lake Charles, LA	36.0695	-91.1543	103	5	564.3	0.5697	C
NM. SIUC	Carbondale, IL	37.7148	-89.2173	120	0	762	0.1	B
TA. W41B	Gary Mavity, Velonia, AR	35.1736	-92.2479	95	5	557.1	0.5697	C
NM. UALR	University of Arkansas, Little Rock	34.7751	-92.3429	138	0	1288	0.1	B
AG. WHAR	Wooly Hollow	35.2902	-92.2885	184	0	1403	0.1	B
TA.X40A	Basin Creek Farm, Malvern, AR	34.4873	-92.8342	158	3	1140.8	0.5711	B
NM. PBMO	Three Rivers Community College, Poplar Bluff, MO	36.7786	-90.4297	143.9	5	543.6	0.5697	C
NM. PLAL	Pickwick Lake, AL	34.9824	-88.0755	165	5	622.1	0.5697	C
NM. CGM3	Cape Girardeau, MO	37.3168	-89.8315	148	5	522	0.5697	C

1.1.5. Digital Seismic Waveform Data for HVSR Study

The waveform data used in this project are from local and regional earthquakes recorded by the three-component seismic stations of the New Madrid Seismic Network (NM), Arkansas Seismic Network (AG), USArray National Seismic Network (US), and US Transportable Array (TA). The instruments are broadband and high-gain broadband seismometers that have 40 Hz and 100 Hz sample rate frequency, respectively. The instrumentation used in this study are in 3 types: CMG-ESP, with a roughly flat response between 0.01 to 50 Hz, STS-2 with a flat response between 0.01 to 100 Hz, and Trillium 120 with 120 seconds to 100 Hz.

More than 580 three-component waveforms recorded from 62 local and regional earthquakes with magnitudes between 3.00 and 4.8, focal depths of less than 19 km, and hypocentral distances less than 450 km that occurred between 2010 and 2016 were obtained from the Incorporated Research Institute for Seismology (IRIS). The location of the earthquakes, as well as their depth and sizes, are depicted in Figure 1-4. The information for the events used in the study and the stations at which they have been recorded are provided in Table 1-2. The event magnitude-distance distributions for the selected stations are shown in Figure 1-5.

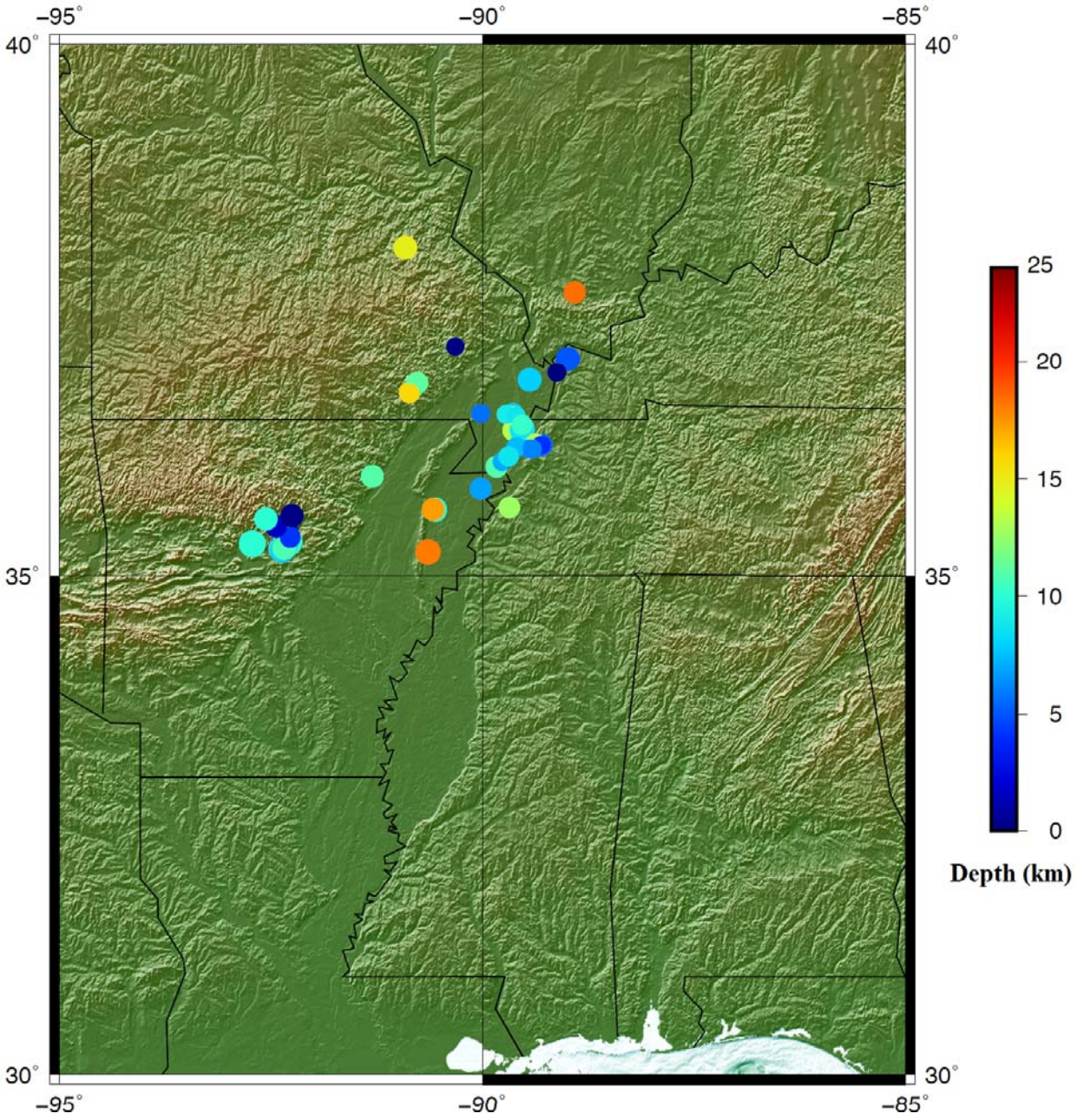

Figure 1-4. The earthquake sizes are scaled by the size of the circles; the depths of the events are matched with the color bar on the right.

Table 1-2. Earthquakes data availability in the study stations.

Date	Lat. N	Lon. E	Depth	ML	UALR	W41B	LCAR	X40A	SIUC	FCAR	WHAR	PBMO	CGM3	PLAL
10/11/2010	35.3177	92.3038	10	4	*		*			*		*		
10/15/2010	35.3069	92.3203	7.5	3.8	*		*			*		*		
10/16/2010	35.3279	92.3547	9.8	3.5	*		*			*		*		
10/18/2010	35.312	92.303	5.5	3.6	*		*			*		*		
11/20/2010	35.4439	92.3166	2.8	3.9	*		*			*		*		
12/13/2010	35.316	92.323	5.3	3.9	*		*			*		*		
2/16/2011	35.2794	92.3465	6.4	3.5	*		*			*		*		
2/17/2011	35.2634	92.3629	7.4	3.8	*		*	*		*		*		
2/18/2011	35.2718	92.3772	5.4	4.1	*		*	*				*		
2/20/2011	35.257	92.356	6.1	3.8	*			*		*		*		
2/25/2011	35.2655	92.3521	8.9	3.5	*			*		*		*		
2/28/2011	35.2374	92.3586	7.4	3.8	*			*	*	*		*		
2/28/2011	35.3264	92.3004	10	4.8	*			*		*		*		
3/3/2011	35.2649	92.3957	13.5	3.5	*			*		*		*		
3/4/2011	35.281	92.345	3	4	*		*	*		*		*		
3/24/2011	35.245	92.368	3.8	3.5	*		*	*		*		*		
4/7/2011	35.2494	92.3829	8.1	3.9	*		*	*		*		*		
4/8/2011	35.2687	92.3426	10.8	3.9	*	*	*	*		*		*		
10/7/2011	35.373	92.27	4.2	3.4	*	*	*	*		*		*	*	
5/22/2013	35.32	92.7014	3.4	3.4	*	*	*	*	*	*	*	*	*	*
5/24/2013	35.3132	92.7221	10	4.4	*	*	*	*		*	*	*	*	*
6/14/2013	35.4808	92.445	1.6	3.6	*	*	*	*	*	*	*	*	*	*
6/4/2014	35.5795	92.245	0.08	3.8	*	*	*	*		*	*	*	*	*
2/23/2013	35.6365	90.5781	17.3	3.7	*	*	*	*		*		*	*	*
4/3/2013	35.5468	92.5633	10	3.8	*	*	*	*	*	*		*	*	*
5/21/2013	35.9578	91.2979	11	3.7	*	*	*	*		*	*	*	*	*
7/17/2013	35.638	90.5642	10	3.9	*	*	*	*		*		*	*	*
4/3/2013	36.3974	89.6288	13.2	3.6	*	*	*	*		*	*	*	*	*
12/29/2011	36.555	89.644	7.8	3.4	*	*	*	*	*	*	*	*	*	
2/21/2012	36.8785	89.4365	7.9	3.9	*	*	*	*	*	*	*	*	*	*
6/17/2012	36.41	89.53	8.7	4.1	*	*	*	*	*	*	*	*	*	*
4/2/2015	36.051	89.8251	10.91	3.6	*	*	*	*	*	*	*	*	*	*

Table 1-3. (Continued)

Date	Lat. N	Lon. E	Depth	ML	UALR	W41B	LCAR	X40A	SIUC	FCAR	WHAR	PBMO	CGM3	PLAL
10/16/2015	36.7613	90.857	16.01	3.5	*	*	*	*	*	*	*	*	*	*
9/22/2011	36.8504	90.7745	11.2	3.6	*	*	*	*	*	*	*	*	*	
8/12/2013	36.2648	89.3015	5.6	3.6	*	*	*	*			*	*	*	*
1/27/2014	37.0767	88.9879	5	4	*	*	*	*	*	*	*	*	*	*
6/7/2011	38.1275	90.9069	14.8	3.9	*	*	*	*	*	*	*	*		
2/28/2015	36.536	89.639	13.44	3.1	*		*			*	*	*	*	*
5/30/2010	36.549	89.715	9.1	3.1	*		*			*	*	*		
11/16/2010	35.835	90.019	6.8	3.6	*	*	*	*		*	*	*		
5/3/2011	36.954	89.121	0	3.1	*	*	*	*	*	*	*	*		
3/1/2012	36.269	89.373	13.1	3.4	*	*		*	*			*	*	*
10/29/2012	35.2287	90.6364	18.1	4.1	*	*	*	*	*	*	*	*	*	*
11/29/2012	36.096	89.767	7.1	3		*	*	*	*	*		*	*	*
1/7/2013	36.224	89.436	6.3	3.1	*	*	*	*	*	*	*	*	*	*
4/5/2013	36.237	89.601	7.4	3.2	*	*	*	*	*	*	*	*	*	*
5/14/2013	35.62	90.55	9.9	3.4		*	*		*	*	*	*	*	*
8/9/2013	36.2635	89.2998	4.1	3	*	*	*	*	*	*	*	*	*	*
4/7/2014	36.2153	89.41	6.1	3.1	*	*	*	*	*	*	*	*	*	*
5/15/2014	36.558	90.02	5.63	3.1	*	*	*	*	*	*	*	*	*	*
8/25/2015	35.66	89.682	12.7	3.5	*	*	*	*	*	*	*	*	*	*
10/16/2015	36.7511	90.86	15.74	3.2	*	*	*	*	*	*	*	*	*	*
11/25/2015	36.538	89.601	8.71	3	*		*		*	*	*	*	*	*
7/5/2016	36.15	89.697	9.02	3	*		*		*	*	*	*	*	*
9/9/2016	36.452	89.534	10.26	3.4	*		*			*	*	*	*	*
11/24/2016	36.1545	89.692	8.75	3.3	*	*	*	*	*	*	*	*	*	*
5/1/2016	37.2136	889.9876	16.26	3.5	*	*		*	*			*	*	*
1/11/2013	37.7093	88.9109	18.4	3.6	*	*	*	*	*	*	*	*	*	*
2/7/2012	37.2	90.316	0.1	3	*	*	*	*		*	*	*	*	*
7/17/2013	35.638	90.564	10	3.9	*	*	*	*	*	*		*	*	*
5/21/2013	35.9578	91.2979	11	3.7	*	*	*	*	*	*	*	*	*	*
2/23/2013	35.6365	90.5781	17.3	3.7	*	*	*	*	*	*	*	*	*	*
TOTAL					60	40	55	49	32	58	36	62	40	37

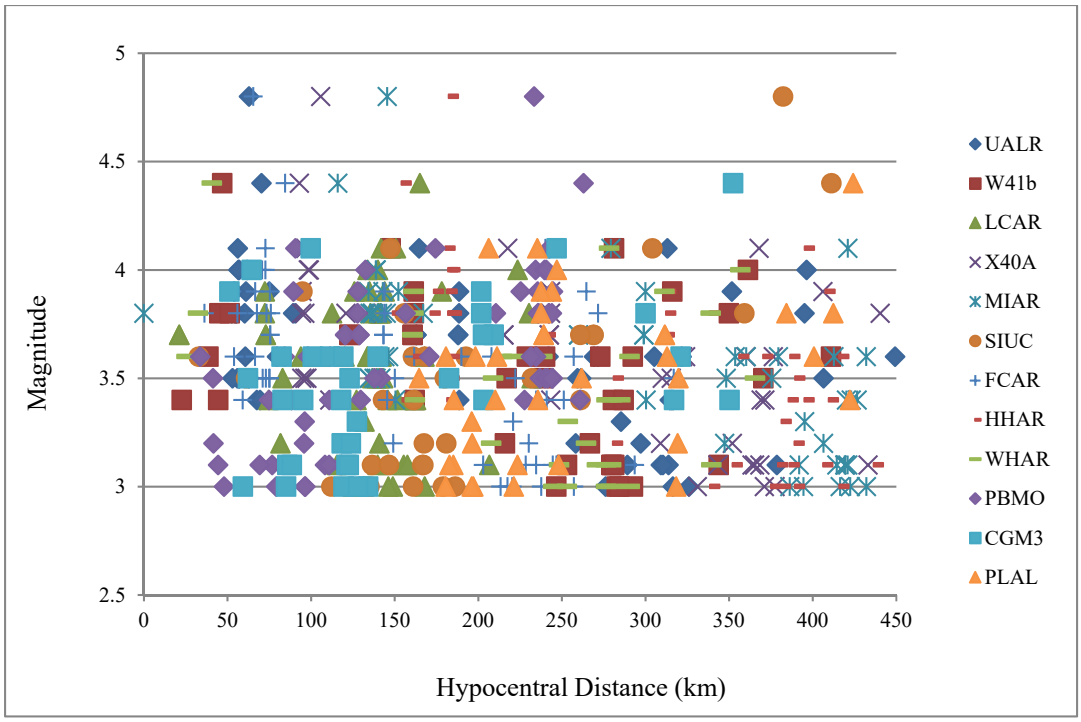

Figure 1-5. Magnitude-distance distribution of 62 earthquakes at 10 stations.

1.1.6. Data Processing

The Fourier spectra of ground acceleration for shear waves are computed using a fast Fourier transform (FFT) for each station and each earthquake. Having the spectra of each waveform, we can calculate the HVSR for different frequencies. The shear-wave window is chosen to extract the shear-wave acceleration-time series, then the onset of P-waves is determined visually considering three-component waveforms, and consequently the S-wave onset is chosen. A noise window of 10 seconds is chosen starting at the origin of each record. The window includes direct S-waves for the close hypocentral distances, and it is contaminated with secondary waves because of reflections from internal crust and the moho (the boundary between the crust and the mantle) discontinuity (Atkinson and Mereu, 1992). We use a window starting with the velocity group of

3.6 km/s and ending on 3 km/s to extract Lg waves. We also use the whole signal of the records to compute the spectral ratios. It was found that all three different windows gave similar results.

In processing the data, after correcting the instrument response, the mean and trend were removed from the acceleration ground motions. Then, the extracted windows were zero-padded to the nearest power of 2, a cosine tapered window of 2% is implemented to the padded signal and noise and the Fourier spectra were smoothed at 5 units of frequency. From the obtained Fourier amplitudes, the signal to noise ratio (SNR) is calculated for individual frequencies and, in each frequency, we omitted those events with a SNR lower than 2 (Zhao et al., 2013). Therefore, we used only the data with high quality for each individual frequency. Figure 1-6 illustrates the shear-wave signal and the noise spectra for a 3.6 magnitude earthquake recorded in LCAR as an example of this process. In Figure 1-6(a) sample frequencies are illustrated on the shear-wave and noise spectra by circles and triangles. The sample frequencies are 47 evenly distributed points on the logarithmic axes between 0.1 Hz and 20 Hz. Figure 1-6(b) clearly shows SNR values in each frequency as well as the threshold of 2. As shown in Figure 1-6(c), the signals with SNR values lesser than 2 are omitted from the analysis.

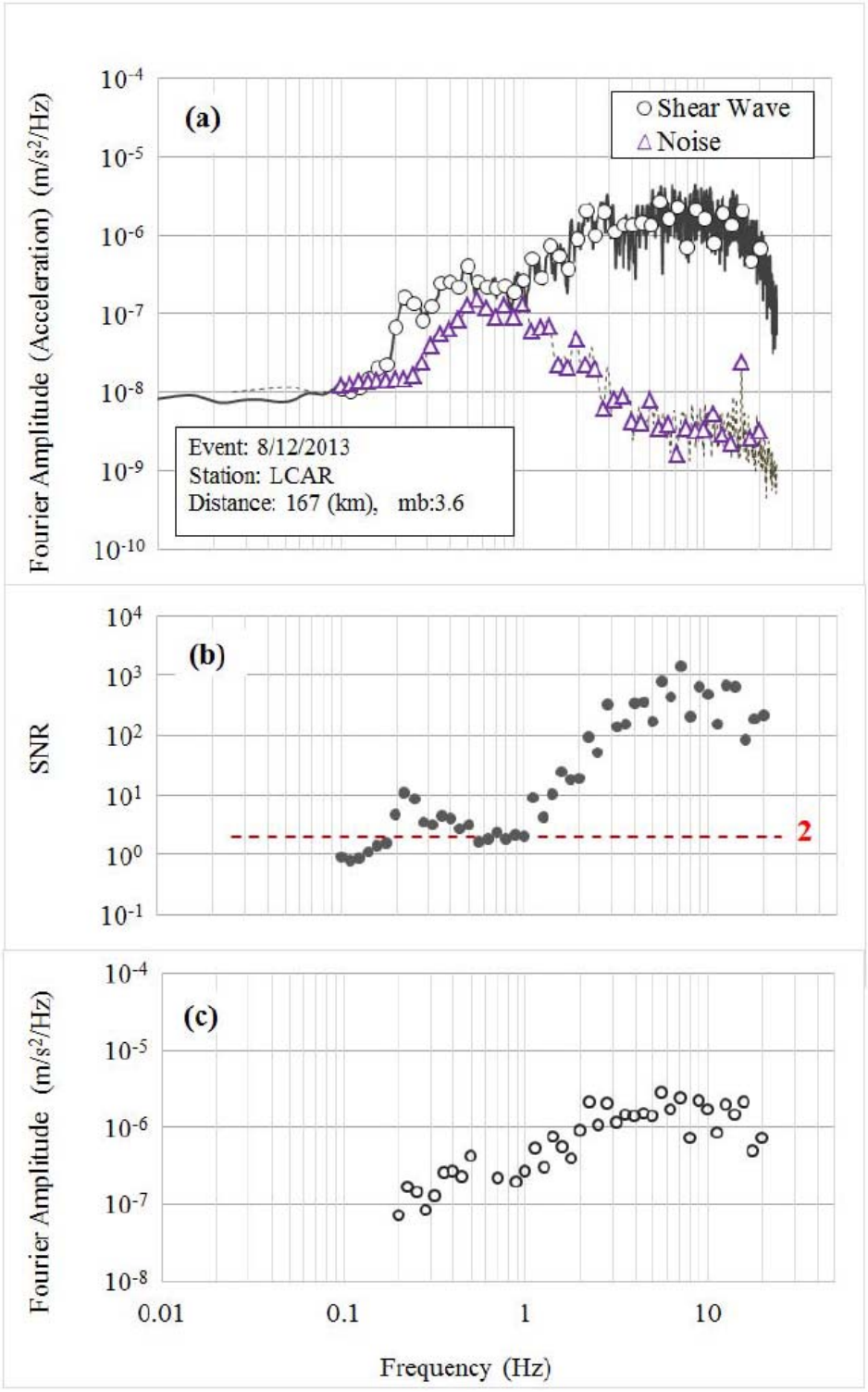

Figure 1-6. (a) Shear-wave spectra (circles) and noise spectra (triangles) recorded at the station. (b) Signal to noise ratio (SNR) and the threshold 2. (c) Shear-wave Fourier amplitudes with SNR higher than 2.

In every frequency the HVSRs are computed for different events and the average of all those HVSRs is calculated. We can also compute the standard deviation in each frequency. HVSRs are obtained in both E-W and N-S directions, and then we used the geometrical mean to combine the results of the two directions to obtain a horizontal to vertical response spectrum.

1.1.7. Results

We calculated the HVSRs for all the selected stations and, for each frequency, we obtained the average of all the events. Note that the number of events used are not equal for all the stations. Table 1-2 provides a list of the events used for each station. Standard deviation in each frequency is computed to find the variability of the site response from the HVSRs mean. The HVSRs have been obtained for both the East-West and North-South components of the seismograms.

We followed the same procedure as Cadet et al. (2010) to find a threshold for f_0 in the ME. We calculated the average of the measured V_{S30} of all the rock stations provided in the NGA-East database. Those are the stations with V_{S30} larger than 760 m/s, which are rock and hard rock site conditions. The f_0 corresponding to a soil layer can be obtained from:

$$f_0 = \frac{\text{average}(V_{S30})}{4H}, \tag{1-4}$$

where H is the corresponding soil layer thickness. The average shear-wave velocity of all the rock stations is computed to be 1100 m/s, and therefore, f_0 for the top 30 meters of a site should be higher than 9 Hz.

In this study, we define two conditions for seismic stations to be considered as rock stations; first, their HVSRs peak frequencies should be higher than 9 Hz, and second, their HVSRs should be lower than 2 in all frequencies. Furthermore, the stations with flat site amplification are more suitable to be considered as reference stations as well.

Each station is studied individually for geological and geotechnical features, and also the amplification factors have been surveyed to find the most suitable reference stations near the ME. The following sections provide in-depth studies of each station considered.

1.1.7.1. SIUC

We begin the survey by considering the SIUC station. SIUC is located at the north of the ME in southern Illinois, and it is close to the stations located within the ME. According to Table 1-1, the V_{S30} of this station is equal to 760 m/s making it a suitable choice to be considered as a reference station for the northern part of the ME. This station is instrumented with a Guralp CMG-3ESP broadband seismometer that belongs to the New Madrid (NM) seismic network and is currently located in the Southern Illinois University campus at Carbondale.

According to the surficial geology map of Carbondale (Nelson, 2013), this station is located on the Glassford formation of Till which is a mixture of clay, silt, sand, gravel, and rocks up to boulder size. Shear-wave velocity profiles for this station were obtained by using the Multichannel Analysis of Surface Waves (MASW) (EPRI 2013a), and have V_{S30} = 760 m/s which correspond to a NEHRP site class B. This station has been in operation since 1999 and is located at a free field near the geology building at Southern Illinois University. To investigate this site for the

characteristics of a reference station, amplification factors were obtained by calculating HVSRs at frequencies between 0.1 Hz and 20 Hz as shown in Figure 1-7.

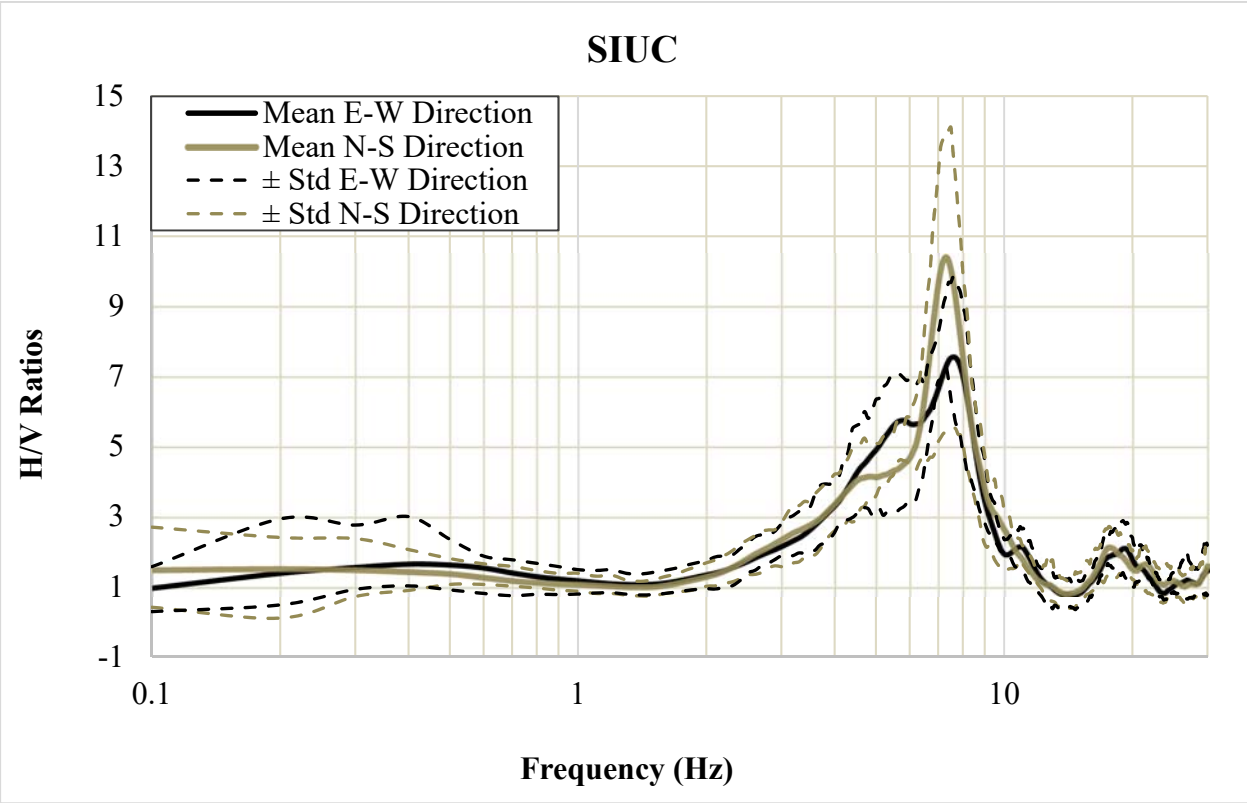

Figure 1-7. Solid lines show average of H/V ratios in East-West (black) and North-South (grey) components and dashed lines show ± standard deviations from the mean.

The f_0 for both directions is the same, and it is equal to 7.4 Hz. However, there is an obvious difference among the amplification factors; the amplification in the N-S component is 10.3, and it is 7.3 in the E-W direction. The HVSRs in both directions are within the one plus and one minus standard deviation band, which means the differences in amplification are about the same in both directions. The amplification factors curve in the low frequencies is almost flat; however, the amplification factors at f_0 increase dramatically. Therefore, this station cannot be considered to be

a reference station because there will be high de-amplifications if we use it as a reference station in methods like SSR to compute the amplification function. Furthermore, the f_0 is 7.4 in both directions, which is lower than the threshold for a reference station f_0 defined earlier.

1.1.7.2. W41B

W41B is a broadband STS-2 seismometer which is one of the 2000 USArray seismic stations which were installed as part of the National Science Foundation's EarthScope initiative in 2011. The station is located 4 miles southwest of Enola, Arkansas, where swarms of earthquakes started in 1982 (Schweig, 1991). It is underlain by the Ross Creek fault and the Morrilton fault (Majenu, 2015). The station's site surface is silt loam and its subsoil consist of silty clay loam up to 6 feet in depth (Natural Resources Conservation Services Soil Survey, 1979). The station is located at the upper part of the Atokan formation which consists of mostly tan to gray silty sandstones alternating with thick intervals of shale (Haley et al., 1993). According to Van Arsdale and TenBrink (2000), this station is located on the Paleozoic rock. The V_{S30} of the station site is 557 m/s according to the Table 1-1 (NGA-East Flatfile) which is estimated from all available proxies where P-wave estimates are not available. This average shear-wave velocity is associated with a NEHRP Site Class C which is stiff soil and soft rock. This is not compatible with our understanding of the site rock condition. To understand the behavior of the soil in this site, the amplification factors were obtained by HVSR. The average of H/V ratios for 40 earthquakes in the frequency range of 0.1 to 20 Hz for the E-W and the N-S directions and their standard deviations are shown in Figure 1-8.

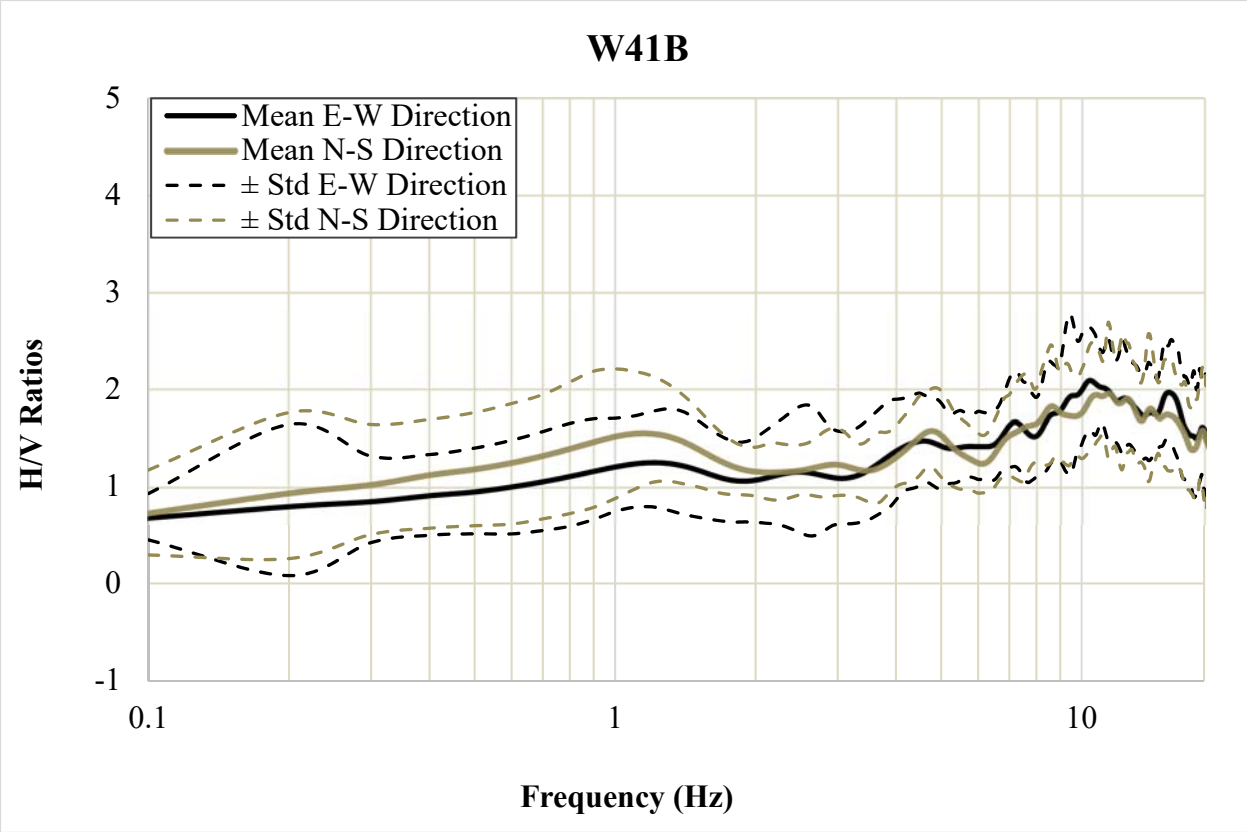

Figure 1-8. Solid lines show average of H/V ratios in East-West (black) and North-South (grey) components and dashed lines show ± standard deviations from the mean.

The HVSRs of the W41B station have a flat trend around unity in the low frequencies. The H/V ratios have a good agreement, and they both are in the range of each other's standard deviations. They have their fundamental resonance frequency around 10 Hz with a value of almost 2, which means the response spectrum curves have the characteristics of a rock reference station. This result is contrary to the NEHRP's soil classification provided in the NGA-East flatfile and agrees with the studies that have been conducted on the geology of the site.

1.1.7.3. CGM3

The CGM3 station is in the northern part of the ME, west of Cape Girardeau in southern Missouri. The level of Paleozoic rock underneath this station is 435 feet from sea level according to the contour map of Van Arsdale and TenBrink (2000) (Figure 1-3). The depth to bedrock in this site reaches to 50 feet. Cape Girardeau County is divided into two division, uplands and lowlands. The uplands area, which occupies the most area of the county, has an average altitude of 495 feet above sea level. The ME is divided into lowlands and uplands as well. The lowlands of the ME, which are generally a smooth plain with a slight slope to the south and south west, begins at a point on the Mississippi river about 1 mile south of Cape Girardeau (Krusekopf and Lewis, 1910). The CGM3 station is located almost in the higher altitude relative to the ME, since the average altitude of the lowlands of the ME is 335 feet above sea level and the site level of the station is around 486 feet. In conclusion, this station is just outside the ME and can be a proper reference station if it carries the determined characteristics for a reference station. According to the soil map of Cape Girardeau County on the Natural Resources Conservation Services (NRCS) website, we realized that this station is located on the Knox silt loam. Knox silt loam consists of a brown or brownish grey silt loam, gets heavier by the texture, and contains more clay in deeper levels. The V_{S30} of the site is 522 m/s according to Table 1-1 (NGA-East Flatfile), which is estimated from all available proxies where the P-wave estimates are not available. This average shear-wave velocity is associated with NEHRP Site Class C, which is stiff soil and soft rock. CGM3 has been operating since 7/2011, and it belongs to the NM seismic network with the ES-T accelerometer. HVSRs are computed for 40 events and their averages are depicted in Figure 1-9.

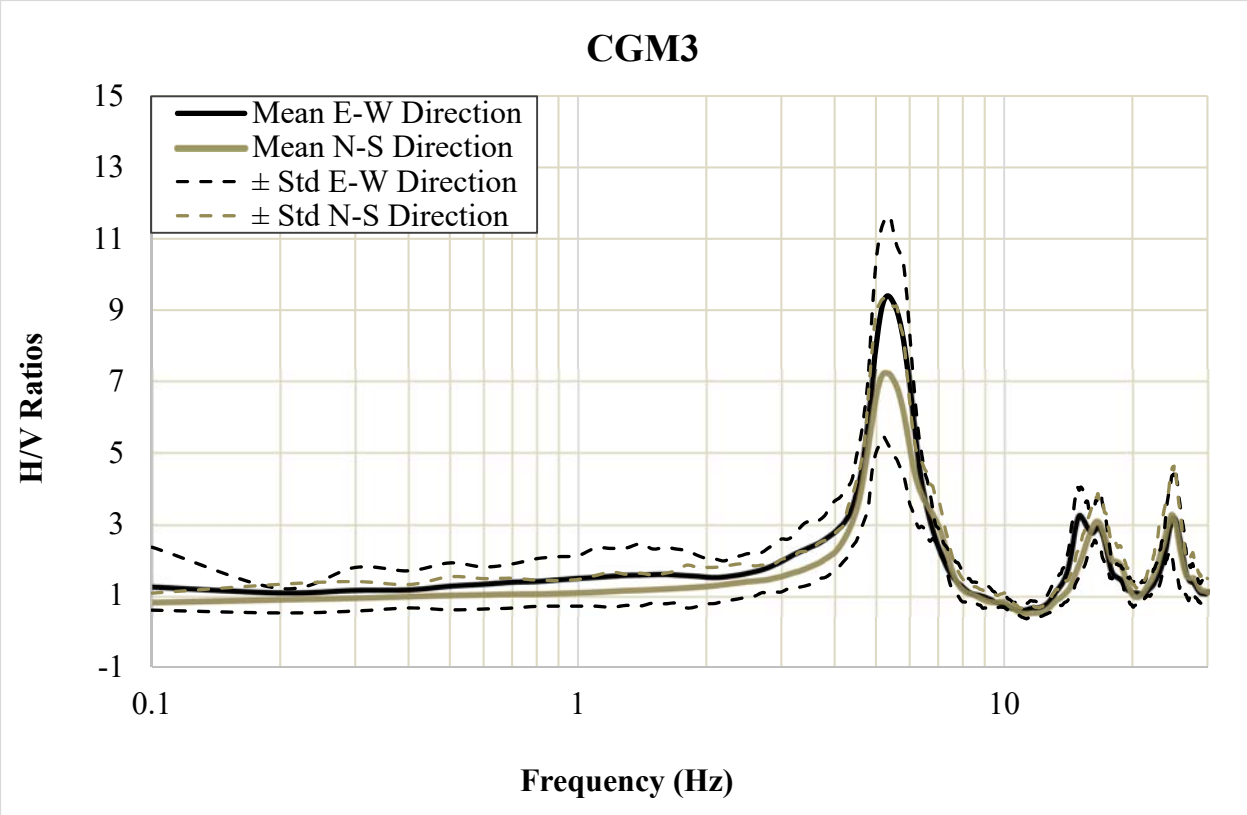

Figure 1-9. Solid lines show average of H/V ratios in East-West (black) and North-South (grey) components and dashed lines show ± standard deviations from the mean.

The f_0 for both directions is around 5.2 Hz and the average HVSRs for N-S and E-W components are 7 and 9.3 respectively. This confirms the fact stated earlier about the soil conditions of this station. Therefore, using this station as a reference station will underestimate the target stations' amplifications dramatically.

1.1.7.4. PBMO

The Poplar Bluff seismic station is a broadband strong motion instrument that has an average shear-wave velocity of 543.6 m/s associated with a NEHRP Site Class site C. According to Van Arsdale and TenBrink (2000), the depth of the Paleozoic rock at this site is 60 feet, and

there are no layers that belong to the ME underneath this station. The site is located on the border of the Ozarks uplands area and the ME lowlands. Gravelly surficial sediments of the Ozark uplands, some weathered residuum from bedrocks and alluvium soil constitute the materials underneath the site between the Paleozoic rock and the surface. Like CGM3, the average shear-wave velocity V_{S30} of this station is estimated from all available proxies where P-wave estimates are not available (Code 5 of the NGA-East flatfile).

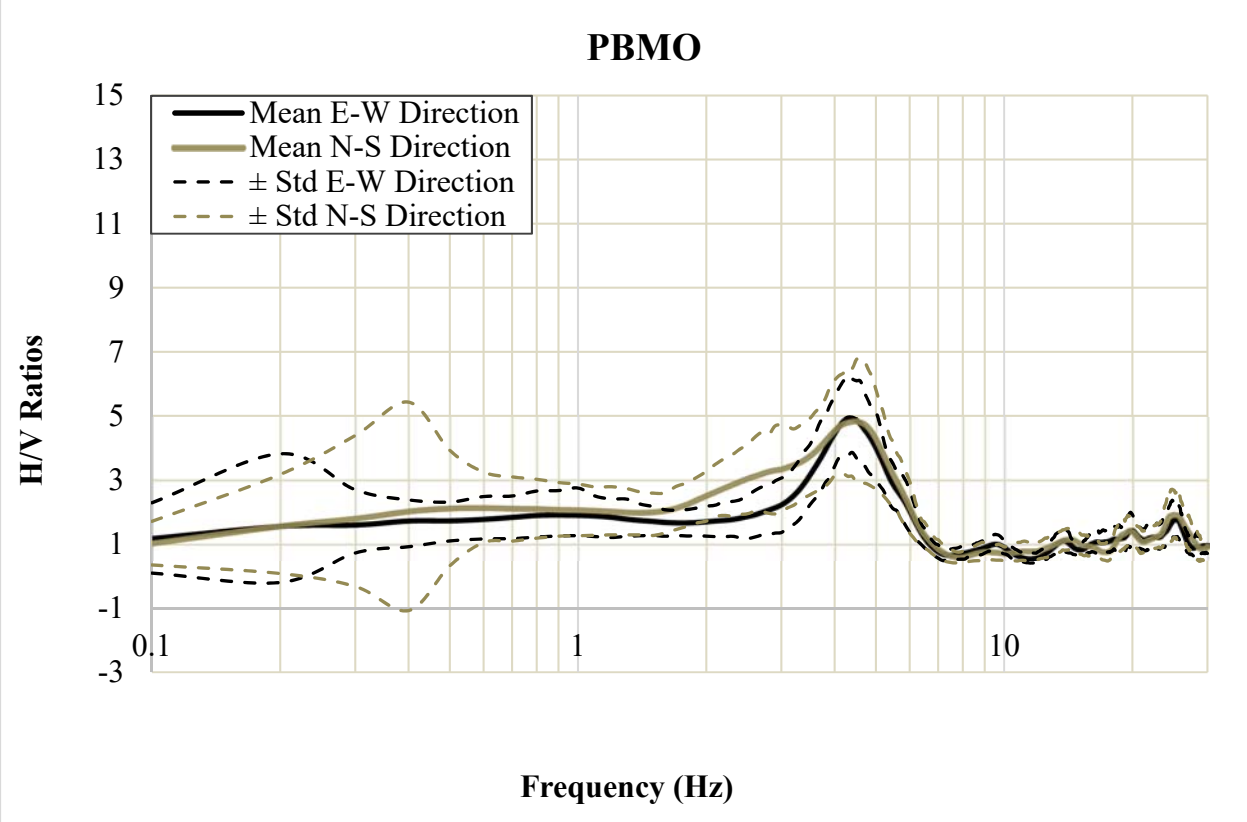

Figure 1-10. Solid lines show average of H/V ratios in East-West (black) and North-South (grey) components and dashed lines show ± standard deviations from the mean.

The HVSR curves in both directions are in very good agreement. The f_0 for the site is 4.4 Hz and the resonance amplification is 4.8. Although the rest of the curve is flat and has values close to 1, the fact that f_0 is so much lower than 9 Hz makes this station incompatible with the reference station specifications.

1.1.7.5. LCAR

LCAR is a strong motion seismic station located in the ME in the Charles Lake state park that belongs to the Arkansas Seismic Network (ASN). LCAR has recorded seismic data since the spring of 2010 when it was established after the 2008 swarm of earthquakes struck near Magnet Cove, Arkansas. LCAR is located near Charles Lake, and is underlain by deposits of the gulf coastal plain on top of Paleozoic rocks of Mississippian age. The V_{S30} of this site is 564.3 m/s associated with NEHRP Site Class C.

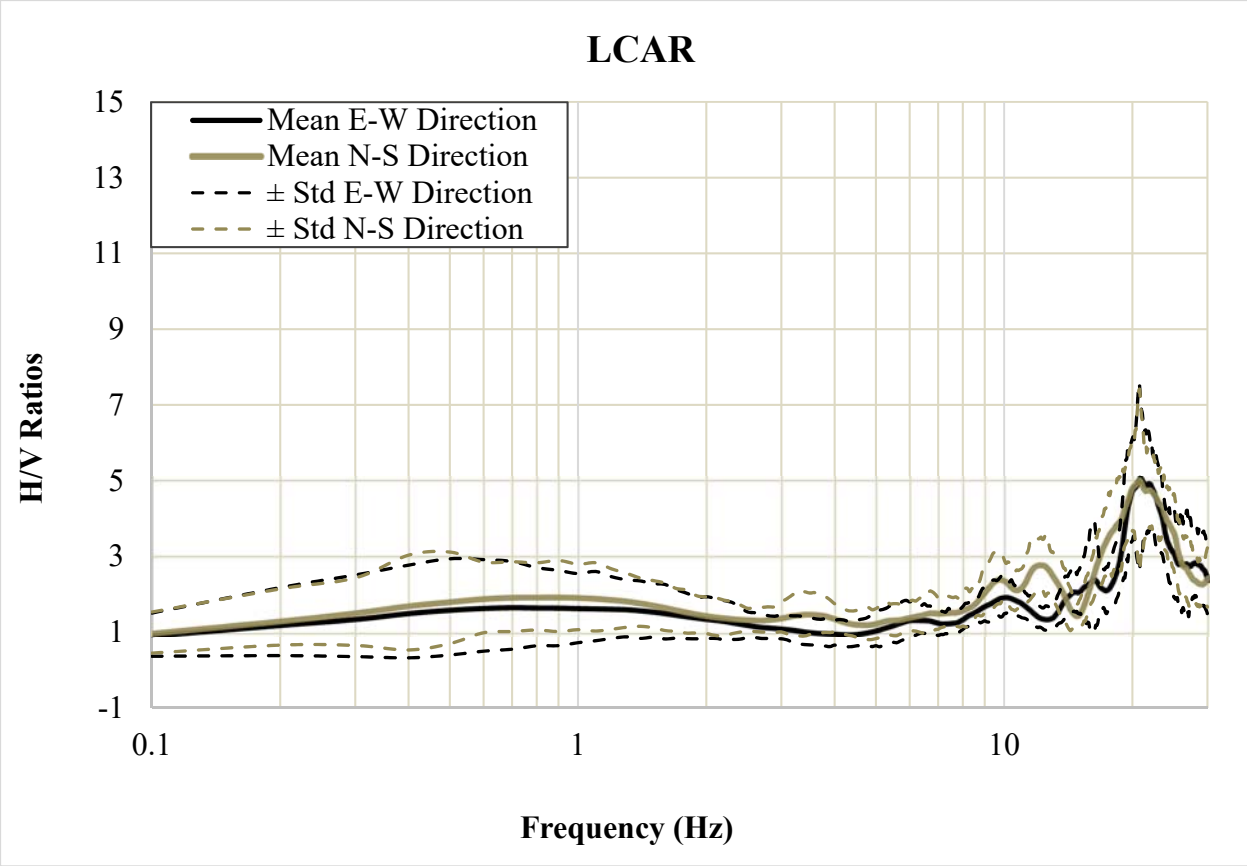

Figure 1-11. Solid lines show average of H/V ratios in East-West (black) and North-South (grey) components and dashed lines show ± standard deviations from the mean.

The peak of the average amplification for this station occurs at 21 Hz. Rapid increase in pore water pressure is the main reason for the high natural frequency of this site. The water level underneath this site is unknown at this point, although the location of this site close to the lake increases the probability of having high levels of ground water. The response spectrum of this station seems to be flat in low frequencies. In the N-S direction, it has a peak equal to an amplification of 2.7 around 11.5 Hz. This is still around the predefined threshold of frequency of a reference station.

1.1.7.6. FCAR

Like the other Arkansas seismic network strong motion stations, FCAR is located near one of the Arkansas state parks. It is a Trillium 120 sensor which has been active since 2010. The V_{S30} at this site is 593 m/s and, considering the geophysical features of the site, this station is located on the Boone formation that belongs to the Mississippian era. It typically consists of thick bedded fine granular to coarse-bioclastic limestone. The Limestone is usually gray, fresh and weathered (Rains and Hutto, 2012).

The soil amplification in both directions matches perfectly when we use the shear-wave window for computing spectrums. The f_0 of this site is 6.5 Hz. The amplification factors in the N-S direction and E-W direction are 2.7 and 2.3, respectively. Van Houtte et al. (2012) suggest a threshold of 2 for amplification factors of reference stations, and because this station has amplification factors greater than 2, it does not carry the characteristics of a reference station.

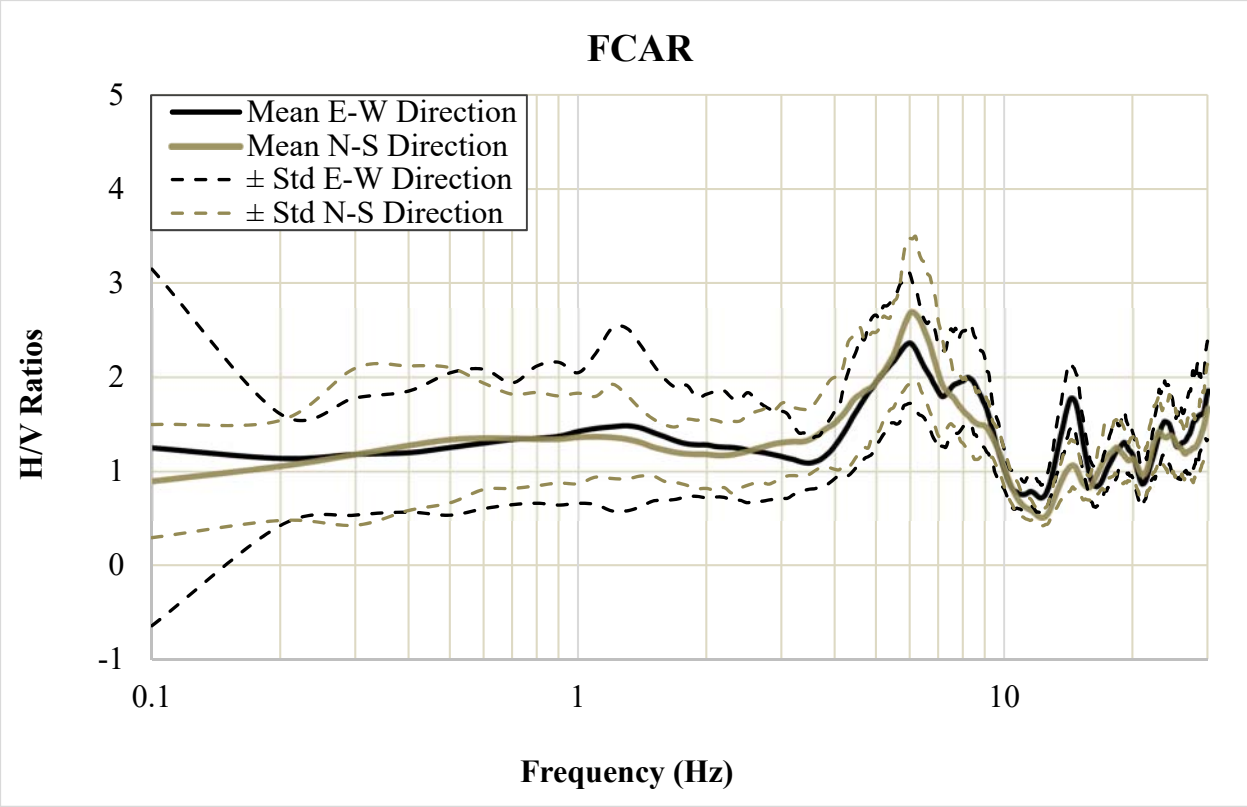

Figure 1-12. Solid lines show average of H/V ratios in East-West (black) and North-South (grey) components and dashed lines show ± standard deviations from the mean.

1.1.7.7. WHAR

One of the broadband seismic stations of ASN is Wooly Hollow, located within approximately 1175 feet of the Wooly Hollow national park visitor center. The station site is located on Mountainburg, a very stony fine sandy loam that is a shallow, well drained, moderately sloping soil on ridge tops and hillsides. The subsoil is strong brown very stony sandy clay loam and hard; massive sandstone bedrock is at a depth of 16 inches (NRCS Soil Survey 1979). Geologically the station is located on the middle part of the Atokan formation of Pennsylvania layers like station W41B. The V_{S30} of WHAR has been measured to be 1403 m/s which is a NEHRP Site Class B, or rock. This station is located in the northeast of the Greenbrier area a few miles

away from the Greenbrier-Guy fault, responsible for earthquake swarms in central Arkansas which are known to be induced earthquakes.

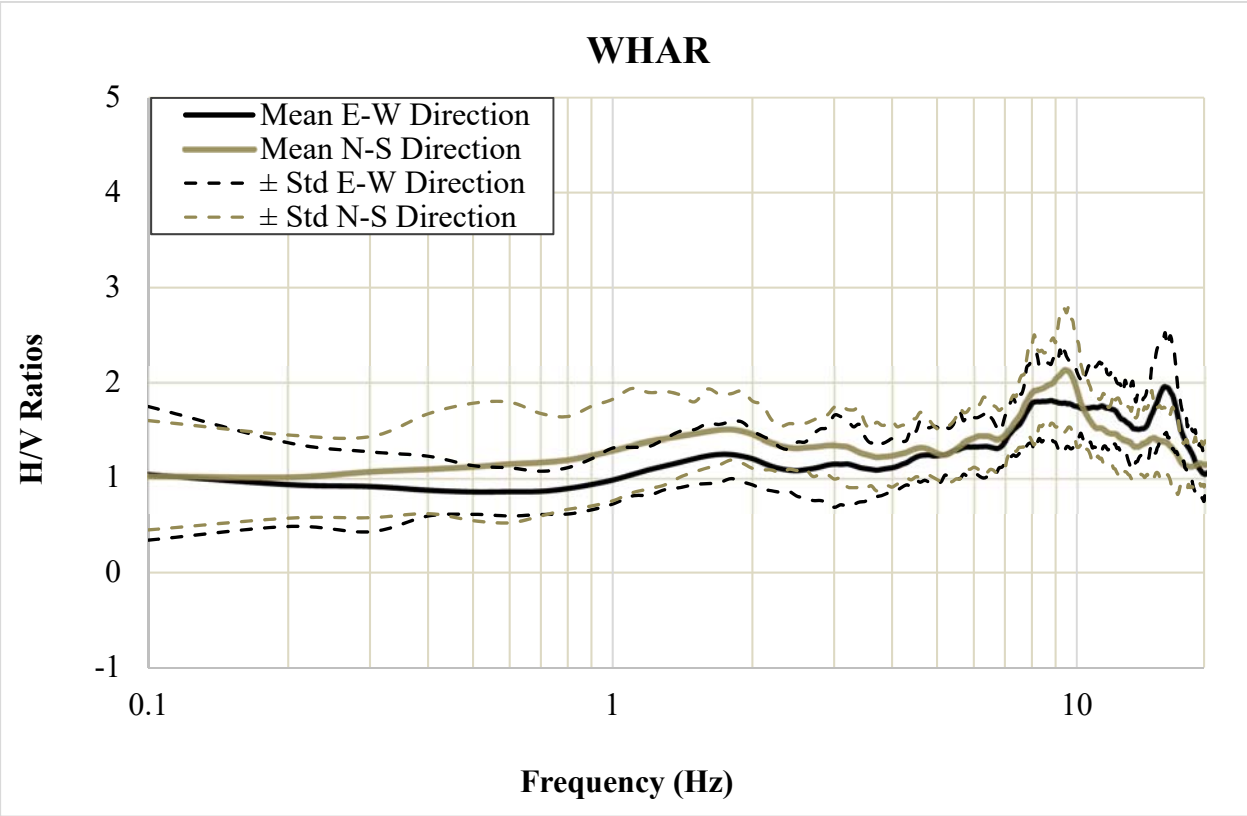

Figure 1-13. Solid lines show average of H/V ratios in East-West (black) and North-South (grey) components and dashed lines show ± standard deviations from the mean.

Average HVSRs of the WHAR station in the E-W and the N-S directions are shown in Figure 1-13. The f_0 for the N-S and the E-W components are 9.5 and 15, respectively. It has almost a flat trend around 1 Hz, which means it is a suitable reference station to be used for obtaining amplification factors in the ME.

1.1.7.8. X40A

X40A is a USArray transposable network station with a STS-2 Streckeisen instrument located in Basin Creek Farm in Hotsprings County in Arkansas. The Paleozoic rock depth underneath this station is around 130 feet, according to Figure 1-3. As for the soil characteristics of the site, the surface layer is dark brown silt loam. The subsoil is red very silty clay loam and below that is massive chert. The V_{S30} of this station is 1140 m/s, estimated by the hybrid slope-geology method. Figure 1-14 shows the average HVSRs in both directions.

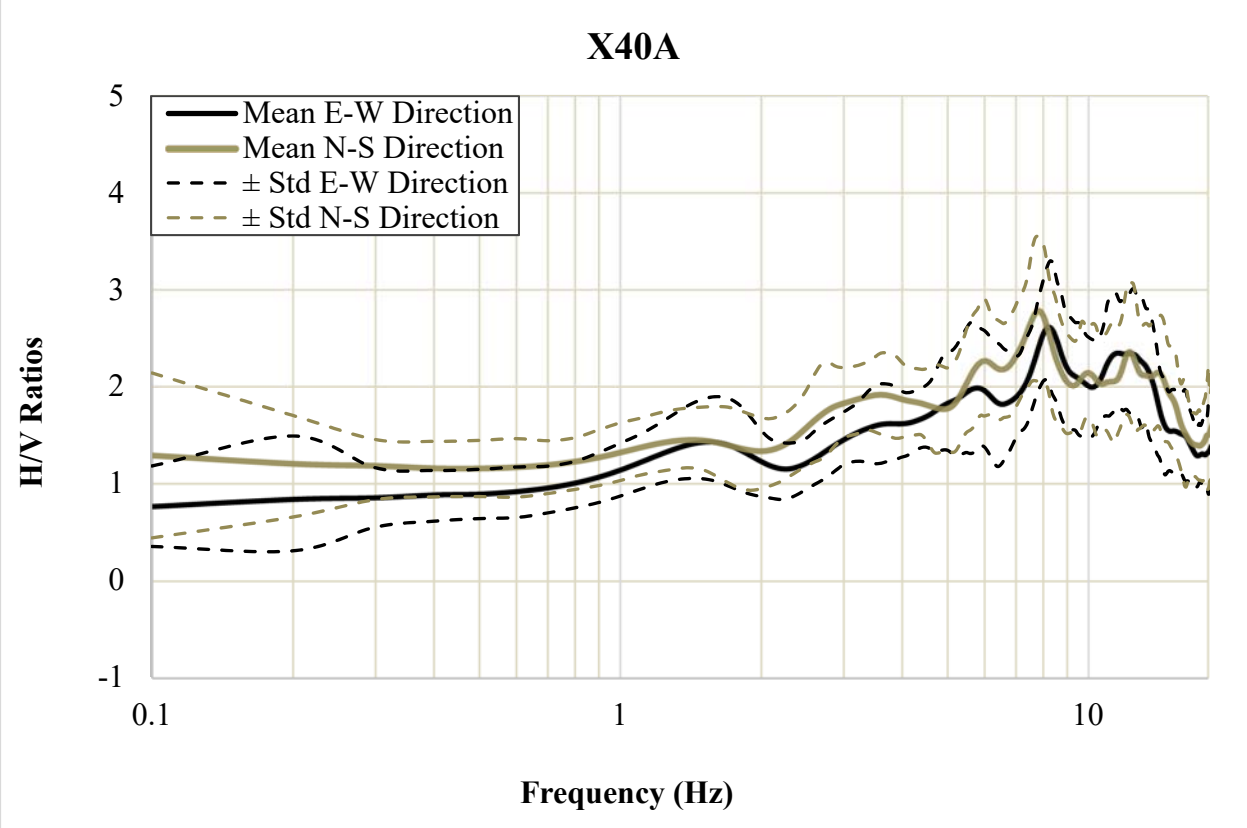

Figure 1-14. Solid lines show average of H/V ratios in East-West (black) and North-South (grey) components and dashed lines show ± standard deviations from the mean.

HVSRs for the N-S components are flat for frequencies less than 2, and the amplification factor curve increases to the peak of 2.8 at 7.7 Hz. The E-W component has the same trend when it reaches to an f_0 of 8 Hz. The response spectra for this site does not have a flat curve and its fundamental resonance frequency is lower than 9 Hz. In conclusion, this station is not a suitable reference station.

1.1.7.9. UALR

UALR is a Guralp broadband triaxial CMG-3ESP seismometer that belongs to the NM seismic network and has been operating since 1999. It is located to the northwest of Little Rock, Arkansas, a few miles outside the lowlands of the ME. Little Rock is close to major faults of Arkansas like the Greenbrier-Guy fault and the recently discovered Marianna fault in the east.

Paleozoic rock is at a depth of 87 feet at the UALR station. The site soil is gravelly silt loam, and it is located on the top of the Jackfork Sandstone according to the geological map of Arkansas. The Jackfork Sandstone is thin- to massive-bedded, fine- to coarse-grained, brown, tan, or bluish-gray quarzitic sandstones with subordinate brown, silty sandstones and gray-black shales (Arkansas Geological Survey website). The V_{S30} of the station has been measured in the field and provided by the NGA-East flatfile to be 1288 m/s which is a NEHRP Site Class B. The site response spectrum of this site in the form of HVSRs for 60 earthquakes is shown in Figure 1-15.

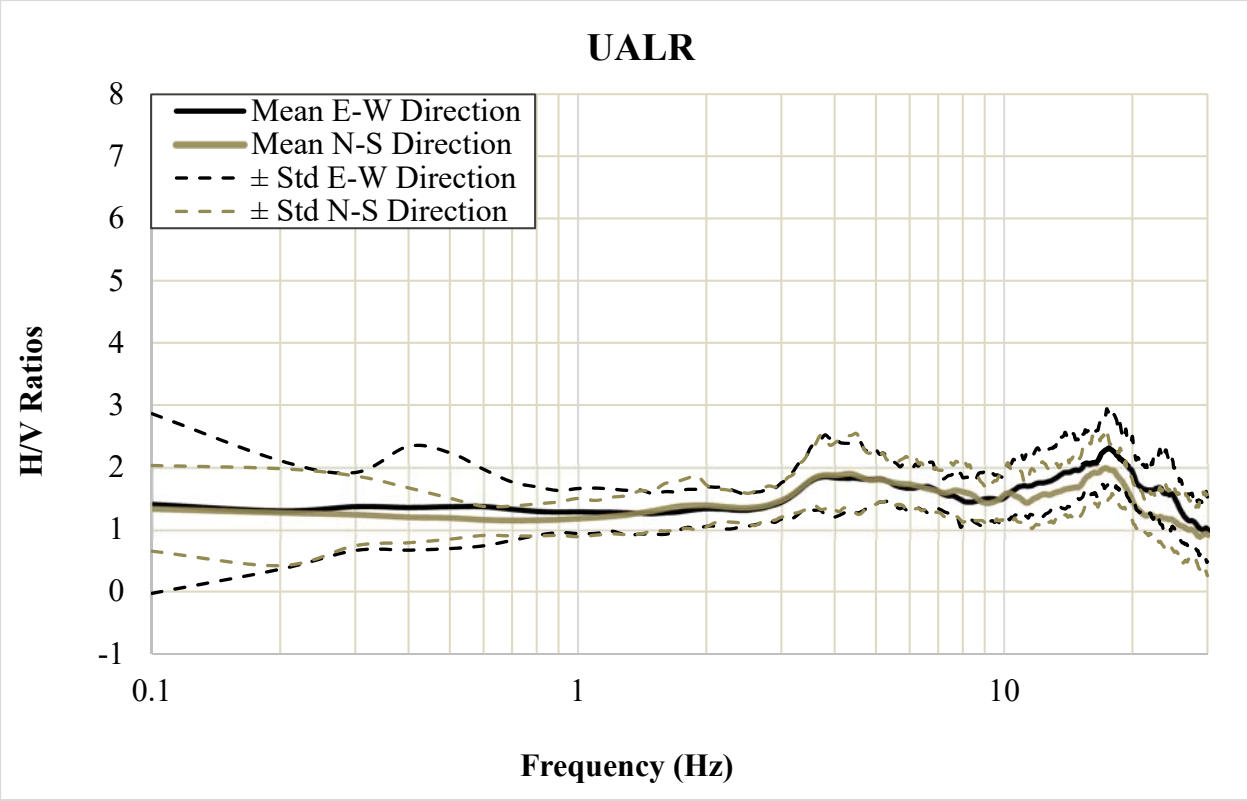

Figure 1-15. Solid lines show average of H/V ratios in East-West (black) and North-South (grey) components and dashed lines show ± standard deviations from the mean.

The average of the H/V ratios in both the E-W and N-S directions are the same for frequencies lower than 10, and they have a flat trend equal to one for frequencies lower than 3 Hz. The average ratios increase to almost 2 in f_0 of the site which is approximately 17 for both components. The fact that the response spectrum of this site is flat and has amplifications lower than 2, and also because its f_0 is higher than 9 Hz are sufficient to choose this station as a reference station in further studies like SSR or basin effects studies in the ME area.

1.1.7.10. PLAL

PLAL is located in the western part of Lauderdale County in Alabama, east of the ME and north of the Tennessee River. It is a broadband seismometer with a CMG-3ESP instrument

belonging to the NM seismic network, operating since 1998. The soil where this station is installed contains mostly cherty silt loam, and the depth of the Paleozoic rock of the ME underneath this site is 128 feet. According to the geological map of Lauderdale County, this station is on top of the Fort Payne Chert layer of the Mississippian time which consists of a limestone containing abundant nodules and beds of gray chert. The V_{S30} of the soil profile of the site has been estimated to be 622 m/s according to the NGA-East flatfile, which is a NEHRP Site Class C. For understanding the behavior of the station to see whether it can be considered to be a reference station, we considered the response spectrum of the site which is depicted in Figure 1-16.

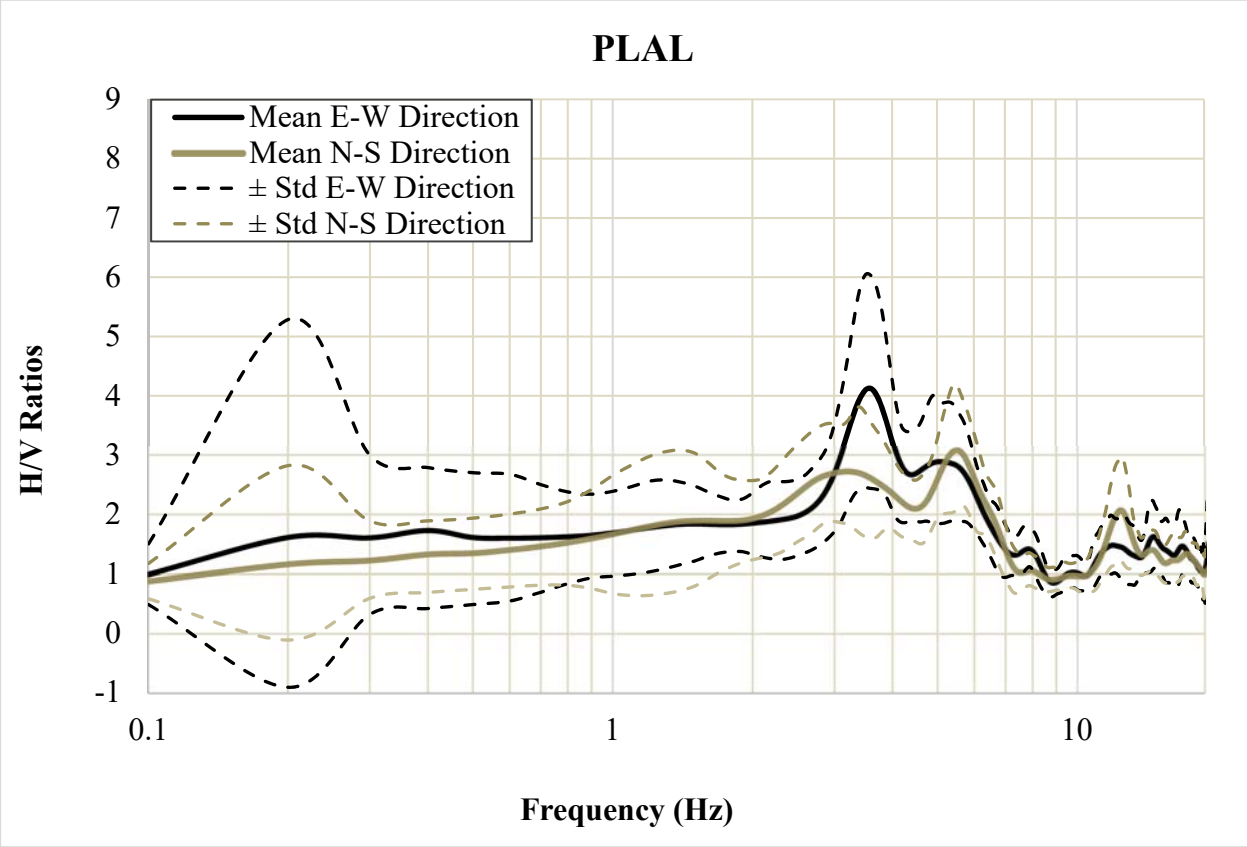

Figure 1-16. Solid lines show average of H/V ratios in East-West (black) and North-South (grey) components and dashed lines show ± standard deviations from the mean.

The average of the HVSRs for the E-W component has a fundamental frequency of 3.7 Hz, and it is 5.5 Hz for the N-S direction. Each way they are less than the fundamental frequency which is defined for a reference station. The amplification peak of average factors for the E-W direction and the N-S direction is 4 and 3, respectively, which gives us another reason not to consider this station as a reference station.

1.1.8. Reference Stations Summary

We computed the HVSRs in frequencies between 0.1 and 20 Hz for all the stations except for LCAR, where we considered frequencies larger than 20 Hz. We investigated the response spectra of these stations and their geological features to find the most suitable ones to use as reference stations in order to calculate site effects in the ME. Site effects can be calculated with methods like SSR. The fact that the stations in the ME are not close enough means that, in future studies, the path effects including the frequency Q factor and geometrical spreading should be accounted for.

Figure 1-17 shows the HVSR geometrical mean for all the stations considered in the study. The summary of the results gained for each station such as fundamental frequency, maximum amplification factor, average V_{S30} of the soil column, and the V_{S30} estimation method of the PEER NGA-East flatfile as explained earlier in the introduction (V_{S30} Code) are summarized in Table 1-4.

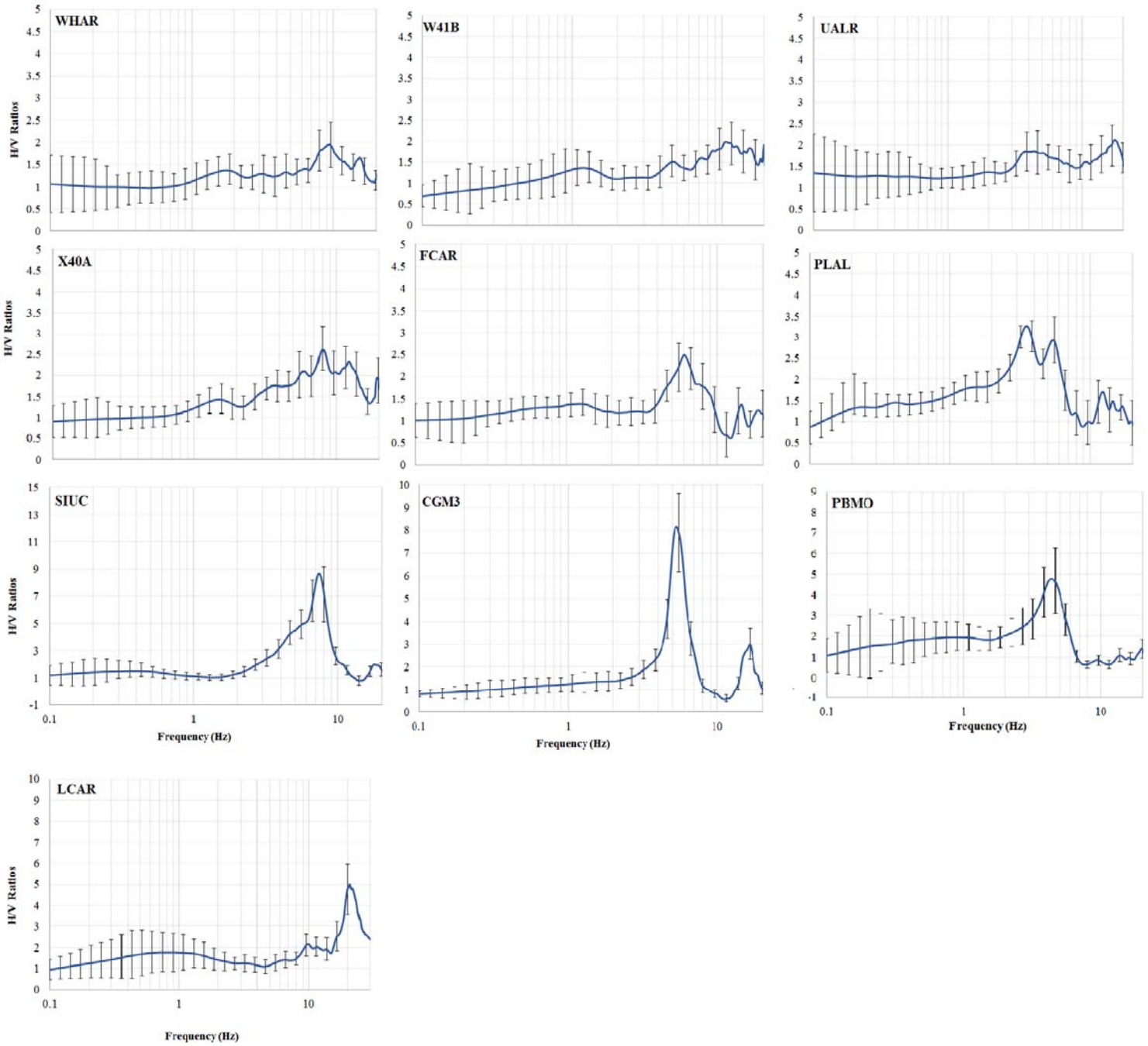

Figure 1-17. Solid lines denote the HVSR Geometrical Mean of the stations and the error bars show the standard deviations in 50 frequencies distributed log evenly.

Three stations (WHAR, W41B, and UALR) have their f_0 larger than 9 Hz and their maximum amplification factors less than or equal to 2. Furthermore, they have a flat response

spectrum compared to the other stations, according to Figure 1-17. Station X40A has characteristics close to a reference station; however, its f_0 is less than 9 Hz and the amplification in this station is not quite in the acceptable range. Another station that is debatable is LCAR, which has a flat HVSRs curve in low frequencies, but has a quite high maximum amplification factor. Most of the other stations have their natural frequency in a low range, resembling the behavior of a soft soil with a noticeable natural frequency that can be related to a thick layer of soil.

Table 1-4. Station Characteristics obtained from NGA-East flatfile and Figure 1-17..

Station ID	V_{S30} **(m/s)**	V_{S30} **Code**	f_0	**Max Amplification Factor**
SIUC	762	0	7.6	8.40
W41B	557.1	5	11.1	1.95
CGM3	522	5	5.5	8.00
PBMO	543.6	5	4.6	4.67
LCAR	564.3	5	19.5	4.76
FCAR	592.9	5	6.3	2.41
WHAR	1403	0	9.2	1.94
X40A	1140.8	3	8.3	2.52
UALR	1288	0	16.6	2.00
PLAL	622.1	5	3.6	2.35

1.2. Estimation of the Site Amplification in the New Madrid Seismic Zone Using Local Earthquake Data with Inversion Method

As stated earlier, the ME is a large area with deep deposits of soil and rock. The shortage of information about its soil layers characteristics can increase the uncertainties of site response analysis. The New Madrid seismic network, as well as other seismic networks, provides researchers a valuable opportunity to perform studies about earthquakes in this region. In this part of the study we select 6 seismic stations from the New Madrid seismic network inside the ME to perform site studies using an inversion method that requires using reference stations adjacent to the target stations. In the previous section the HVSR method was used considering the V_{S30} of a few rock stations close to the ME, to find the most suitable reference stations. Stations WHAR, UALR, and W41B showed the closest characteristics to a references station. We can use any of them in the inversion. Considering the limitations of large earthquake data and the fact that events we select should have records in both target stations and the reference stations we ended up using WHAR as the reference station.

1.2.1. Methodology

The standard spectral ratio method was first introduced by Borcherdt (1970) and developed further by Andrews (1986). It defined a generalized inversion method to decompose ground motion spectra into source, path and site components. The inversion method used in this study has been used by many researchers (Frankel et al. 1990; McNamra et al. 1996; Erikson et al. 2004) to investigate path effects. According to these studies the path effect can be defined by:

$$P_{ij}(f) = R_{ij}^{-\gamma}(f)\exp(-\frac{\pi f R_{ij}}{Q(f)V_s}), \tag{1-4}$$

where R is the hypocentral distance of the i^{th} event to the j^{th} station, γ is the geometrical spreading, $Q_s(f)$ and V_s denote the average quality factor and the average velocity of the S-waves in the medium, respectively. Applying the equation above to Equation 1-2, when the source of the earthquakes is the same, we conclude:

$$\frac{A_{ij}(f)}{A_{ir}(f)} = \frac{G_j(f).R_{ij}^{-\gamma}(f)\exp(-\frac{\pi f R_{ij}}{Q(f)V_s})}{G_r(f).R_{ir}^{-\gamma}(f)\exp(-\frac{\pi f R_{ir}}{Q(f)V_s})}, \tag{1-5}$$

By taking the logarithm of each side of Equation 1-5 the results can be rewritten at a fixed frequency as:

$$\ln A_{ij} + \gamma \ln R_{ij} = \ln G_i(f) - \pi f R_{ij}/QV_s, \tag{1-6}$$

where $\ln(A_{ij})$ is the logarithm of the ratio of the amplification factor for the target station and the reference staion at a fixed frequency. $\ln(R_{ij})$ is the logarithm of the ratio of the target station and the refernce staion distances to the event, $G_{ij}(f)$ is the site amplification factor of each station in i events, and V_s is the shear wave velocity in the region. The subscripts i and j denote the total

number of events and stations, respectively, and in Eq 1-5, r denotes the refernce station. For all events and stations, the Equation 1-6 can be expressed in matrix form by:

$$Gm = d \Rightarrow m = (G^T G)^{-1} G^T d, \tag{1-7}$$

where *m*, which is the model vector to be obtained, is the site amplification factors of the stations and *d* is the spectral ratios of the target stations to the reference station plus the product of the logartihm of distances ratio and gamma. The inversion is executed by finding a solution for *m* through the singular value decomposition method.

1.2.2. **Waveforms and Data**

The stations we used to determine the site amplification factors are shown in Table 1-5. The information is obtained from the flatfile of the NGA-East program. There is not much information about the geological features of these sites except their V_{S30} which shows that they are mostly located on soft layers of soil. The average shear-wave velocities of 4 stations (Code = 0) are measured in the field by geotechnical means and other stations are estimated by weighted proxy methods (Code = 5). These methods, which were addressed in the introduction of this part, are explained in detail in the NGA-East flatfile document report by Goulet et al., 2014.

To obtain the site amplification factors of these stations, we use the inversion method explained earlier, using 35 earthquakes that occurred in the NMSZ and Arkansas seismic zone. The data processing of this section is similar to the previous section, which means the spectrum values that have a signal to noise ratio lower than 2 are removed from the analysis (for more information about this procedure see Figure 1-6).

Table 1-5. Considered target stations close to the ME and their corresponding information.

Station ID	Station Name	Latitude	Longitude	Elevation (m)	V_{S30} code	V_{S30} (m/s)	Standard Deviation	NEHRP
NM.LPAR	Lepanto, AR	35.6019	-90.3002	67	0	225	0.1	D
NM.HBAR	Harrisburg, AR	35.555	-90.6572	74	0	225	0.1	D
NM.GNAR	Gosnell, AR	35.9652	-90.0178	71	5	224.8	0.57	D
NM.PVMO	Portageville, MO	36.4137	-89.6997	98.3	5	235.2	0.57	D
NM.PEBM	Pemiscot Bayou, MO	36.1131	-89.8623	76	0	160	0.1	E
NM.UTMT	Martin, TN	36.3498	-88.8636	120	0	300	0.1	D

Figure 1-18 shows the location and depth of the local events of the NMSZ and Arkansas region. These events are shallow and close enough to the station under study that they do not generate shear wave secondary reflections or refractions. Therefore, the S-wave window is used to extract the signal from the time series. The records are demeaned and detrended after the instrument responses are removed from them. Six target stations inside the ME and a rock reference station WHAR is adjacent to this area.

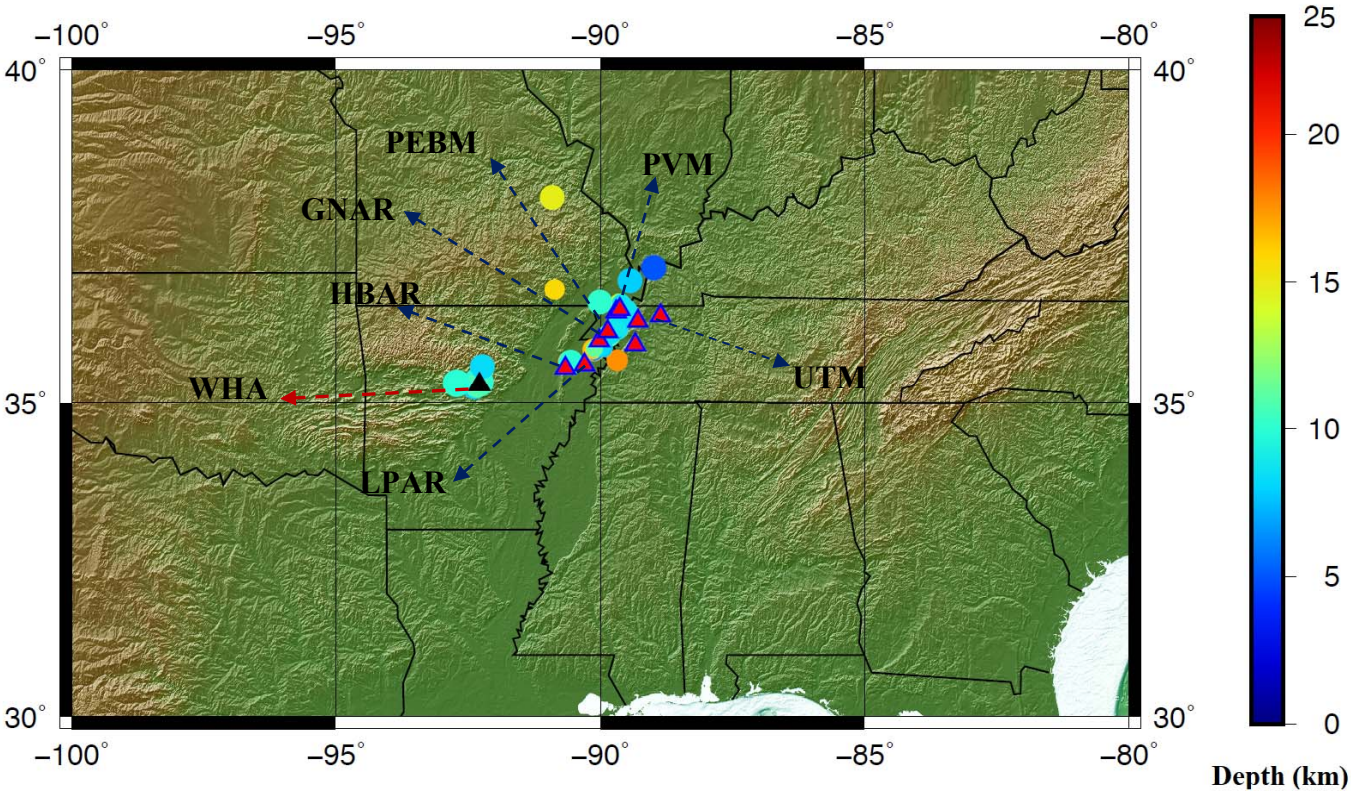

Figure 1-18. Six seismic target stations and WHAR as reference station for site effect studies in the Mississippi embayment area as well 35 earthquakes. Colored bar depicts the depths of the events.

1.2.3. Inversion results

By solving the inversion problem, we obtained the model vector of Equation 1-7 using 35 events in 200 frequencies. In this equation *m* is the site factor matrix, which show the ratio of the amplification factors of the target stations to the reference stations in each frequency, assuming the site amplification factor of the reference station WHAR to be almost equal to 1. As stated earlier this method incorporates a joint inversion method to solve site amplification factors and Q factors in the region. The vector *m* is calculated to find site amplifications and also the Q factor. Because of a trade-off between *Q* and geometrical spreading, the accuracy of quality factor cannot be confirmed. The advantages of the inversion method are the low value of standard deviation with

respect to the standard spectra ratio method and averaging out the effects of directivity and radiation patterns on site amplification. the values of Q factor in 20 distinct frequencies are shown in Figure 1-19.

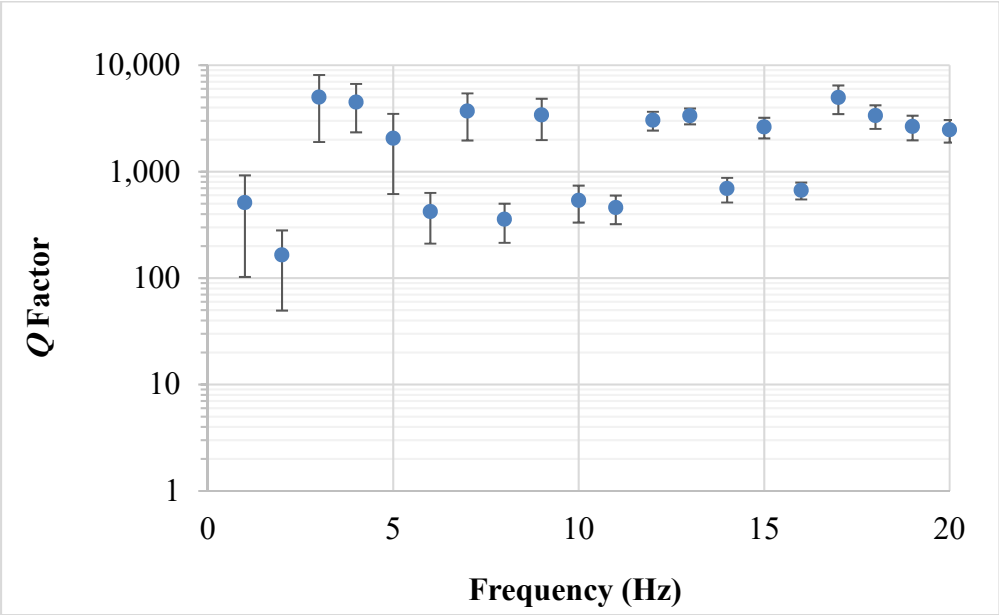

Figure 1-19. Quality factor obtained by inversion method.

Geometrical means of the two horizontal directions are obtained by computing the square root of the spectral values in each frequency. The geometrical mean of the horizontal spectral values is the site amplification factors in each station. The site amplification factors for 6 targets stations inside the ME are depicted in Figure 1-20.

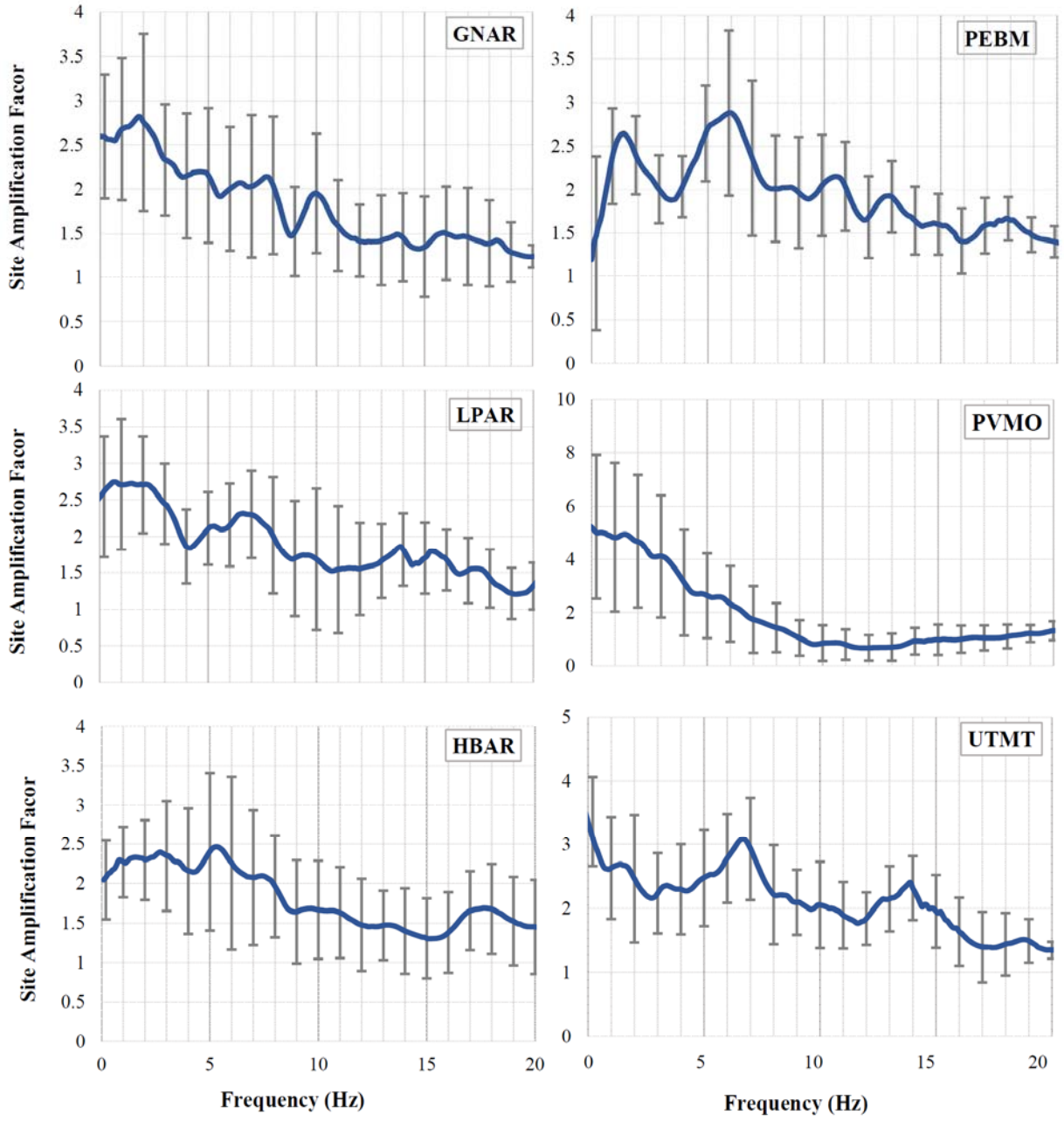

Figure 1-20. Geometrical mean of horizontal site amplification factors calculated through inversion method for 6 stations in the Mississippi embayment area using WHAR as the reference station.

As noted previously, the fundamental frequency f_0 in the site amplification factors reveals geological features of the site. In the previous section the f_0 of rock stations have been shown to

be higher than 8 Hz while sites with softer soils tend to have lower fundamental frequencies. As it is shown in Figure 1-20, which shows the site amplification factors using horizontal earthquake records, most of the target sites have very low fundamental frequencies. Bodin et al. (2001) investigated site effects in the Memphis, Tennessee area of the ME and concluded that the fundamental periods of different sites in this area are dependent on the thickness of the embayment and are between 2 and 5 seconds. The f_0 for the GNAR, LPAR, PVMO, and UTMT stations in our study are lower than 2 Hz and are associated with the fundamental periods introduced in Bodin et al. (2001). HBAR has a similar trend to the other stations and its fundamental frequencies occurs at 5 HZ. As it is shown in Figure 1-20, the standard deviation in the fundamental frequency is relatively higher than the other frequencies. We can conclude that the f_0 can occur in a lower frequency like 3 Hz, which has relatively lower deviation. The site amplification factors of the HBAR stations have similar values and trends to the H/V study performed by Zandieh and Pezeshk in 2011. The site amplification computed in this study for seismic station PEBM has almost identical values with the HVSR values represented in Zandieh and Pezeshk (2001). In the following the site amplification factor is obtained using the vertical component of the seismograms. These curves are shown in the figure below.

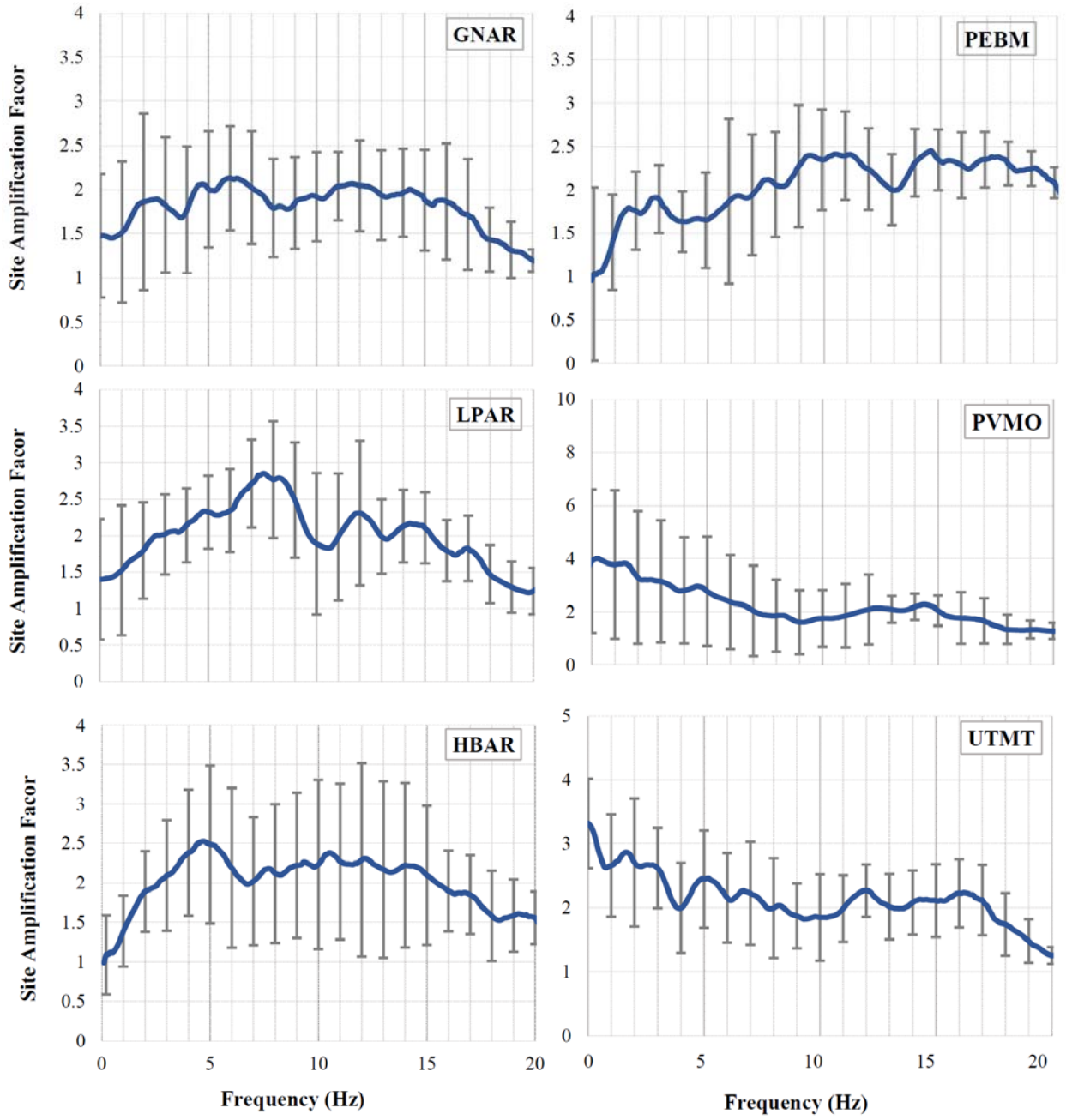

Figure 1-21. Vertical site amplification factors calculated through inversion method for 6 stations in the Mississippi embayment area, using WHAR as the reference station.

It is evident in Figure 1-21 that the fundamental frequency of the vertical component is higher than for the horizontal components, which is compatible with the assumption that the vertical components of the earthquake records are less affected by local site conditions than the horizontal earthquakes' records. Amplification factors of most of the target sites are between 2 and 4. Comparing the PVMO station with the UTMT station, we realize that although PVMO has a lower V_{S30}, it has a higher amplification factor at its fundamental frequency. According to Table 1-5, V_{S30} of this station is estimated by proxy measures. However, the V_{S30} of UTMT is measured in the field geotechnically and is more accurate. This observation shows that the V_{S30} value, especially if it is estimated by topographic or proxy methods, cannot be accurate enough to be used in seismic hazard analysis. As stated earlier, by increasing the number of events in this study we can decrease the levels of uncertainty and improve the results of this site-effect research.

2. Uncertainties Evaluation in Site Response Analysis

Abstract

Uncertainties exist inherently in seismic site amplification functions, and site-specific response analysis results are partly originated from variabilities in soil and local site conditions. These uncertainties can affect the results of surface seismic hazards or surface ground motions obtained by site response analysis (SRA). In SRA these uncertainties are accounted for by generating random cases of soil parameters. Choosing suitable randomization bounds can decrease the effects of the uncertainties in soil parameters on SRA results like predicted spectral accelerations. These bounds are quantified by the coefficient of variation (COV), which can be defined for different soil parameters. Vertical seismometer arrays provide a great opportunity to study the variability that exists in SRA by comparing predicted and observed surface ground motions.

In this study we evaluate COVs for different parameters of the soil that are the main input parameters of equivalent-linear SRA. These input parameters are the shear-wave velocity, thickness, shear modulus reduction (G/G_{max}) and damping values of each soil layer. Besides providing COVs for each individual parameter we provide COVs for two mixtures of parameters: $COV_{Profile}$, which is the coefficient for randomizing thickness and shear-wave velocity together, and COV_{DYN}, which is the coefficient for randomizing shear modulus reduction and damping together. We show that they vary by different periods. We perform 1-D equivalent-linear SRA with the SHAKE91 program for ground motions with peak ground accelerations (PGAs) of more than 0.05g for four vertical seismic stations with different site classes. The seismic stations belong to the KIK-Net seismic network in Japan. We also perform a nonlinear SRA on one of the stations

using the Deepsoil program and conclude that, by incorporating uncertainties in site response analysis the need for performing nonlinear analysis, can be resolved.

Coefficients of variation that generate minimum root means square errors are obtained for different site classes. The results are presented in several frequency distribution tables that show that how often a given COV range, which produces the minimum RMSE, occurs in selected ground motions.

2.1. Introduction

The characteristics of earthquake waves can be influenced dramatically by the soil and geological features of a particular site by the time they reach the ground surface. There are several examples throughout the history of earthquakes that show how local conditions can amplify or de-amplify the destructive effects of an earthquake. It is important to understand the characteristics of local features and how they affect earthquake wave propagation. Furthermore, it is important to be able to predict surface ground motion time series for a specific site for different purposes like evaluating the site-specific design response spectrum or evaluating liquefaction potentials.

2.1.1. Site-Specific Ground Response Analysis

In designing critical infrastructure and building structures such as bridges, dams, and nuclear facilities, it is required to perform site specific seismic hazard analysis, which utilizes ground motion prediction equations (GMPEs). Most of the GMPEs are modeled to predict the earthquake intensities on rock surfaces; in some other GMPEs that account for local site conditions, they only use the average shear-wave velocity of the upper 30 meters of the soil (V_{S30}). However, the local site effects have more aspects to account for than just considering V_{S30}. Therefore, different methods of site effect evaluation like site specific response analysis are used.

According to many building codes and seismic risk documents there are different circumstances that encourage engineers and researchers to perform site-specific response analysis. The following is a list of conditions for which a site-specific ground motion response analysis should be considered (Pezeshk and Yarahmadi, 2016):

- Site Class F,
- Critical and very important facilities and infrastructures,

- Liquefiable soil conditions,
- Deep soil deposits,
- Thin soil layers over rock (less than 40 to 50 ft),
- To obtain ground surface PGA for abutment walls or other designs, and
- To obtain better information.

Site specific ground response analysis is used to predict surface ground motions using soil characteristics of a site when the bedrock underneath that site is subjected to a motion that is obtained by seismic hazard techniques.

Basically, when the earthquake waves propagate through the Earth, they are travelling in the rock layers with different velocities. As they reach shallower depths, their velocity decreases which makes their direction inclined more vertically towards the soil and surface of the Earth (Kramer, 1996).

In a site response analysis (SRA), the soil is first modeled considering characteristics like the shear-wave velocity profile and dynamic properties. Then, an earthquake record obtained by seismic hazard means is applied to the base of the modeled column of soil to obtain the surface ground motion.

2.1.2. Linear Site-Specific Ground Response Analysis

In one-dimensional site response analysis (1-D SRA) the assumption is that the soil layers are distributed infinitely horizontally. When the waves hit the bottom of the soil profile, the harmonic horizontal motion of the bedrock produces vertically propagating shear waves in the soil layers above (Kramer, 1996). In linear SRA the surface motion is evaluated by multiplying a transfer function in the frequency domain by the bedrock transformed wave displacement time

series in the frequency domain. The transformed displacement in the frequency domain can be computed using traditional fast Fourier transform (FFT) methods. We can write the equation of horizontal motion of a soil layer as follows:

$$u(z,t) = A e^{i(\omega t + k z)} + B e^{i(\omega t - k z)}, \tag{2-1}$$

where ω is the circular frequency of ground shaking; k is the wave number, which is equal to ω/V_s; and A and B are the amplitudes of the wave when traveling upward or downward, respectively (Kramer, 1996). Having the horizontal displacement, we can compute the shear strain and consequently the shear stress of each soil layer. By applying boundary conditions to the equations of motion, the transfer function can be evaluated considering each soil layer's properties. This means the goal in linear SRA is finding a suitable transfer function.

2.1.3. **Nonlinear Site-Specific Ground Response Analysis**

The behavior of the soil under cyclic earthquake loads is inherently nonlinear, especially when the earthquake intensity is high. The shear stress versus strain relation follows a hysteresis loop when the soil is subjected to a cyclic load like the loads generated by seismic shear waves. In ideal circumstances, the shape of a hysteresis loop can be illustrated as shown in Figure 2-1(a). The shear modulus can be found at each point by the tangent of the curve, and the damping can be found by evaluating the area inside the loop. The hysteresis loop shape changes while unloading and reloading during a cyclic load. By obtaining the location of the maximum shear stress and strain of the loops we can obtain the backbone curve, which helps to find the shear modulus of a material in different cyclic strain amplitudes (Kramer, 1996). Soil nonlinear models utilize

different kinds of backbone curves along with a series of controlling rules that direct unloading and reloading behavior, stiffness degradation and other behavior. Figure 2-1 (b) illustrates a very simple backbone curve, which can be more complex for other models.

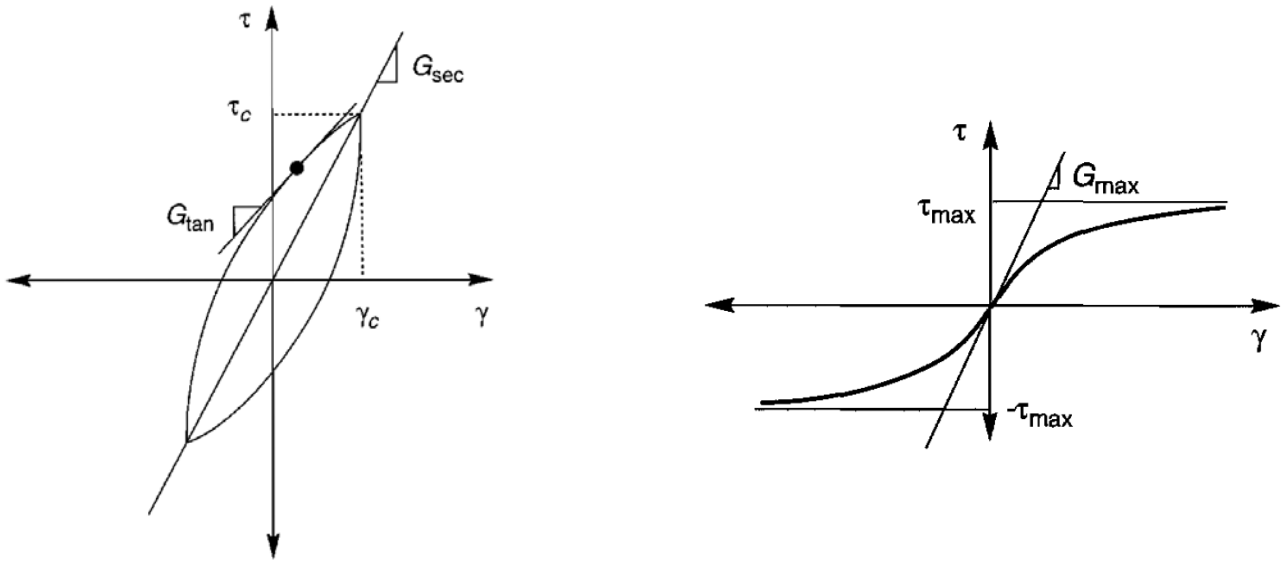

Figure 2-1. (a) Ideal hysteresis loop under cyclic load. (b) Hyperbolic backbone curve (Kramer, 1996).

In nonlinear SRA a direct numerical integration is performed in the time domain. The motion of each layer is computed in incremental time steps from the bottom of the soil column until it arrives at the ground surface. This approach can be very complex and time consuming when there are multiple layers of soil in the SRA model. Another factor of complexity in nonlinear approaches is accounting for the nonlinear stress-strain behavior of the soils, which follows the actual stress-strain path in a backbone curve during cyclic loading (Kramer, 1996).

There are various tools developed to perform nonlinear site response analysis. The most well-known are Deepsoil, D-MOD, DESRA, and NOAH. Each of these tools follows different methods to perform site response analysis. While the NOAH does not use damping and shear

modulus curves of the soil layers and considers pore water pressure, Deepsoil delivers many options to choose different methods that can help to perform the procedures more simply. In general, performing nonlinear models can be sophisticated and time consuming.

2.1.4. Equivalent Linear Site-Specific Response Analysis

The tangent slope of the backbone curve represents the shear modulus at that strain in the soil element. As can be observed from Figure 2-2, this slope decreases when the shear strain increases. Shear modulus reduction curves for each soil material are generated by obtaining values of G/G_{max} for each strain.

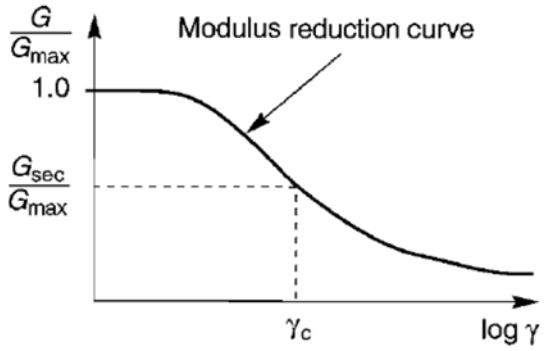

Figure 2-2. Shear modulus reduction curve (Kramer, 1996).

Performing a nonlinear SRA can be complicated and time consuming; therefore, equivalent linear models have been developed which consider shear modulus reduction and damping curves to estimate the nonlinearity of the soil during seismic cyclic loading. Having the shear modulus and damping ratio at each strain, we can perform equivalent linear seismic response analysis (EL-SRA). First, we calculate the maximum shear strain using an initial estimate of shear modulus and damping ratio. Having the maximum shear strain, the effective shear strain can be computed and

new values for shear modulus and damping can be found by using shear modulus reduction and damping ratio curves. This iteration stops when a compatible shear strain value is achieved in two consecutive steps.

EL-SRA is widely used by researchers and engineers. This method is less time consuming than nonlinear procedures because of its iteration and approximation nature. In addition, equivalent linear (EL) models need fewer input parameters than their nonlinear counterparts. Shear-wave velocity profile, damping ratio, and shear modulus reduction curves of the soil layers as well as the input rock ground motions for bedrock underneath the soil are the main parameters EL models need to perform site-specific response analysis. These parameters are very significant parameters for nonlinear models too; therefore, finding appropriate soil properties and input ground motions affect the performance of both EL and NL site response analysis dramatically.

There are a variety of laboratory and in-situ methods to find soil properties. Each of these methods have different ranges of variability associate with, which leads to uncertain results in site response analysis. Addressing the uncertainties in EL-SRA may decrease the need to perform fully nonlinear analysis, which have the same uncertainties in their input parameters. Therefore, in this study we are concentrating on finding suitable uncertainties in different parameters of the soil, and how to consider them while performing site response analysis.

2.1.5. Sources of Uncertainties

There are two sources of uncertainty in performing SRA. First is the variability that exists in different seismic input records; and second, there are uncertainties that exist in characterizing the represented soil properties at the site under study. Parameters such as shear-wave velocities,

layer thickness, shear modulus reduction G/G_{max} and damping curves have significant roles in SRA.

In general, uncertainties can be divided into two categories: the "epistemic uncertainties" are associated with a lack of knowledge and data in modeling a process; and the "aleatory variability" is associated with the natural randomness that exists inherently in performing a process (Green et al., 2016).

While PSHA gives us the seismic hazard at the location, even having a site amplification function doesn't guarantee a precise seismic hazard prediction at the ground surface. Site amplification factors are dependent on the soil's properties and its dynamic behavior under the seismic excitation. Many studies have focused on how to incorporate uncertainties in PSHA of the surface. Cramer (2003) proposed a completely probabilistic method to consider the uncertainties of site amplifications in seismic hazard analysis to obtain the site-specific probabilistic ground motion estimate, and Bazzurro and Cornell (2004) proposed a method to reduce those variabilities that affect the surface seismic hazard. Therefore, defining the soil uncertainties and their effects on the site amplification factors have a major impact on surface hazard estimates.

The distinction between epistemic uncertainties and aleatory variabilities in the SRA can be vague (Green et al., 2016). For instance, we can account for shear-wave velocity aleatory variability by producing random shear-wave profiles following a normal distribution. We can account for epistemic uncertainties by determining the bounds of random cases considering the epistemic uncertainty defined for the soil.

Asimaki et al. (2008) performed a comprehensive study on different methods of SRA by comparing real observations from downhole array ground motions at the ground surface with the

predicted ground motions obtained using various SRA models. They ran SRA with different models to minimize the cumulative normalized error of the predicted and the observed spectral acceleration at the surface for different ground motions, represented as follows:

$$e_{SA} = \frac{1}{n}\sqrt{\sum_{i=1}^{n}\left[\frac{SA_o(T_i) - SA_P(T_i)}{SA_o(T_i)}\right]^2}. \quad (2\text{-}2)$$

where, SA_o is the observed spectral acceleration, and SA_P is the predicted spectral acceleration in one period and, n is the number of iterations.

Li and Asimaki (2010) investigated the propagation of uncertainties in SRA. They evaluated the standard deviation of differences in pseudo acceleration of predicted and observed ground motions at the ground surface of downhole arrays by randomizing the dynamic properties of the soil considering different ground motion intensities.

Kaklamanos et al. (2015) quantified uncertainties in linear, equivalent linear, and nonlinear site response models by studying vertical seismometers of the Kiban-Kioshin Network (KIK-Net) by comparing the predicted site response results with observed surface ground motions. By comparing different models, they found that linear models fail to predict short-period ground motion in shear strains of 0.01% to 0.1% while equivalent linear and nonlinear models offer more realistic predictions. For performing site response models, they used shear-wave profiles provided in the KIK-Net database, while they used models proposed by Zhang et al. (2005) and Darendeli (2001) to obtain shear modulus reduction and damping curves.

Andrade and Borja (2006) investigated the relative sensitivity of the equivalent linear and nonlinear SRA to variability of the soils using two site response codes: SHAKE and SPECTRA. In order to reach this goal, they modeled the variability of the soil by generating random uncertainties and adding them to the input parameters of the SHAKE and SPECTRA codes. In defining the variabilities in soil parameters, they used the correlation between shear modulus and damping while assuming all other soil parameters are independent.

According to the Electric Power Research Institute seismic evaluation report for post-Fukushima incident studies (EPRI, 2012), the aleatory variability in SRA can be captured by generating a specific number of random cases of the soil parameters. The main soil parameters in equivalent linear SRA are the shear-wave velocity, thickness, damping and shear modulus reduction (G/G_{max}) values of each soil layer. We need to treat these soil parameters as random variables. For this purpose, random cases are generated repeatedly and SRA is performed for each randomized case. Choosing suitable randomization bounds can decrease the effects of the uncertainties in soil parameters on SRA results. These bounds are quantified by the coefficient of variation (COV), which can be defined for different soil parameters. The value of COV for these soil parameters has been employed differently in different studies. For critical infrastructures like power plants numerous shear wave profiles are measured in the field. Obtaining the standard deviations of the shear wave velocities of each layer, the coefficient of variations can be estimated.

2.2. Purpose of the Study

When performing SRA for critical infrastructure like nuclear power plants it is common to measure several shear-wave profiles at the site of the study. Using these measurements, the shear-

wave velocities' standard deviation can be obtained. Using these standard deviations, coefficients of variation can be defined to perform randomization in order to account for aleatory variabilities.

Toro et al. (1993), using generic soil profiles, suggested the standard deviation of the natural logarithm of the shear-wave velocity, σ_{lnv}, to be 0.39, which corresponds to a COV of 0.41 for shear-wave velocities. It is common for researchers and engineers to use Toro's values to perform randomization of the shear wave profile when the borehole measurements/data in the field are not enough to establish the standard deviation of the measured soil shear-wave profiles.

The main objective of this study is to present a different procedure to find σ_{lnv} values for shear-wave profiles and COV values for other parameters of the soil when there is a need to generate random cases. Here we show this procedure using four different stations in the KIK-Net network. This procedure can be used in other regions when vertical array data is available.

To reach this goal, sets of ground motions from vertical arrays of seismometers are employed. We use the equivalent linear software SHAKE91, which performs 1-D equivalent linear SRA. We take advantage of KIK-Net vertical seismometer arrays that provide both rock-level and surface ground motions for various earthquakes. Another benefit this database provides is that the site soil information is available for each station. The information available, such as shear-wave velocity, p-wave velocity, soil layer thicknesses, and the geological and material characteristics of each layer of the soil, are essential in a site response analysis.

2.3. Randomization Procedure

For generating random realizations of different soil parameters, we generate random numbers from a normal distribution with a mean of zero and a unit standard deviation within the

bounds of ±2σ, multiply that random number by the coefficient of variation (or σ_{lnV} in the case of shear wave velocity), and multiply the product with the soil parameter base case. The result is then added to the soil parameter base case:

$$X_r = X + \varepsilon_r \cdot \sigma_X = X + \varepsilon_r \cdot X \cdot COV_X \tag{2-3}$$

where X is a measured or estimated soil parameter like the thickness of each soil layer, shear modulus reduction (G/G_{max}), or damping, $\sigma_X = X \cdot COV_X$ is the standard deviation of X, ε_r is the generated N [0,1] random variate, and X_r is the generated random soil property.

2.3.1 Randomization of Dynamic Properties

If there are no field measurements or laboratory tests performed on the site under the study to find shear modulus reduction (G/G_{max}) and damping curves, there are generic models to produce them. The EPRI 2012 report and studies like Zhang et al. (2005) and Darendeli (2001) recommend generic models to be used in SRA. No matter if one uses generic models or obtains the modulus reduction and damping curves of the soil layers by real in-situ or laboratory means, there are still uncertainties that need to be addressed. Therefore, as recommended by the EPRI 2012 report, one needs to account for these uncertainties by generating random cases of the base case.

To generate random shear modulus reduction and damping curves according to the EPRI 2012 report, a log normal distribution can be assumed with a COV in the natural scale. These values are computed at a cyclic shear strain of 0.003% for both damping and shear modulus. The

computed change of the shear modulus or damping at 0.003% is then applied to all the strains. The random perturbation factor is reduced or tapered near the ends of the strain range to preserve the general shape of the base-case curves. For defining the shear modulus reduction and damping curves in this study, we use 11 strains. For tapering the randomizations near the ends of the strain range in this study, we multiply the first term of Equation 2-3 ($COV \cdot \varepsilon_r \cdot X$) by zero for shear strains number 1 and 11 (strains on each end of the strain range), and multiply this term by 0.5 for shear strains numbers 2 and 10. Damping should be limited to a maximum value of 15% in this application, and an upper and lower band of ±2σ should be applied to the random numbers. A sample of the shear modulus and damping curves of a sandy material is illustrated in Figure 2-3 for a coefficient of variation of 0.3.

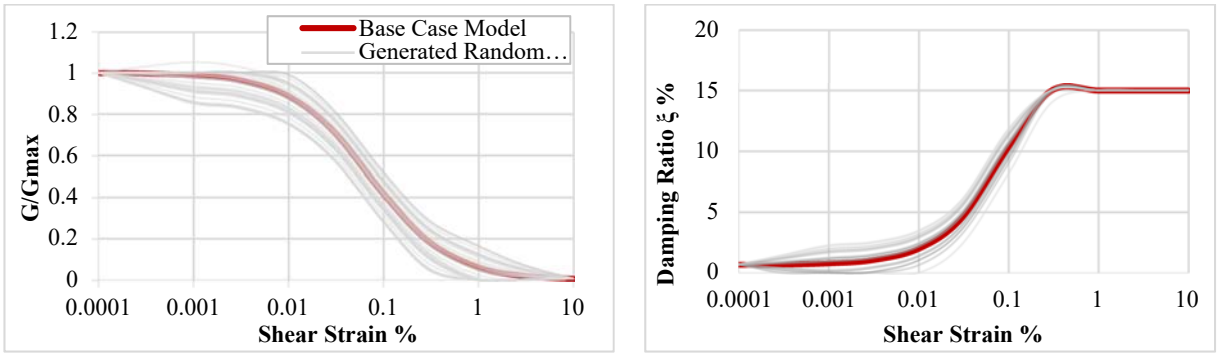

Figure 2-3. Dynamic properties 30 randomizations.

2.3.2 Randomization of Shear-Wave Profile

Each shear-wave profile has two aspects: the shear-wave velocity and thickness of each layer of the soil. For generating random thicknesses for each soil layer, we follow the same approach we have for dynamic properties of the soil and as given in Equation 2-3.

For shear-wave velocity we use the Toro et al. (1993) randomization model, which assumes that the shear-wave velocities are log normally distributed and there is a correlation between the shear-wave velocities of adjacent soil layers. Toro's model is associated with the normal distribution model:

$$Z_i = \frac{\ln(V_i) - \ln[V_{\text{median}}(h_i)]}{\sigma_{\ln V_i}}, \tag{2-4}$$

where V_i is the shear-wave velocity at layer *i,* h_i is the midpoint depth of the *i*, and $\sigma_{\ln V_i}$ is the lognormal standard deviation of shear-wave velocity at layer *i*. They defined this normal distribution based on a database of 580 shear wave profiles. V_{median} in Toro's study is the median of the shear-wave velocities they used in their study. In this study, however, we replace it with the base shear-wave velocity we obtained from the KIK-Net database.

The standard deviation $\sigma_{\ln V}$ determines the randomization bounds that are used to generate random shear wave velocities. This sigma is unitless because it is the standard deviation of the natural logarithm of the shear wave velocity and it is associated to the coefficient of variation. The COV is the ratio of the standard deviation to the average on the natural scale, where for a log-normal distribution:

$$COV = \sqrt{e^{\sigma^2} - 1}, \tag{2-5}$$

Toro et al. (1993) characterized the log normal distribution of velocities and the correlation they have among the layers by performing a first order auto regression in a shear-velocity profile database, where the random values of each layer correlate with their adjacent layers with auto correlation coefficient ρ:

$$Z_1 = \varepsilon_1$$
$$Z_i = \rho Z_{i-1} + \sqrt{1-\rho^2}\,\varepsilon_i \tag{2-6}$$

where ε_1, ε_2, ε_3... are random normal variables about zero with a unit standard deviation. The correlation coefficient ρ is dependent on the depth and layer thicknesses proposed by Toro et al. (1993) by Equations 2-7 to 2-9:

$$\rho(h,t) = (1-\rho_d(h))\rho_t(t) + \rho_d(h) \tag{2-7}$$

where:

$$\rho_d(h) = \begin{cases} \rho_{200}\left[\dfrac{h+h_0}{200+h_0}\right]^{\beta} & \begin{cases} For \quad h \le 200 \\ \\ For \quad h > 200 \end{cases} \\ \rho_d(h) = \rho_{200} \end{cases} \tag{2-8}$$

$$\rho_t = \rho_0 \exp\left[\frac{-t}{\Delta}\right] \tag{2-9}$$

where h is the average midpoint depths of layers i and i-1, and ρ_{200}, h_0, β, ρ_0 and Δ are the model parameters provided in Table 2-1, which depend on the National Earthquake Hazard Reduction Program (NEHRP) site classification (BSSC, 1998). The stations used in this research are located in different site classes; therefore, we should adjust Toro's equations accordingly per the parameters represented in this table.

In this study we evaluate the sigma of the log-normal distribution for shear wave velocities when performing randomization for shear wave velocities. For all the other parameters, i.e., shear modulus reduction (G/G_{max}), damping and thickness of soil layers, we evaluate the COV on the natural scale.

Table 2-1. Correlation Parameters by Toro et al. (1996).

	Site Class			
Parameter	A	B	C	D
ρ_0	0.95	0.97	0.99	0
Δ	3.4	3.8	3.9	5
ρ_{200}	0.42	1	0.98	0.5
h_0	0	0	0	0
b	0.063	0.293	0.344	0.744

An example of a random shear-wave profile of a seismic station that belongs to the KIK-Net seismic network is depicted in Figure 2-4. In this example, a sigma of 0.3 is used to generate 60 random shear wave velocities for each soil layer based on the relations above, and also a COV of 0.30 is used to generate 60 random layer thicknesses for each soil layer, from the base shear-wave profile of station IBRH13 of the KIK-Net database.

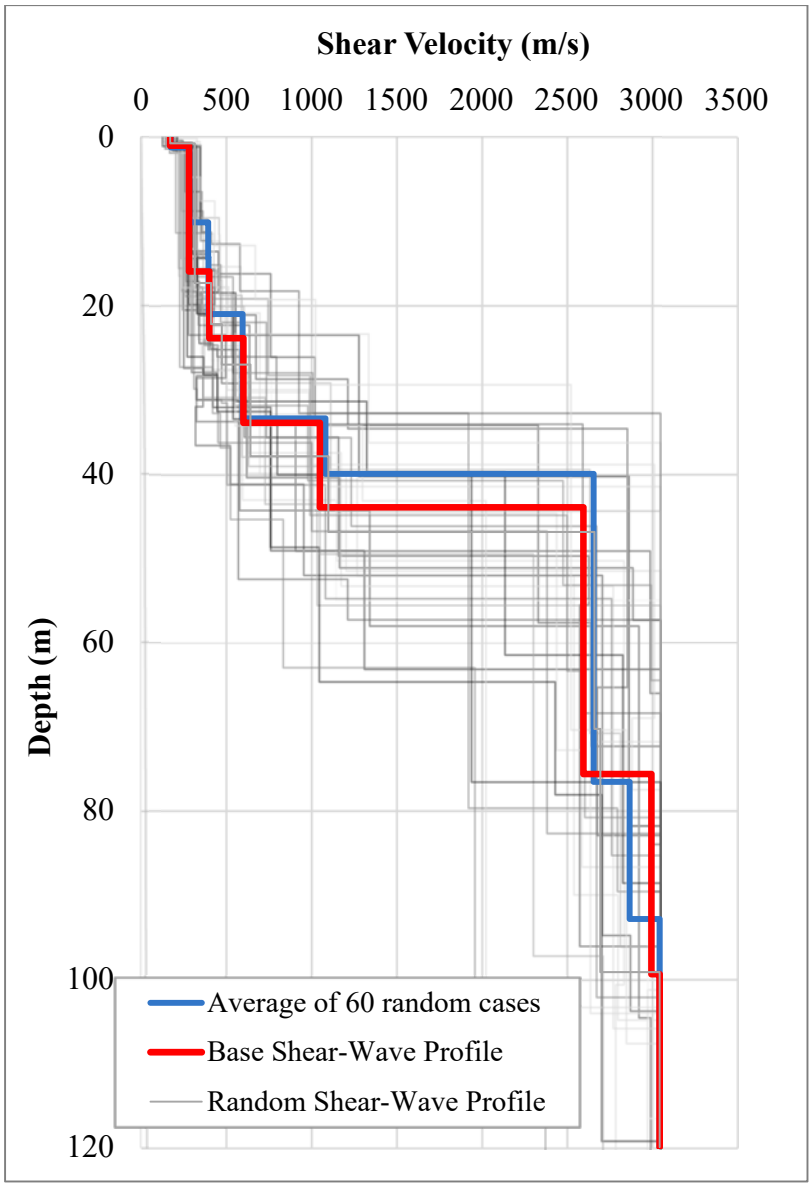

Figure 2-4. IBRH13 shear-wave profile randomization.

2.4. Shear Modulus Reduction and Hysteretic Damping Curves

In EL-SRA, in which the input parameters are limited to a few, shear modulus and damping can affect the results dramatically. Therefore, special consideration should be given to the selection of the shear modulus and damping curves. In some projects, laboratory or in-situ tests are performed to gain the dynamic properties of the soil, while in other projects, where the test

availability is limited, researchers and engineers use generic curves. Generic dynamic parameter curves have been developed in different studies. One of the most popular is the one provided in the guidelines for determining design basis ground motions by the Electric Power Research Institute (EPRI 1993). According to EPRI (1993), the shear modulus reduction and damping ratio curves of different soil materials like sand, gravel, and clay with different depths are gathered from other studies. Zhang et al. (2005) and Darendeli (2001) developed generalized modulus reduction and damping relationships. The Zhang et al. (2005) and Darendeli (2001) models need different soil parameters like the soil normal effective stress, the plasticity index, and the ground water level of the site to generate dynamic relationships. Kaklamanos et al. (2015) used these models to perform SRA and compared the results based on these two models.

The shear modulus and damping curves in this study are obtained based on the assumptions and procedures of Kaklamanos et al. (2015). Following their article, the shear modulus reduction and damping curves of soil layers are computed by Zhang et al. (2005), which proposed relationships for generating shear modulus and damping for the soils using the mean effective confining pressure σ_m, plasticity index PI, and the geological age (Quaternary, Tertiary, and older or residual soils) of the soil layers as input parameters.

The density of the soil layers is not provided in the KIK-Net database. Boore (2007) proposed sets of equations from different studies to estimate the density of the soils based on their *P*-wave velocities:

$$V_P < 1.50 \text{ km/sec} \qquad \rho = 1.93 \text{ gm/cm}^3 \qquad (2\text{-}10)$$

$$1.50 \text{ km/sec} < V_P < 6.0 \text{ km/sec} \qquad \rho = 1.74\, V_P^{0.25} \qquad (2\text{-}11)$$

$$\rho=1.6612V_P-0.4721V_P^2+o.0671V_P^3-0.0043V_P^4+0.000106V_P^5 \quad 6.0 \text{ km/sec}<V_P \tag{2-12}$$

where ρ is the density in gm/cm^3 and V_P is the P-wave velocity in km/sec.

Having the density of the soil and the shear-wave velocity of each layer of the soil, the maximum soil shear modulus related to small strain levels can be calculated by:

$$G_{max}=\rho V_S^2 \tag{2-13}$$

The shear modulus reduction relation can be obtained by (Zhang et al., 2005):

$$G/G_{\max}=\frac{1}{(1+\frac{\gamma}{\gamma_r})^{\alpha}} \tag{2-14}$$

where γ_r is related to the mean effective confining stress of the soil and α is the regression constant proposed in the paper for different layers of the soil based on their plasticity index and their geological age.

The mean effective confining stress of the soil is a combination of vertical and horizontal effective stresses. The vertical effective stress can be estimated by the density of the soil and the level of underground water. The horizontal effective stress can be computed by applying K_0 to the vertical effective confining stress:

$$K_0 = \frac{\upsilon}{1-\upsilon} \qquad \text{where} \quad \upsilon = \frac{V_P^2 - 2V_S^2}{2V_P^2 - 2V_S^2} \tag{2-15}$$

Damping is dependent on the shear modulus reduction value at each strain level, plasticity index (PI), and the mean effective confining stress of the soil.

2.5. Data

For this study, we take advantage of the strong-motion KIK-Net seismic network because of its vast ground motion database and the information they provide for each seismic station such as the shear-wave profiles, P-wave velocity profiles, soil layer profiles, and geological features.

The KIK-Net seismic network consists of pairs of seismographs installed in a borehole together with high sensitivity seismographs at the ground surface, deployed at nearly 700 locations in Japan. The pairs of seismographs in the bottom of a borehole and at the surface of the ground give the opportunity to compare the SRA results and the observed ground motions on the surface.

One of the objectives of this study is to determine uncertainties of nonlinear properties of the soil while performing site response analysis; therefore, strong ground motions are used as inputs to the SRA. High intensities take the analysis into the nonlinear range because the higher intensities (peak ground acceleration) induce larger strains, and the larger strains in stress-strain curves like backbone curves (that were represented earlier), are far from the linear phase. To have high intensity ground motions in our study, we tried to use ground motions with PGA higher than 0.05g. Peak ground acceleration of the surface is basis for choosing ground motion records. These ground motions resulted from earthquakes recorded between 2002 to 2018 with magnitudes between 2 and 6.

Four stations representing four different soil site classes (B, C, D, and E) are chosen from the KIK-Net database. The stations and their corresponding ground motion are provided in Table 2-2. Information such as the average shear-wave velocity, depth of borehole, and shear-wave velocity at the bottom of the hole can be obtained from the database. The KIK-Net network stations cover the Japan seismic zone, which is considered to be one of the most seismically active places in the world. Locations of the selected stations are shown in Figure 2-5 and provided in Table 2-2.

Table 2-2. Four Seismic Stations in KIK-Net Database.

Station ID	Latitude	Longitude	V_{S30} (m/s)	V_{Shole} (m/s)	D_{hole} (m)	NEHRP Site Class	Number of Ground Motions	PGA
NMRH04	43.39	145.12	168	410	216	E	28	> 0.05g
IBRH14	36.69	140.55	829	3200	100	B	137	>0.05g
IWTH27	39.03	141.53	670	2790	100	C	80	>0.05g
IBRH13	36.79	140.57	335	3000	100	D	87	>0.1g

V_{S30}: Average shear velocity in top 30 meters.
V_{Shole}: Shear-wave velocity of the bottom of the borehole.
D_{hole}: Depth of the bore hole.
PGA: Peak Ground Acceleration of the surface ground motions used in the research for each station.

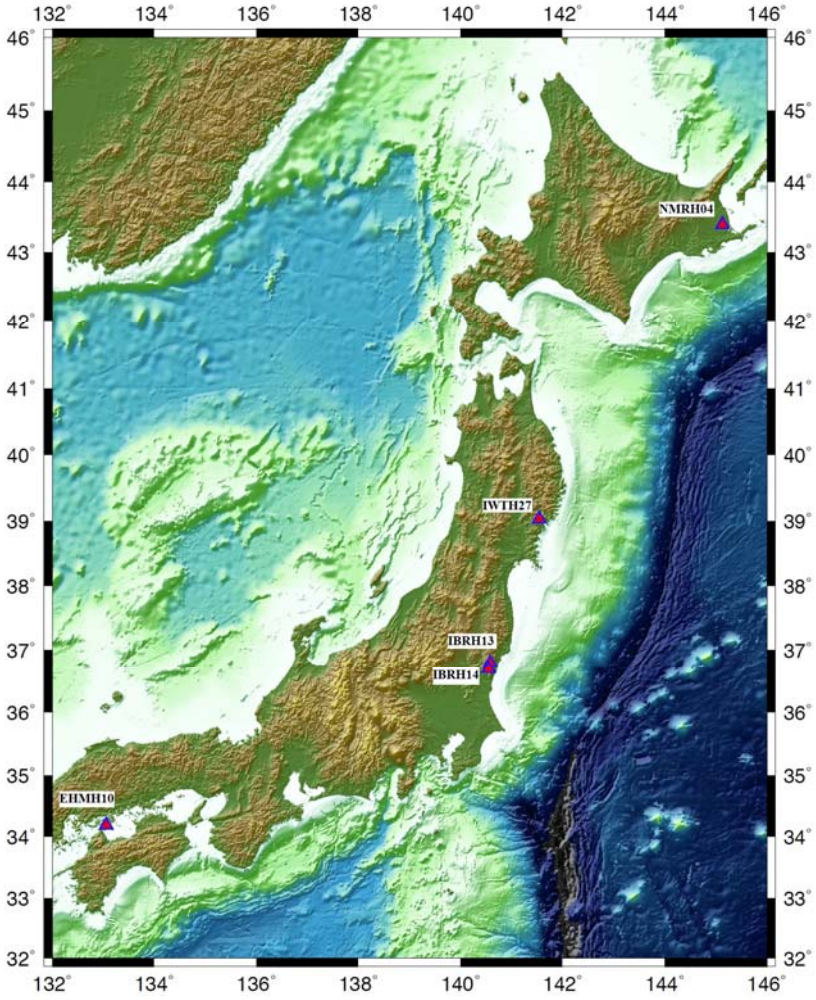

Figure 2-5. Seismic zone of Japan and selected stations for this study.

2.6. Methodology

In this section, we are going to explain our research approach and illustrate the procedure thoroughly using one of the stations under study.

- First, we pick one of the input soil parameters of the equivalent linear SRA. We generate 60 random cases with a specified coefficient of variation based on the procedure explained in Section 2.3. Having these 60 profiles we perform SRA with SHAKE91 using one input ground motion to obtain 60 acceleration spectra on the surface.
- Next we compute the root mean square error (RMSE) between these 60 predicted spectra and the observed acceleration spectrum of the same ground motion for each of 16 periods between 0.1 and 9.5 seconds.
- We repeat this for forty-five different COVs (0.05-0.49) resulting in forty-five RMSE values at each period. Then, we find the minimum of the RMSE values at each period and find the COV associated with that minimum RMSE, COV_{min}.
- Then, we repeat all these procedures with more ground motions. In the case of station IBRH13, for which we have eighty-seven input ground motions, we repeat the procedure eighty-seven times.
- Now we have eighty-seven COV_{min} values for each period that we can process statistically to see which COV provided the best result across different periods.
- We perform these steps for various equivalent linear SRA input parameters such as soil layer thickness, soil shear modulus reduction (G/G_{max}), and damping.
- We also perform the exact same steps for shear-wave velocity, but instead of obtaining COV_{min} we compute the best value for σ_{lnv} introduced in Section 2.3 in the Toro et al. (1993) equations.

In this study, we obtain the most suitable COV for each SRA input parameter individually by randomizing that one parameter, for example the damping curve, while keeping all the other input parameters constant. We also obtain the most suitable COV to use for combinations of input parameters by randomizing both inputs simultaneously using the same COV. The names we assigned for are:

- COV_{Thk}: Coefficient of variation when randomizing just the thickness of each layer.
- $COV_{G/Gmax}$: Coefficient of variation when randomizing just the shear modulus reduction curves.
- COV_{Damp}: Coefficient of variation when randomizing just the damping curves.
- $Sigma_{Vs}$: lognormal standard deviation when randomizing shear-wave velocities based on the Toro et al. (1993) randomization relationships (Equation 2-4).
- COV_{DYN}: Coefficient of variation when randomizing both the shear modulus reduction (G/G_{max}) and damping curves with the same COV.
- $COV_{Profile}$: Coefficient of variation when randomizing both the soil layer shear-wave velocity and thickness with a same value for COV and sigma.

2.6.1 Example Methodology for IBRH13 station

In this part of the study we elaborate on the methodology of the research for just one seismic station, IBRH13. Station IBRH13 is located on layers of weathered granite with an average shear velocity (V_{S30}) of 335 m/s, which is categorized as site class D based on the NEHRP soil classification. The shear-wave profile and the soil properties of the top 100 meters of this station are provided in the KIK-Net database. The shear wave velocity of the bedrock is near 3000 m/s.

Having the shear-wave profile of the station, the depth of bedrock can be found. Having the seismograph at the bottom of the borehole, which is placed at the bedrock level, shows that this station is a suitable candidate to conduct our study of SRA.

A total of 87 earthquake ground motions recorded at this station from 2003 to 2018 are used as ground motion inputs for site response analyses. The earthquake records have magnitudes between 2.3 and 6.0 with epicentral distances between 2 and 249 km, which generate PGAs between 0.1g and 1.08 g on the surface seismograph.

Figure 2-6 and Figure 2-7 show the soil profile, modulus reduction curves, and damping curves of different layers of the IBRH13 station. Considering the soil profile, we can identify 7 distinct layers of soils. Damping and shear modulus reduction values of these layers are computed with the Zhang e al. (2005) models.

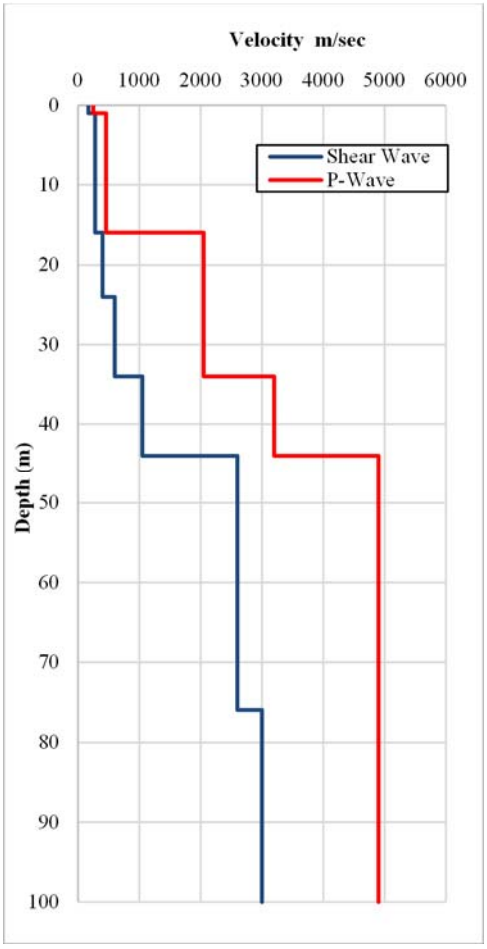

Figure 2-6. Shear wave and P-wave profile of the IBRH13 station.

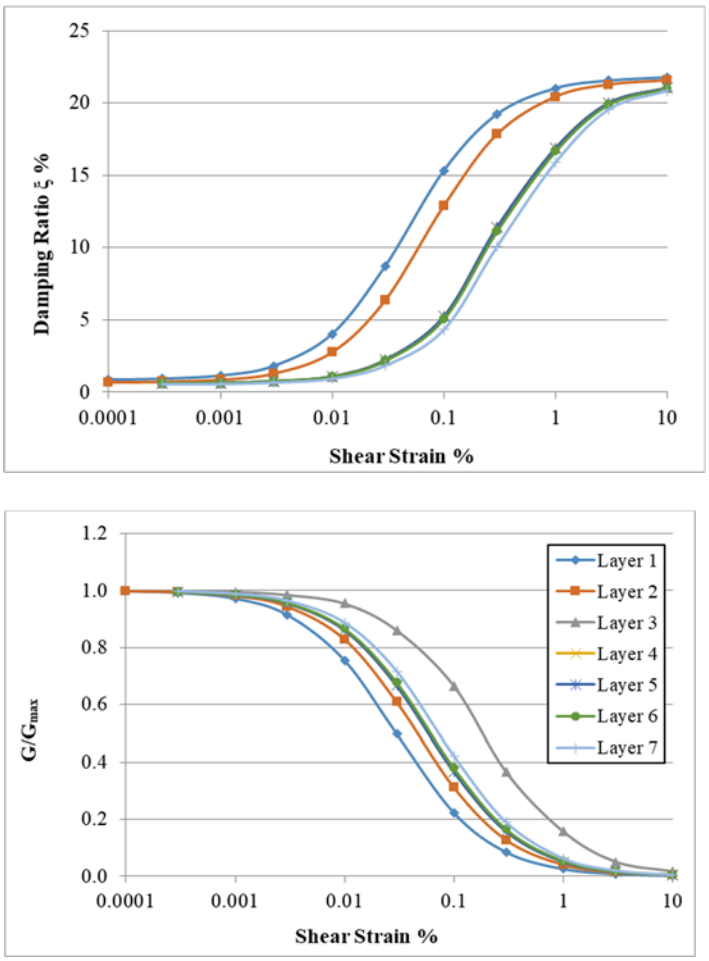

Figure 2-7. (a) Damping and (b) Shear modulus reduction curve of 7 layers of the soil.

As stated earlier, the variability that exists inherently in soil parameters can be accounted for by adding random uncertainties. We take advantage of this randomization for different input parameters in site response analysis models. This means we can generate artificial soil parameters like soil layer shear-wave velocities, shear modulus reduction values and damping ratios from their corresponding base cases. For generating random cases we need to specify a range of variation that is a product of random numbers with a suitable coefficient of variation. The EPRI 2012 report recommends generating at least 30 random cases for each parameter of the soil while performing SRA, while in this study we generate 60 random cases for each parameter.

The observed spectral acceleration on the surface most likely falls between the upper bound and lower bound of the 60 predicted spectral accelerations that resulted from randomization. This is the main justification to use randomization for performing SRA. In most of the cases, the nonlinear site response results fall in the range of results from the EL-SRA random cases; therefore, the need for performing time-consuming sophisticated nonlinear models can be eliminated. Figure 2-8 shows the results of EL-SRA for 60 randomized shear-wave profiles using the computer software SHAKE91 as well as the observed spectral acceleration of the surface ground motion. Also, the spectral acceleration of the surface ground motion obtained by NL-SRA using the computer software DeepSoil is depicted in this figure.

In performing NL-SRA, the same input parameters (shear-wave velocity, G/G_{max} and damping curves) used as inputs for EL-SRA for station IBRH13 (Figure 2-6 and Figure 2-7) are used. P-wave velocities of 1000-2000 m/s are associated with characteristics of saturated soil by several studies, such as the Kaklamanos et al. (2015) study in which they assumed that the groundwater is located where the P-wave velocity first surpasses 1500 m/s. In this study, we use the same assumption in our analysis to find the location of the ground water level. The randomized spectral accelerations shown in Figure 2-8 come from randomizing the IBRH13 station shear-wave profiles using a COV of 0.25 for randomizing soil layers thicknesses and sigma (σ_{lnV}) of 0.25 for randomizing the shear-wave velocity of each layer.

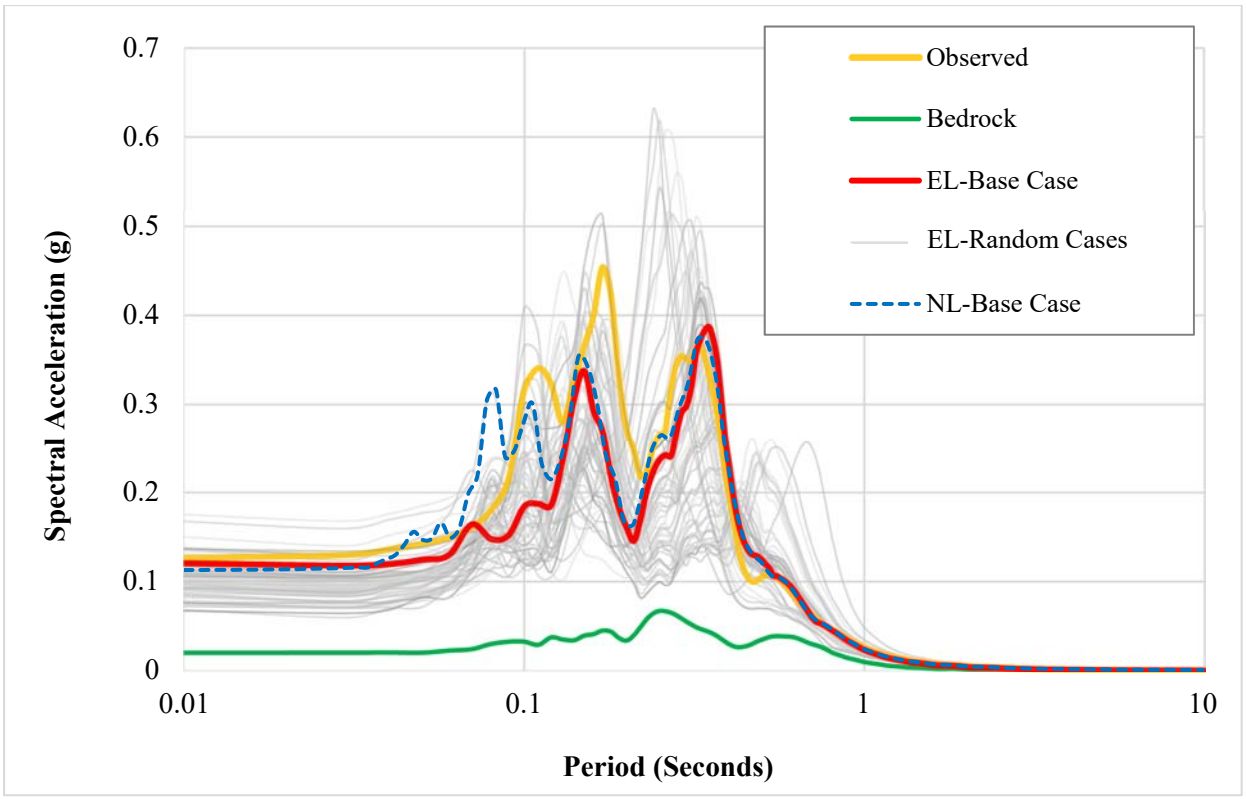

Figure 2-8. Site response results comparison.

Figure 2-8 shows that the observed and the nonlinear spectral acceleration curves fall between the spectral accelerations resulting from SRA using randomized shear-wave profiles. This demonstrates that by defining an appropriate uncertainty bound for different input parameters, we can predict suitable results such that both the observed and the nonlinear SRA spectral accelerations fit within the randomized bound results. These results were obtained using a COV of 0.25 to produce 60 artificial shear-wave profiles. [This means that artificial profiles are generated when we add random uncertainties with coefficient of variations of 0.25 with a normal distribution to layer thickness, and σ_{lnv} of 0.25 to the shear-wave velocity logarithm.] The input earthquake record used in the SRA is from an earthquake with a magnitude of 6.2, an epicentral

distance of 62 km and a depth of 32 km, which resulted in a ground motion record with a peak ground acceleration (PGA) of 0.125g.

In this specific example, we investigate the uncertainties by obtaining the most suitable COV for the shear-wave velocity (COV_{Vs}), and soil layer thicknesses (COV_{Thk}). Also, we find the most suitable COV for the shear-wave profiles (COV_{Pofile}) by randomizing the shear-wave velocity and thickness of the soil layers simultaneously. The coefficients of variation for the shear modulus reduction ($COV_{G/Gmax}$) and damping curves (COV_{Damp}) and their combination (COV_{Dyn}) are studied for each station as well. For this purpose, we generated 60 random base case parameters using the methodologies explained earlier for 45 different coefficients of variability (values from 0.05 to 0.49 with 0.01 increments). We performed SRA for these random cases; then we compared the response spectra of the observed ground motion (real earthquake records at the ground surface) with the predicted response spectra of the ground motions (obtained through EL-SRA).

The geometrical mean of two orthogonal components (East-West and North-South) of the spectral accelerations are obtained by computing the square root of their products. The geometrical mean for the observed spectral acceleration SA_{obs} and all 60 randomly predicted spectral accelerations SA_{pr} in 16 distinct periods for different earthquakes were computed.

There are different procedures to compare the predicted random results with the observed spectral acceleration. In one approach, the logarithmic difference between the average of 60 random SA_{pr} and SA_{obs} values at the period T_i can be calculated (Equation 2-16), while in another approach the root mean of the squared differences of SA_{obs} and each random SA_{pr} at the period T_i can be computed as given in Equation 2-17 below.

$$\sigma_{lnSA} = \ln\left(\frac{\sum_{i=1}^{60}(SA_{pr}^{i})}{60}\right) - \ln\left(SA_{obs}\right) \tag{2-16}$$

$$RMSE = \sqrt{\frac{\sum_{i=1}^{60}(SA_{pr}^{i} - SA_{obs})^{2}}{60}} \tag{2-17}$$

In this study, we use the latter approach to perform the comparison. Table 2-3 provides RMSE values that resulted from randomizing the shear-velocity profiles using one ground motion with a PGA of 0.125g at the IBRH13 station location.

The randomization was performed assuming the correlations that exist between soil layers; therefore, the random shear-wave velocities are generated considering correlation coefficients computed using Equations 2-6 to 2-9 and the correlation parameters of Table 2-1. The station's average shear-wave velocity V_{S30} is equal to 335 m/s, which is a site class D according to the NEHRP classification. Therefore, the shear-wave velocity correlation parameters for the site class D according to Table 2-1 are used.

Table 2-3. RMSE of Observed and Predicted Spectral Acceleration at the Ground Surface for an Event with PGA of 0.125g.

	Period (Seconds)															
COV	0.1	0.25	0.5	0.74	1	1.25	1.5	1.75	2	2.25	2.5	3	4	5	7.4	9.5
0.05	0.1060	0.0325	0.0118	0.0074	0.0024	0.0013	0.0010	0.0008	0.0007	0.0008	0.0008	0.0005	0.0004	0.0004	0.0003	0.0002
0.06	0.1130	0.0344	0.0139	0.0082	0.0026	0.0015	0.0011	0.0008	0.0007	0.0008	0.0008	0.0005	0.0004	0.0004	0.0003	0.0002
0.07	0.1098	0.0368	0.0144	0.0077	0.0027	0.0016	0.0011	0.0008	0.0008	0.0008	0.0008	0.0005	0.0004	0.0004	0.0003	0.0002
0.08	0.1098	0.0424	0.0128	0.0074	0.0026	0.0016	0.0011	0.0008	0.0007	0.0008	0.0007	0.0005	0.0004	0.0004	0.0003	0.0002
0.09	0.1236	0.0449	0.0196	0.0091	0.0031	0.0019	0.0013	0.0010	0.0008	0.0009	0.0008	0.0005	0.0004	0.0004	0.0003	0.0002
0.1	0.1090	0.0425	0.0160	0.0079	0.0029	0.0017	0.0012	0.0009	0.0008	0.0008	0.0008	0.0005	0.0004	0.0004	0.0003	0.0002
0.11	0.1174	0.0538	0.0233	0.0094	0.0034	0.0021	0.0015	0.0011	0.0009	0.0009	0.0008	0.0005	0.0004	0.0004	0.0003	0.0002
0.12	0.1156	0.0709	0.0276	0.0091	0.0036	0.0021	0.0014	0.0010	0.0008	0.0009	0.0008	0.0005	0.0004	0.0004	0.0003	0.0002
0.13	0.1176	0.0527	0.0214	0.0082	0.0030	0.0020	0.0013	0.0010	0.0008	0.0008	0.0008	0.0005	0.0004	0.0004	0.0003	0.0002
0.14	0.1177	0.0776	0.0321	0.0099	0.0038	0.0023	0.0015	0.0011	0.0009	0.0008	0.0008	0.0005	0.0004	0.0004	0.0003	0.0002
0.15	0.1178	0.0733	0.0292	0.0089	0.0031	0.0019	0.0013	0.0009	0.0008	0.0008	0.0008	0.0005	0.0004	0.0004	0.0003	0.0002
0.16	0.1277	0.0776	0.0302	0.0096	0.0037	0.0022	0.0015	0.0011	0.0009	0.0009	0.0008	0.0005	0.0004	0.0004	0.0003	0.0002
0.17	0.1286	0.0709	0.0312	0.0096	0.0033	0.0020	0.0013	0.0010	0.0008	0.0008	0.0008	0.0005	0.0004	0.0004	0.0003	0.0002
0.18	0.1259	0.0705	0.0306	0.0098	0.0035	0.0022	0.0014	0.0010	0.0008	0.0008	0.0007	0.0005	0.0004	0.0004	0.0003	0.0002
0.19	0.1272	0.0898	0.0335	0.0109	0.0039	0.0022	0.0014	0.0010	0.0008	0.0008	0.0007	0.0004	0.0004	0.0004	0.0003	0.0002
0.2	0.1247	0.0850	0.0414	0.0160	0.0043	0.0024	0.0016	0.0011	0.0009	0.0008	0.0008	0.0005	0.0004	0.0004	0.0003	0.0002
0.21	0.1337	0.0860	0.0425	0.0128	0.0038	0.0023	0.0015	0.0011	0.0008	0.0008	0.0007	0.0005	0.0004	0.0004	0.0003	0.0002
0.22	0.1251	0.1108	0.0475	0.0170	0.0051	0.0027	0.0017	0.0012	0.0009	0.0009	0.0008	0.0005	0.0003	0.0004	0.0003	0.0002
0.23	0.1284	0.1095	0.0471	0.0255	0.0065	0.0031	0.0020	0.0014	0.0011	0.0010	0.0009	0.0005	0.0003	0.0004	0.0003	0.0002
0.24	0.1247	0.0964	0.0378	0.0204	0.0049	0.0024	0.0016	0.0011	0.0009	0.0008	0.0008	0.0005	0.0004	0.0004	0.0003	0.0002
0.25	0.1328	0.1236	0.0462	0.0221	0.0058	0.0029	0.0018	0.0013	0.0009	0.0009	0.0008	0.0005	0.0004	0.0004	0.0003	0.0002
0.26	0.1334	0.1001	0.0510	0.0295	0.0070	0.0032	0.0020	0.0014	0.0011	0.0009	0.0008	0.0005	0.0003	0.0003	0.0003	0.0002
0.27	0.1383	0.1048	0.0505	0.0263	0.0065	0.0032	0.0021	0.0015	0.0011	0.0010	0.0009	0.0005	0.0004	0.0004	0.0003	0.0002
0.28	0.1366	0.0998	0.0524	0.0167	0.0048	0.0025	0.0016	0.0012	0.0009	0.0008	0.0008	0.0005	0.0003	0.0004	0.0003	0.0002
0.29	0.1438	0.0922	0.0492	0.0235	0.0061	0.0031	0.0020	0.0014	0.0011	0.0010	0.0008	0.0005	0.0004	0.0004	0.0003	0.0002
0.3	0.1474	0.1532	0.0445	0.0443	0.0090	0.0037	0.0023	0.0017	0.0013	0.0010	0.0009	0.0005	0.0004	0.0003	0.0003	0.0002
0.31	0.1418	0.1267	0.0567	0.0444	0.0090	0.0039	0.0024	0.0017	0.0013	0.0010	0.0008	0.0005	0.0003	0.0003	0.0002	0.0002
0.32	0.1551	0.0940	0.0591	0.0395	0.0085	0.0038	0.0024	0.0016	0.0012	0.0010	0.0009	0.0005	0.0003	0.0003	0.0003	0.0002
0.33	0.1480	0.1145	0.0513	0.0280	0.0066	0.0032	0.0020	0.0015	0.0011	0.0010	0.0008	0.0005	0.0003	0.0003	0.0003	0.0002
0.34	0.1577	0.1239	0.0457	0.0519	0.0104	0.0042	0.0025	0.0018	0.0014	0.0011	0.0009	0.0006	0.0004	0.0003	0.0003	0.0002
0.35	0.1545	0.0895	0.0483	0.0292	0.0075	0.0034	0.0021	0.0014	0.0011	0.0009	0.0008	0.0005	0.0004	0.0003	0.0003	0.0002
0.36	0.1568	0.1065	0.0569	0.0388	0.0094	0.0040	0.0024	0.0017	0.0013	0.0010	0.0009	0.0005	0.0003	0.0003	0.0003	0.0002
0.37	0.1447	0.1055	0.0558	0.0400	0.0078	0.0034	0.0021	0.0014	0.0011	0.0009	0.0008	0.0005	0.0003	0.0003	0.0003	0.0002
0.38	0.1627	0.1310	0.0537	0.0454	0.0108	0.0045	0.0028	0.0019	0.0014	0.0011	0.0009	0.0006	0.0003	0.0003	0.0002	0.0002
0.39	0.1597	0.1678	0.0471	0.0401	0.0097	0.0038	0.0023	0.0016	0.0012	0.0010	0.0009	0.0005	0.0003	0.0003	0.0003	0.0002
0.4	0.1631	0.1247	0.0506	0.0538	0.0116	0.0046	0.0027	0.0018	0.0014	0.0011	0.0009	0.0006	0.0003	0.0003	0.0002	0.0002
0.41	0.1574	0.1423	0.0436	0.0412	0.0088	0.0036	0.0021	0.0015	0.0012	0.0010	0.0008	0.0005	0.0003	0.0003	0.0003	0.0002
0.42	0.1611	0.1293	0.0672	0.0481	0.0107	0.0043	0.0026	0.0018	0.0014	0.0011	0.0009	0.0005	0.0003	0.0003	0.0002	0.0002
0.43	0.1639	0.1412	0.0575	0.0544	0.0113	0.0045	0.0026	0.0018	0.0014	0.0011	0.0009	0.0005	0.0003	0.0003	0.0002	0.0002
0.44	0.1672	0.1099	0.0593	0.0504	0.0111	0.0046	0.0027	0.0018	0.0014	0.0011	0.0009	0.0006	0.0003	0.0003	0.0002	0.0002
0.45	0.1760	0.1358	0.0612	0.0514	0.0102	0.0045	0.0028	0.0019	0.0015	0.0012	0.0010	0.0006	0.0004	0.0003	0.0002	0.0002
0.46	0.1690	0.1376	0.0556	0.0694	0.0142	0.0056	0.0032	0.0022	0.0017	0.0013	0.0010	0.0006	0.0004	0.0003	0.0002	0.0002
0.47	0.1615	0.1574	0.0569	0.0399	0.0111	0.0046	0.0027	0.0018	0.0013	0.0011	0.0009	0.0005	0.0003	0.0003	0.0002	0.0002
0.48	0.1710	0.1250	0.0483	0.0577	0.0135	0.0052	0.0029	0.0019	0.0015	0.0011	0.0009	0.0006	0.0003	0.0003	0.0002	0.0002
0.49	0.1661	0.1326	0.0555	0.0629	0.0126	0.0050	0.0029	0.0020	0.0015	0.0012	0.0009	0.0006	0.0003	0.0003	0.0002	0.0002
COV_{min}	**0.18**	**0.24**	**0.02**	**0.26**	**0.34**	**0.34**	**0.34**	**0.34**	**0.34**	**0.22**	**0.22**	**0.22**	**0.22**	**0.24**	**0.24**	**0.24**

The COV for which the minimum RMSE occurs at each period is also provided in Table 2-3. For example, as is indicated in Table 2-3, the minimum RMSE at a period of 0.1 second is 0.1259, which occurs when a COV of 0.18 is used. This is done for all 16 periods. The last row of Table 2-3 shows the COV_{min} for all periods. The results shown in Table 2-3 were obtained for one ground motion. To reduce the uncertainties that exist in different earthquake records, we follow this procedure for all 87 available ground motions. The COV_{min} for 16 different periods using 87 ground motions at site IBRH13 are provided in Table 2-4. By assessing these coefficients statistically, we can determine a COV_{min} to use when we are randomizing the shear-wave profiles (randomizing thicknesses and shear-wave velocities simultaneously).

Table 2-4. COV_{min} for 87 Ground Motions at 16 periods Considering Randomization of Shear-Wave Profiles.

Ground Motion	Period (Seconds)															
	0.1	0.25	0.5	0.74	1	1.25	1.5	1.75	2	2.25	2.5	3	4	5	7.4	9.5
1	0.08	0.14	0.08	0.08	0.08	0.24	0.37	0.37	0.37	0.37	0.48	0.44	0.44	0.44	0.24	0.24
2	0.05	0.32	0.24	0.22	0.37	0.37	0.38	0.46	0.46	0.46	0.46	0.46	0.47	0.47	0.47	0.47
3	0.05	0.11	0.08	0.21	0.24	0.48	0.48	0.48	0.48	0.48	0.48	0.48	0.48	0.48	0.14	0.24
4	0.07	0.16	0.05	0.05	0.08	0.05	0.05	0.08	0.08	0.08	0.05	0.05	0.05	0.08	0.06	0.12
5	0.14	0.12	0.05	0.05	0.05	0.05	0.08	0.21	0.08	0.05	0.21	0.22	0.28	0.06	0.22	0.16
6	0.23	0.23	0.44	0.48	0.47	0.48	0.48	0.48	0.48	0.48	0.48	0.48	0.48	0.48	0.49	0.48
7	0.05	0.05	0.05	0.08	0.05	0.05	0.05	0.05	0.05	0.08	0.08	0.19	0.43	0.48	0.44	0.48
8	0.19	0.14	0.05	0.08	0.08	0.21	0.08	0.08	0.08	0.41	0.41	0.41	0.41	0.41	0.41	0.42
9	0.05	0.07	0.07	0.05	0.05	0.07	0.09	0.05	0.11	0.11	0.11	0.06	0.05	0.44	0.48	0.43
10	0.08	0.09	0.08	0.13	0.14	0.42	0.42	0.47	0.43	0.08	0.24	0.08	0.23	0.42	0.47	0.05
11	0.06	0.09	0.08	0.08	0.05	0.18	0.41	0.23	0.11	0.05	0.11	0.29	0.09	0.11	0.22	0.08
12	0.05	0.14	0.21	0.21	0.48	0.48	0.37	0.05	0.05	0.05	0.05	0.05	0.14	0.14	0.14	0.05
13	0.22	0.47	0.44	0.46	0.05	0.05	0.05	0.24	0.24	0.24	0.24	0.07	0.07	0.24	0.24	0.24
14	0.05	0.09	0.3	0.28	0.28	0.49	0.42	0.38	0.38	0.42	0.38	0.49	0.49	0.49	0.49	0.49
15	0.05	0.05	0.08	0.08	0.05	0.05	0.05	0.08	0.08	0.13	0.33	0.44	0.48	0.44	0.42	0.42
16	0.05	0.05	0.08	0.08	0.44	0.21	0.44	0.08	0.44	0.44	0.05	0.05	0.22	0.05	0.11	0.05
17	0.15	0.46	0.44	0.48	0.47	0.47	0.47	0.47	0.47	0.47	0.47	0.47	0.47	0.36	0.44	0.36
18	0.05	0.09	0.24	0.21	0.05	0.05	0.37	0.46	0.28	0.24	0.28	0.28	0.07	0.1	0.07	0.05
19	0.05	0.06	0.16	0.21	0.05	0.21	0.28	0.06	0.06	0.22	0.22	0.22	0.22	0.44	0.05	0.47
20	0.05	0.05	0.08	0.08	0.05	0.08	0.08	0.21	0.21	0.21	0.08	0.06	0.08	0.06	0.48	0.48
21	0.05	0.05	0.08	0.05	0.06	0.05	0.05	0.25	0.05	0.05	0.05	0.49	0.49	0.48	0.47	0.47
22	0.05	0.14	0.05	0.21	0.21	0.05	0.48	0.48	0.41	0.41	0.41	0.41	0.05	0.05	0.05	0.46
23	0.05	0.23	0.24	0.46	0.41	0.41	0.41	0.41	0.41	0.41	0.4	0.24	0.24	0.24	0.14	0.14
24	0.05	0.23	0.08	0.48	0.4	0.24	0.24	0.24	0.24	0.24	0.24	0.24	0.24	0.14	0.14	0.14
25	0.22	0.23	0.08	0.21	0.48	0.42	0.48	0.48	0.48	0.48	0.48	0.48	0.48	0.44	0.44	0.41
26	0.05	0.23	0.24	0.48	0.05	0.07	0.07	0.24	0.24	0.24	0.24	0.24	0.24	0.24	0.24	0.24
27	0.05	0.3	0.3	0.3	0.46	0.46	0.3	0.24	0.24	0.4	0.05	0.05	0.05	0.05	0.05	0.3
28	0.08	0.09	0.05	0.14	0.05	0.05	0.2	0.26	0.48	0.48	0.48	0.48	0.48	0.48	0.48	0.48
29	0.05	0.23	0.21	0.44	0.48	0.48	0.41	0.41	0.41	0.41	0.41	0.41	0.41	0.05	0.05	0.05
30	0.22	0.23	0.3	0.21	0.48	0.48	0.48	0.05	0.05	0.05	0.05	0.05	0.05	0.14	0.14	0.14
31	0.22	0.23	0.08	0.26	0.48	0.24	0.24	0.24	0.24	0.24	0.24	0.24	0.24	0.24	0.24	0.24
32	0.22	0.11	0.08	0.16	0.23	0.24	0.24	0.24	0.24	0.24	0.24	0.14	0.14	0.14	0.14	0.33
33	0.05	0.11	0.24	0.48	0.24	0.06	0.06	0.06	0.06	0.24	0.06	0.24	0.07	0.24	0.24	0.14
34	0.15	0.23	0.24	0.48	0.48	0.24	0.24	0.24	0.24	0.24	0.24	0.24	0.24	0.24	0.24	0.24
35	0.23	0.23	0.24	0.21	0.37	0.48	0.48	0.05	0.05	0.05	0.05	0.05	0.05	0.07	0.07	0.14
36	0.05	0.06	0.05	0.21	0.21	0.21	0.05	0.06	0.05	0.05	0.06	0.05	0.06	0.46	0.06	0.05
37	0.05	0.23	0.08	0.14	0.21	0.05	0.05	0.05	0.14	0.14	0.07	0.07	0.14	0.14	0.14	0.14
38	0.06	0.05	0.08	0.21	0.21	0.05	0.08	0.08	0.05	0.05	0.05	0.08	0.21	0.21	0.21	0.42
39	0.15	0.14	0.05	0.15	0.37	0.49	0.49	0.49	0.49	0.49	0.49	0.46	0.49	0.24	0.14	0.14
40	0.05	0.41	0.21	0.21	0.37	0.24	0.24	0.24	0.24	0.24	0.24	0.05	0.24	0.05	0.05	0.05
41	0.06	0.23	0.08	0.21	0.48	0.48	0.48	0.48	0.48	0.48	0.48	0.48	0.48	0.48	0.24	0.24
42	0.06	0.23	0.41	0.24	0.41	0.41	0.41	0.41	0.41	0.41	0.41	0.41	0.41	0.41	0.41	0.41
43	0.05	0.28	0.09	0.05	0.28	0.05	0.08	0.37	0.05	0.42	0.48	0.46	0.47	0.48	0.48	0.48
44	0.22	0.23	0.24	0.38	0.24	0.24	0.24	0.24	0.24	0.24	0.24	0.24	0.24	0.24	0.24	0.24
45	0.05	0.41	0.24	0.46	0.41	0.24	0.24	0.24	0.24	0.24	0.24	0.24	0.24	0.24	0.28	0.28
46	0.08	0.05	0.08	0.05	0.05	0.05	0.05	0.05	0.42	0.38	0.38	0.42	0.05	0.42	0.38	0.38
47	0.05	0.09	0.05	0.05	0.05	0.05	0.21	0.37	0.37	0.41	0.41	0.41	0.41	0.41	0.41	0.41
48	0.05	0.28	0.08	0.08	0.44	0.42	0.48	0.48	0.24	0.24	0.24	0.24	0.24	0.24	0.49	0.38
49	0.22	0.23	0.24	0.08	0.2	0.28	0.28	0.28	0.24	0.24	0.24	0.24	0.24	0.24	0.14	0.14
50	0.05	0.05	0.05	0.05	0.08	0.08	0.08	0.05	0.08	0.41	0.41	0.41	0.41	0.41	0.05	0.05
51	0.06	0.23	0.21	0.47	0.41	0.41	0.24	0.24	0.24	0.24	0.24	0.24	0.24	0.28	0.14	0.14
52	0.22	0.05	0.08	0.16	0.21	0.21	0.3	0.48	0.48	0.48	0.48	0.48	0.48	0.48	0.48	0.41
53	0.05	0.28	0.05	0.37	0.24	0.05	0.08	0.24	0.24	0.24	0.24	0.05	0.05	0.05	0.05	0.24
54	0.07	0.23	0.37	0.48	0.48	0.24	0.24	0.24	0.24	0.24	0.24	0.24	0.24	0.24	0.14	0.14
55	0.05	0.23	0.24	0.44	0.48	0.48	0.05	0.05	0.06	0.05	0.08	0.06	0.24	0.24	0.14	0.14
56	0.05	0.23	0.3	0.48	0.05	0.05	0.05	0.05	0.05	0.05	0.05	0.07	0.07	0.24	0.24	0.24

Table 2-4. (Continued)

Ground Motion	Period (Seconds) 0.1	0.25	0.5	0.74	1	1.25	1.5	1.75	2	2.25	2.5	3	4	5	7.4	9.5
57	0.06	0.23	0.05	0.49	0.05	0.05	0.05	0.05	0.05	0.05	0.05	0.05	0.24	0.24	0.24	0.24
58	0.22	0.28	0.06	0.3	0.38	0.38	0.38	0.38	0.38	0.26	0.26	0.26	0.26	0.28	0.28	0.28
59	0.05	0.14	0.08	0.21	0.37	0.37	0.24	0.24	0.24	0.42	0.41	0.41	0.41	0.41	0.41	0.36
60	0.05	0.14	0.24	0.23	0.41	0.41	0.41	0.41	0.41	0.41	0.41	0.41	0.28	0.14	0.14	0.14
61	0.05	0.05	0.05	0.07	0.05	0.05	0.05	0.05	0.05	0.05	0.05	0.06	0.05	0.06	0.23	0.47
62	0.05	0.23	0.24	0.48	0.24	0.24	0.14	0.14	0.14	0.14	0.14	0.14	0.14	0.14	0.14	0.14
63	0.14	0.11	0.08	0.08	0.19	0.21	0.21	0.48	0.37	0.37	0.22	0.28	0.48	0.3	0.05	0.05
64	0.05	0.05	0.24	0.05	0.21	0.33	0.31	0.48	0.48	0.48	0.48	0.43	0.43	0.14	0.14	0.14
65	0.05	0.46	0.21	0.38	0.46	0.24	0.24	0.24	0.24	0.24	0.24	0.24	0.24	0.14	0.14	0.14
66	0.05	0.09	0.08	0.21	0.24	0.08	0.08	0.08	0.08	0.19	0.08	0.05	0.08	0.08	0.14	0.14
67	0.05	0.05	0.13	0.22	0.22	0.31	0.48	0.48	0.47	0.47	0.47	0.47	0.47	0.24	0.14	0.14
68	0.13	0.05	0.24	0.48	0.36	0.22	0.22	0.22	0.22	0.22	0.24	0.24	0.24	0.24	0.14	0.24
69	0.05	0.05	0.05	0.08	0.05	0.08	0.08	0.44	0.08	0.05	0.05	0.05	0.24	0.24	0.24	0.14
70	0.07	0.08	0.17	0.18	0.14	0.18	0.13	0.08	0.08	0.07	0.05	0.05	0.05	0.05	0.05	0.07
71	0.22	0.09	0.08	0.28	0.48	0.48	0.41	0.41	0.41	0.41	0.41	0.41	0.41	0.41	0.41	0.24
72	0.05	0.05	0.08	0.21	0.37	0.48	0.48	0.48	0.14	0.14	0.14	0.08	0.08	0.37	0.19	0.14
73	0.08	0.06	0.08	0.08	0.21	0.21	0.13	0.48	0.48	0.48	0.48	0.48	0.48	0.48	0.48	0.31
74	0.05	0.05	0.06	0.2	0.05	0.14	0.14	0.14	0.14	0.28	0.28	0.28	0.28	0.28	0.24	0.24
75	0.1	0.16	0.05	0.05	0.05	0.21	0.05	0.05	0.05	0.05	0.08	0.21	0.05	0.45	0.05	0.08
76	0.05	0.08	0.06	0.06	0.05	0.1	0.06	0.06	0.06	0.05	0.05	0.05	0.05	0.05	0.05	0.05
77	0.22	0.46	0.44	0.48	0.24	0.24	0.22	0.24	0.24	0.24	0.24	0.24	0.24	0.24	0.24	0.24
78	0.05	0.05	0.05	0.05	0.05	0.05	0.14	0.14	0.14	0.14	0.14	0.14	0.14	0.14	0.14	0.14
79	0.05	0.24	0.05	0.21	0.44	0.48	0.48	0.48	0.37	0.37	0.47	0.47	0.48	0.24	0.24	0.24
80	0.05	0.09	0.08	0.21	0.21	0.21	0.21	0.24	0.21	0.18	0.21	0.21	0.05	0.05	0.05	0.05
81	0.05	0.1	0.08	0.21	0.21	0.21	0.37	0.48	0.48	0.48	0.48	0.48	0.48	0.44	0.28	0.28
82	0.08	0.09	0.06	0.48	0.24	0.24	0.24	0.24	0.24	0.24	0.24	0.24	0.24	0.24	0.24	0.14
83	0.05	0.09	0.05	0.1	0.07	0.05	0.09	0.09	0.09	0.06	0.06	0.06	0.41	0.47	0.34	0.34
84	0.06	0.11	0.13	0.2	0.48	0.24	0.24	0.08	0.08	0.08	0.08	0.08	0.08	0.05	0.05	0.05
85	0.05	0.09	0.08	0.08	0.21	0.48	0.48	0.41	0.24	0.24	0.41	0.41	0.41	0.24	0.28	0.28
86	0.05	0.28	0.21	0.42	0.46	0.46	0.46	0.41	0.41	0.41	0.3	0.3	0.3	0.05	0.05	0.05
87	0.13	0.06	0.08	0.28	0.44	0.44	0.44	0.44	0.44	0.44	0.44	0.44	0.24	0.4	0.4	0.4

2.7. Results

2.7.1. IBRH13 Seismic Station

There are different ways to analyze the COV_{min} values provided in Table 2-4. We used a frequency distribution procedure to statistically analyze the data. We divided the 45 possible COV values into nine bins and determined how many ground motions fell within each bin. Table 2-5 is a frequency distribution table of COV_{min} values when randomizing the shear-wave profile. To make it easier to read we added color intensities to this table; the higher the number of ground motions in each COV bin, the darker green the color.

Table 2-5. Frequency distribution of COV_{min} of 87 ground motions for the **shear-wave profile** randomization.

Bin	Bin	Period (seconds)															
Start	End	0.1	0.25	0.5	0.74	1	1.25	1.5	1.75	2	2.25	2.5	3	4	5	7.4	9.5
0.05	0.09	65	36	52	26	27	27	27	26	26	21	24	26	23	17	18	16
0.10	0.14	5	14	2	4	2	2	5	3	7	6	5	3	5	12	21	22
0.15	0.19	4	2	2	4	1	2	0	0	0	2	0	1	0	0	1	1
0.20	0.24	13	22	21	24	21	25	19	22	23	23	23	20	24	23	19	16
0.25	0.29	0	5	0	4	2	1	2	3	1	2	3	5	4	3	4	4
0.30	0.34	0	2	4	2	0	2	3	0	0	0	2	1	1	1	1	4
0.35	0.39	0	0	1	3	8	3	6	5	6	4	2	0	0	2	1	4
0.40	0.44	0	2	5	3	10	8	10	9	11	16	12	15	12	15	10	9
0.45	0.49	0	4	0	17	16	17	15	19	13	13	16	16	18	14	12	11

As seen in Table 2-5, 65 of the 87 ground motions have COV_{min} values between 0.05 and at period of 0.1 second. This is a high percentage of the ground motions we investigated for this site. Also, For the other periods, a large number of ground motions also have COV_{min} values lower than 0.09. This means that the shear-wave profile for those ground motions does not need to be randomized because the observed response acceleration spectrum on the surface matches closely

to the response spectrum obtained using SRA. This can have two explanations; One is that the base case shear-wave profile we used to perform the SRA in this study is close to reality and does not contain much uncertainty. Another is that, the shear-wave profile might have been obtained by inverse methods that use observed ground motion records to estimate shear-wave profiles. In that case, the base case profile reproduces the average of the ground motions from which it was derived. In this research we are trying to find a proper coefficient of variation to use when the base case does not produce the observed result. Therefore, it can be reasonable to ignore the ground motions that produced the low COVs and investigate the ground motions that have higher COV_{min} values. We modified Table 2-5 by omitting the row with the 0.05 to 0.09 bin. The results are provided in Table 2-6.

Table 2-6. Modified frequency distribution of COV_{min} of 87 ground motions for the **shear-wave profile** randomization.

Bin	Bin	Period (seconds)															
Start	End	0.1	0.25	0.5	0.74	1	1.25	1.5	1.75	2	2.25	2.5	3	4	5	7.4	9.5
0.05	0.09																
0.10	0.14	5	14	2	4	2	2	5	3	7	6	5	3	5	12	21	22
0.15	0.19	4	2	2	4	1	2	0	0	0	2	0	1	0	0	1	1
0.20	0.24	13	22	21	24	21	25	19	22	23	23	23	20	24	23	19	16
0.25	0.29	0	5	0	4	2	1	2	3	1	2	3	5	4	3	4	4
0.30	0.34	0	2	4	2	0	2	3	0	0	0	2	1	1	1	1	4
0.35	0.39	0	0	1	3	8	3	6	5	6	4	2	0	0	2	1	4
0.40	0.44	0	2	5	3	10	8	10	9	11	16	12	15	12	15	10	9
0.45	0.49	0	4	0	17	16	17	15	19	13	13	16	16	18	14	12	11

Omitting the first row of Table 2-5, which is associated with the ground motions that have the lowest coefficient of variations means we are omitting the ground motions that somehow produce matched results to the observed response spectrum, and we investigate the variabilities in

other ground motions that produce uncertain results. Most ground motions in Table 2-6 have their COV_{min} in the ranges of 0.20 to 0.24 and 0.40 to 0.49. Considering Table 2-6, we may conclude that there is no single COV for randomizing a given shear-wave profile across all periods for all ground motions.

Following the same procedure, we obtained $sigma_{min}$, $COV_{G/Gmax}$, COV_{Damp}, COV_{DYN}, and COV_{THK} and provide the results in Tables 2-7 to 2-11. The $sigma_{min}$ values provided in Table 2-7 are the same as the σ_{lnv} defined in Section 2.3. These are the standard deviation in natural logarithm of shear-wave velocity of soil layers in which the RMSE is minimum. The results are similar to those obtained for $COV_{Profile}$.

Table 2-10 provides COV_{THK} values. Interestingly, COV_{THK} shows a strong frequency in the range of 0.45 to 0.49 for all periods. $COV_{G/Gmax}$ (COV of shear modulus reduction curves) are provided in Table 2-9 and has the most frequencies in the range of 0.3 to 0.34. The COV_{Damp} results are provided in Table 2-10; the optimal values fall with the range of 0.35 to 0.39. Also, as it is provided in Table 2-11, COV_{DYN} has a dominant value within the range of 0.35 to 0.39.

Table 2-7. Modified frequency distribution of $Sigma_{min}$ of 87 ground motions for the **shear-wave velocity** randomization.

Bin	Bin	Period (Seconds)															
Start	End	0.1	0.25	0.5	0.74	1	1.25	1.5	1.75	2	2.25	2.5	3	4	5	7.4	9.5
0.05	0.09																
0.10	0.14	14	27	8	1	3	0	3	4	8	3	1	1	3	1	1	5
0.15	0.19	0	1	2	1	0	1	1	0	1	3	5	6	5	10	9	9
0.20	0.24	23	1	23	21	15	19	17	19	20	19	18	10	13	11	13	10
0.25	0.29	2	10	2	4	3	2	6	7	9	9	9	9	6	6	3	5
0.30	0.34	0	0	3	6	4	5	2	4	1	3	3	3	0	0	0	0
0.35	0.39	0	1	6	6	5	6	4	6	3	3	1	2	1	0	1	0
0.40	0.44	0	4	7	10	11	8	17	14	12	12	17	14	17	20	23	17
0.45	0.49	0	15	1	22	24	22	19	16	18	16	14	16	20	19	13	14

Table 2-8. Modified frequency distribution of COV_{min} of 87 ground motions for the soil layers **thickness** randomization.

Bin	Bin	Period (seconds)															
Start	End	0.1	0.25	0.5	0.74	1	1.25	1.5	1.75	2	2.25	2.5	3	4	5	7.4	9.5
0.05	0.09																
0.10	0.14	3	20	10	11	9	5	9	7	11	9	9	4	4	4	1	5
0.15	0.19	1	1	10	3	6	2	4	4	4	5	2	4	3	2	2	3
0.20	0.24	20	15	1	3	2	4	1	6	8	5	6	6	8	9	7	6
0.25	0.29	0	3	7	6	5	6	2	1	0	2	1	1	2	2	1	0
0.30	0.34	0	0	1	3	2	0	0	0	0	0	1	1	2	3	3	4
0.35	0.39	1	0	0	1	1	1	0	1	0	0	0	2	0	0	0	1
0.40	0.44	12	22	2	7	15	9	18	19	21	19	17	17	11	13	8	10
0.45	0.49	0	7	7	23	21	30	25	23	21	25	27	25	29	30	40	37

Table 2-9. Modified frequency distribution of COV_{min} of 87 ground motions for the **shear modulus reduction (G/G_{max}) curve** randomization.

Bin	Bin	Period (seconds)															
Start	End	0.1	0.25	0.5	0.74	1	1.25	1.5	1.75	2	2.25	2.5	3	4	5	7.4	9.5
0.05	0.09																
0.10	0.14	4	6	6	4	6	7	6	7	4	8	8	15	9	9	15	18
0.15	0.19	0	2	1	1	0	1	1	0	0	0	0	1	0	2	0	1
0.20	0.24	6	2	8	2	1	0	3	4	6	4	3	4	3	2	8	7
0.25	0.29	0	0	1	0	0	0	0	1	0	0	1	0	2	2	3	4
0.30	0.34	26	8	37	26	32	26	25	23	27	28	22	17	19	25	17	17
0.35	0.39	0	11	0	1	1	2	2	2	1	1	1	1	1	3	7	9
0.40	0.44	10	9	8	16	16	13	15	13	11	15	17	14	15	8	6	5
0.45	0.49	12	8	10	18	9	20	18	19	20	15	20	18	23	16	15	13

Table 2-10. Modified frequency distribution of COV_{min} of 87 ground motions for the **damping curves** randomization.

Bin	Bin	Period (seconds)															
Start	End	0.1	0.25	0.5	0.74	1	1.25	1.5	1.75	2	2.25	2.5	3	4	5	7.4	9.5
0.05	0.09																
0.10	0.14	1	1	1	2	1	1	1	1	1	1	1	1	3	2	2	2
0.15	0.19	1	0	1	0	1	0	0	2	2	5	2	2	0	2	4	3
0.20	0.24	3	3	2	2	5	9	9	4	7	10	8	7	5	8	7	4
0.25	0.29	0	0	0	0	0	0	0	0	0	0	0	0	3	1	1	0
0.30	0.34	0	0	0	1	0	0	0	0	0	0	0	0	0	0	1	2
0.35	0.39	40	50	45	52	58	53	54	56	56	54	58	57	59	56	56	53
0.40	0.44	0	0	0	0	0	0	0	0	0	0	0	0	1	1	2	2
0.45	0.49	0	4	1	0	1	3	2	1	1	2	1	2	2	5	6	12

Table 2-11. Modified frequency distribution of COV_{min} of 87 ground motions for the **dynamic property** randomization.

Bin	Bin	Period (seconds)															
Start	End	0.1	0.25	0.5	0.74	1	1.25	1.5	1.75	2	2.25	2.5	3	4	5	7.4	9.5
0.05	0.09																
0.10	0.14	0	0	2	2	2	2	3	3	1	0	0	1	2	3	5	7
0.15	0.19	2	1	2	0	0	1	1	1	2	1	0	2	1	1	1	1
0.20	0.24	4	4	19	11	12	12	11	12	9	11	9	7	9	6	6	6
0.25	0.29	0	0	0	1	0	1	1		0	0	1	1	0	0	1	1
0.30	0.34	2	0	7	7	3	4	1	2	2	2	5	4	7	8	9	8
0.35	0.39	35	47	27	42	47	45	52	51	54	53	49	52	51	50	51	51
0.40	0.44	2	2	0	0	0	0	0	1	3	3	4	5	3	5	0	1
0.45	0.49	2	4	1	0	0	2	2	2	3	4	3	2	6	7	6	7

2.7.2. Other Stations

Now that we have elaborated on how the uncertainty investigation was done for the IBRH13 station with a site class D, we discuss uncertainties of other site classes by investigating the rest of the stations introduced in Table 2-2. The shear-wave profiles of the stations with site classes B (IBRH14), C(IWTH27), and D (IBRH13) are shown in Figure 2-9. As shown in Figure 2-9, the station IBH14 and IWTH27 profiles corresponding to B and C site classes are investigated. The shear-wave profile of the NMRH04 station corresponds to a site class E and is very different compared to the other stations.

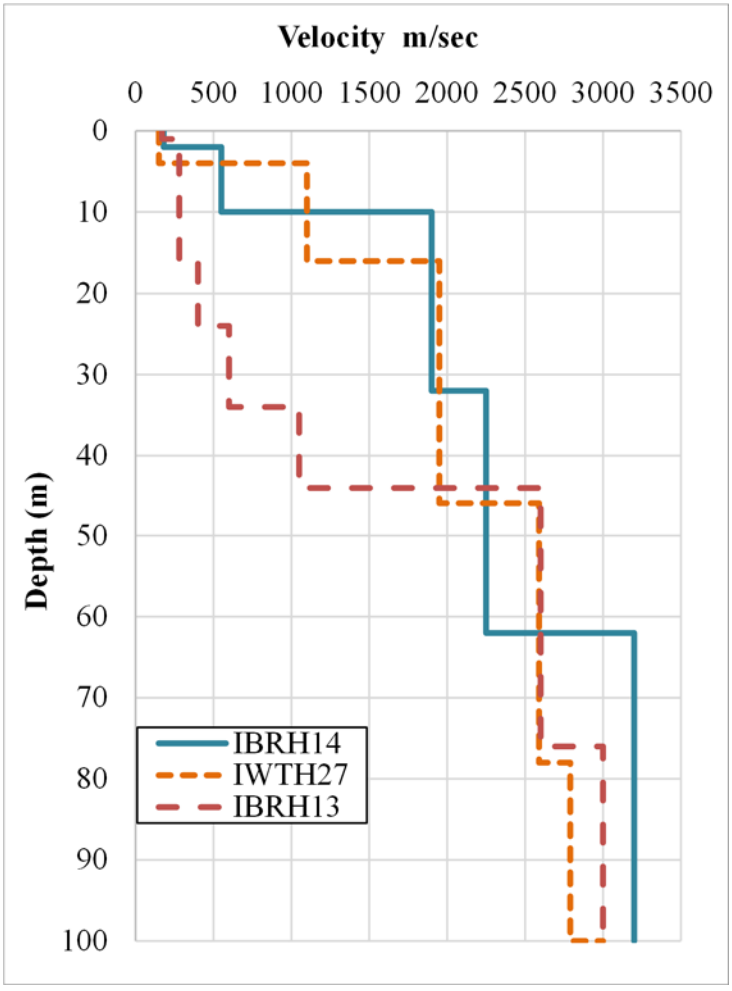

Figure 2-9. Seismic stations' shear-wave profiles.

2.7.2.1. IBRH14 Station

This station is located on a site class B soil. 137 ground motions with PGAs greater than 0.05g are used to find the most suitable COV for different SRA input parameters. The number and intensities of this set of ground motions are suitable to perform this research. The same method used in the previous section for station IBRH13 is conducted for the IBRH14 station. The frequency distribution of ground motions that have COV_{min} in different ranges at different periods are shown in Tables 2-12 to 2-17.

Table 2-12. Modified frequency distribution of COV_{min} of 137 ground motions for the **shear-wave** profile randomization.

Bin	Bin	Period (seconds)															
Start	End	0.1	0.25	0.5	0.74	1	1.25	1.5	1.75	2	2.25	2.5	3	4	5	7.4	9.5
0.05	0.09																
0.10	0.14	12	6	9	10	7	13	14	9	12	10	12	8	8	10	14	19
0.15	0.19	12	3	14	19	18	17	18	19	11	11	7	9	4	2	1	1
0.20	0.24	0	0	1	2	3	3	5	3	2	3	2	2	5	4	2	2
0.25	0.29	1	0	4	6	12	13	22	33	32	35	34	28	24	27	18	16
0.30	0.34	0	0	1	1	1	2	2	1	4	3	4	4	7	9	11	15
0.35	0.39	2	0	2	1	1	3	5	2	6	6	5	5	5	3	2	6
0.40	0.44	1	0	0	1	1	2	1	0	0	1	0	1	6	11	19	16
0.45	0.49	0	5	5	4	3	3	6	12	16	18	25	37	40	37	32	22

Table 2-13. Modified frequency distribution of $Sigma_{min}$ of 137 ground motions for the **shear-wave velocity** randomization.

Bin	Bin	Period (seconds)															
Start	End	0.1	0.25	0.5	0.74	1	1.25	1.5	1.75	2	2.25	2.5	3	4	5	7.4	9.5
0.05	0.09																
0.10	0.14	11	16	14	15	20	20	20	10	12	12	13	14	7	10	10	13
0.15	0.19	8	12	12	21	14	14	12	8	4	2	4	1	1	2	1	2
0.20	0.24	1	0	7	4	6	5	4	6	3	4	5	2	0	1	1	1
0.25	0.29	4	0	5	5	9	4	7	6	10	12	9	14	9	13	14	25
0.30	0.34	0	0	3	3	8	10	10	14	16	10	7	9	6	8	2	5
0.35	0.39	0	0	1	4	4	10	10	13	15	18	18	25	25	20	23	21
0.40	0.44	4	0	0	0	0	1	8	7	6	3	3	6	18	16	24	20
0.45	0.49	0	5	5	5	6	7	13	16	18	27	33	29	28	25	14	12

Table 2-14. Modified frequency distribution of COV_{min} of 137 ground motions for the **thickness** randomization.

Bin	Bin	Period (seconds)															
Start	End	0.1	0.25	0.5	0.74	1	1.25	1.5	1.75	2	2.25	2.5	3	4	5	7.4	9.5
0.05	0.09																
0.10	0.14	26	12	11	14	10	17	8	4	9	8	8	7	12	7	4	2
0.15	0.19	10	6	10	10	8	9	11	7	5	11	10	8	5	5	4	2
0.20	0.24	3	5	7	3	5	7	5	4	5	5	2	5	3	3	2	2
0.25	0.29	23	6	14	7	14	15	24	34	37	41	48	50	54	54	38	28
0.30	0.34	0	1	2	4	7	2	3	1	3	3	2	3	2	2	1	1
0.35	0.39	4	1	4	5	4	11	11	11	12	11	7	5	2	2	5	6
0.40	0.44	0	0	3	6	4	5	4	5	6	6	5	6	4	4	13	14
0.45	0.49	7	4	4	8	6	9	10	15	10	9	10	12	12	14	16	14

Table 2-15. Modified frequency distribution of COV_{min} of 137 ground motions for **shear modulus reduction (G/G_{max}) curve** randomization.

Bin	Bin	Period (seconds)															
Start	End	0.1	0.25	0.5	0.74	1	1.25	1.5	1.75	2	2.25	2.5	3	4	5	7.4	9.5
0.05	0.09																
0.10	0.14	10	12	7	11	9	7	6	6	7	5	3	7	9	9	15	13
0.15	0.19	9	16	10	14	8	5	7	5	3	1	2	1	0	1	1	2
0.20	0.24	17	4	14	5	5	5	5	7	7	2	5	2	5	7	9	13
0.25	0.29	7	2	5	2	2	6	2	1	1	4	3	2	4	3	4	4
0.30	0.34	26	16	9	14	14	6	9	1	4	3	3	5	4	4	12	15
0.35	0.39	6	3	6	3	2	5	3	4	6	6	6	5	8	7	9	5
0.40	0.44	16	1	11	16	17	24	23	25	26	28	27	25	28	31	34	22
0.45	0.49	13	8	15	18	27	34	46	56	54	59	63	65	59	53	25	30

Table 2-16. Modified frequency distribution of COV_{min} of 137 ground motions for the **damping curve** randomization.

Bin	Bin	Period (seconds)															
Start	End	0.1	0.25	0.5	0.74	1	1.25	1.5	1.75	2	2.25	2.5	3	4	5	7.4	9.5
0.05	0.09																
0.10	0.14	63	33	39	38	38	28	22	17	16	14	9	3	3	1	2	4
0.15	0.19	8	6	6	7	4	7	5	9	5	9	9	11	5	6	1	1
0.20	0.24	3	3	1	3	4	2	3	0	1	0	1	0	1	0	0	2
0.25	0.29	7	6	16	11	6	14	6	9	10	9	12	9	8	4	5	5
0.30	0.34	2	6	4	6	8	6	5	7	8	3	3	2	5	3	3	1
0.35	0.39	8	6	4	7	9	16	14	18	16	14	18	18	17	20	18	17
0.40	0.44	10	6	3	7	8	9	15	12	15	13	16	16	11	10	10	6
0.45	0.49	22	45	37	40	40	42	47	44	49	62	56	63	73	73	78	80

Table 2-17. Modified frequency distribution of COV_{min} of 137 ground motions for the **dynamic properties** randomization**.**

Bin	Bin	Period (seconds)															
Start	End	0.1	0.25	0.5	0.74	1	1.25	1.5	1.75	2	2.25	2.5	3	4	5	7.4	9.5
0.05	0.09																
0.10	0.14	11	16	15	15	17	14	9	12	7	8	5	10	7	8	14	9
0.15	0.19	7	10	6	12	8	5	8	4	7	2	3	0	1	1	2	2
0.20	0.24	18	7	14	7	6	8	4	3	2	2	1	2	2	5	6	12
0.25	0.29	5	2	7	2	4	4	5	4	2	4	7	2	0	2	5	0
0.30	0.34	24	13	7	12	9	13	11	13	13	8	6	6	10	9	6	4
0.35	0.39	9	1	4	3	5	3	2	4	9	8	10	8	9	16	21	15
0.40	0.44	22	6	9	19	18	20	21	24	24	29	26	34	27	27	14	12
0.45	0.49	7	3	13	14	21	27	38	41	45	50	53	53	59	50	46	45

Investigating $COV_{Profile}$ and $Sigma_{VS}$ at this station shows that we cannot define a specific trend. The COV_{min} when randomizing the shear wave profile are distributed over different ranges and, they have a bi-modal distribution with COV ranges of 0.25 to 0.29 and 0.45 to 0.49. Further investigation should be performed to find the characteristics of the ground motions that lead to these results. However, for COV_{THK} we can define and propose a value of 0.27 to be used for periods higher than 1 second. For dynamic properties the results show that in the majority of ground motions, a suitable COV might be 0.47 for purpose of randomizing.

2.7.2.2. IWTH27 Station

Station IWTH27 seismic instrumentations are located on layers of soil with V_{S30} of 670 m/s which has layers of tuff and shales. 80 ground motions with PGAs more than 0.05g were used to find the most suitable COVs for different soil parameters. Results are provided in Tables 2-18 to 2-23.

Table 2-18. Frequency distribution of COV_{min} of 80 ground motions for the **shear-wave profile** randomization.

Bin	Bin	Period (seconds)															
Start	End	0.1	0.25	0.5	0.74	1	1.25	1.5	1.75	2	2.25	2.5	3	4	5	7.4	9.5
0.05	0.09																
0.10	0.14	16	1	6	6	8	9	10	14	14	10	9	9	4	8	8	7
0.15	0.19	3	0	2	5	5	7	8	10	9	12	13	10	10	3	2	5
0.20	0.24	12	0	0	0	0	0	1	1	2	1	3	0	2	4	10	13
0.25	0.29	0	0	0	1	1	1	2	3	3	5	6	9	10	8	4	2
0.30	0.34	0	0	0	0	0	0	1	0	0	0	0	0	1	0	2	2
0.35	0.39	1	0	0	0	1	1	0	0	0	0	1	1	2	9	7	6
0.40	0.44	6	0	0	1	2	2	1	1	1	1	2	1	1	2	5	10
0.45	0.49	5	0	0	0	0	0	1	1	2	3	4	10	16	14	16	12

Table 2-19. Modified frequency distribution of $Sigma_{min}$ of 80 ground motions for the **shear-wave velocity** randomization.

Bin	Bin	Period (seconds)															
Start	End	0.1	0.25	0.5	0.74	1	1.25	1.5	1.75	2	2.25	2.5	3	4	5	7.4	9.5
0.05	0.09																
0.10	0.14	10	5	8	14	19	13	15	20	20	13	9	9	3	3	1	2
0.15	0.19	9	0	5	2	5	5	8	5	9	4	9	2	9	6	9	1
0.20	0.24	0	1	0	0	3	3	3	0	4	3	3	6	5	4	5	7
0.25	0.29	0	0	1	4	4	1	3	4	3	5	6	6	3	4	2	1
0.30	0.34	2	0	0	0	0	0	0	0	0	1	2	0	0	1	3	3
0.35	0.39	28	0	0	0	0	0	0	0	1	3	5	8	5	5	3	1
0.40	0.44	0	0	0	0	0	1	1	1	1	2	3	5	2	3	6	6
0.45	0.49	1	0	0	0	1	1	2	2	2	2	1	5	10	16	16	24

Table 2-20. Modified Frequency distribution of COV_{min} of 80 ground motions for the **soil layers thickness** Randomization.

Bin	Bin	Period (seconds)															
Start	End	0.1	0.25	0.5	0.74	1	1.25	1.5	1.75	2	2.25	2.5	3	4	5	7.4	9.5
0.05	0.09																
0.10	0.14	0	5	10	8	5	4	10	8	12	9	7	3	2	9	7	12
0.15	0.19	26	4	4	7	8	3	6	6	5	6	4	6	3	1	3	3
0.20	0.24	0	0	6	5	8	4	1	5	4	5	4	6	2	0	3	0
0.25	0.29	15	0	2	1	3	2	8	5	9	10	12	8	6	7	5	4
0.30	0.34	2	0	0	1	1	2	1	1	2	0	1	0	4	2	0	0
0.35	0.39	0	0	0	0	0	0	3	2	1	1	2	2	2	4	1	2
0.40	0.44	1	0	0	0	1	1	1	0	0	0	1	2	2	4	6	12
0.45	0.49	0	1	0	2	6	4	2	3	4	6	4	5	5	3	8	6

Table 2-21. Modified frequency distribution of COV_{min} of 80 ground motions for the **shear modulus reduction (G/G_{max}) curve** randomization.

Bin	Bin	Period (seconds)															
Start	End	0.1	0.25	0.5	0.74	1	1.25	1.5	1.75	2	2.25	2.5	3	4	5	7.4	9.5
0.05	0.09																
0.10	0.14	6	9	4	10	6	9	5	11	4	4	6	11	9	5	5	4
0.15	0.19	11	5	3	7	5	3	2	6	1	3	2	2	1	1	1	2
0.20	0.24	1	1	2	6	2	3	5	1	3	2	3	2	1	4	1	3
0.25	0.29	7	3	7	4	6	6	3	4	6	5	6	3	2	6	2	6
0.30	0.34	1	3	5	1	3	0	1	2	3	4	4	1	3	3	0	2
0.35	0.39	0	0	0	2	5	5	3	3	5	5	5	2	1	3	3	0
0.40	0.44	3	3	9	6	10	13	16	8	12	8	5	10	5	6	9	8
0.45	0.49	4	0	3	5	6	4	11	14	18	12	16	10	15	6	15	15

Table 2-22. Modified frequency distribution of COV_{min} of 80 ground motions for the **damping curves** randomization

Bin	Bin	Period (seconds)															
Start	End	0.1	0.25	0.5	0.74	1	1.25	1.5	1.75	2	2.25	2.5	3	4	5	7.4	9.5
0.05	0.09																
0.10	0.14	1	8	2	4	3	4	6	2	3	3	3	3	2	3	3	5
0.15	0.19	0	3	2	4	4	7	4	4	3	4	4	3	1	2	3	5
0.20	0.24	1	1	4	5	5	9	7	7	10	10	8	8	4	3	3	2
0.25	0.29	3	4	3	7	3	1	3	4	3	4	6	5	3	4	4	3
0.30	0.34	0	0	1	0	3	3	4	1	1	2	1	1	1	2	5	5
0.35	0.39	5	1	2	4	5	4	3	5	6	5	4	6	9	8	6	8
0.40	0.44	10	10	10	12	7	11	16	22	25	22	24	23	22	19	16	10
0.45	0.49	1	6	7	3	8	10	9	9	8	4	9	7	10	11	11	8

Table 2-23. Modified frequency distribution of COV_{min} of 80 ground motions for the **dynamic properties** randomization**.**

Bin	Bin	Period (seconds)															
Start	End	0.1	0.25	0.5	0.74	1	1.25	1.5	1.75	2	2.25	2.5	3	4	5	7.4	9.5
0.05	0.09																
0.10	0.14	3	10	4	12	11	13	6	11	11	5	3	11	11	9	8	5
0.15	0.19	1	5	3	5	2	5	1	4	1	3	3	3	2	2	2	3
0.20	0.24	0	4	3	5	4	6	9	5	8	4	6	8	2	5	6	2
0.25	0.29	1	4	7	3	8	6	9	11	15	11	11	7	6	6	3	3
0.30	0.34	0	1	4	3	0	4	1	4	4	3	3	0	4	1	0	0
0.35	0.39	0	0	2	2	1	2	6	3	3	5	6	5	4	6	4	6
0.40	0.44	5	0	5	5	9	2	10	6	9	10	6	7	7	5	6	6
0.45	0.49	0	0	0	0	1	1	1	3	4	3	8	8	6	6	12	18

Considering the results of the IWTH27 station, which is a site class C and has a softer soil compared to the stations studied earlier, we realize the distribution of COV_{min} has different trends than seismic stations IBRH13 and IBRH14. For periods longer than 0.1 seconds and shorter than 3 seconds the $COV_{Profile}$ occurs mostly in the range of 0.1 to 0.14 and for longer periods the $COV_{Profile}$ is in the range of 0.45 to 0.49. Although there is a similar trend for $Sigma_{Vs}$ the COV_{THK} has a different trend, the range of COV_{min} for periods lower than 2 seconds are between 0.1 and 0.14 and for longer periods they fall in the range of 0.25 to 0.29. According to Table 2-21 the COV_{min} for the shear modulus reduction curve occurred mostly on the last two rows, showing that the most suitable $COV_{G/Gmax}$ has a value between 0.4 and 0.49. For damping, COV_{min} occurred the most in the range of 0.4 to 0.45. Considering the Table 2-23 a consistent trend cannot be defined when randomizing both shear modulus reduction and damping curves with that same COV.

2.7.2.3. NMRH04 Station

This station is located on layers of pumice, sand, humus soil, gravel, and fine gravel with an average shear-wave velocity of 168 m/s in the first 30 meters of depth. The shear-wave profile is shown in Figure 2-10. There are not many ground motions with high intensities recorded in this station. We found only 28 ground motions with PGAs higher than 0.05g to use in our investigation. The same procedure used for site classes B, C, and D was followed for this station as well. Considering Table 2-24 it is evident that for most of the ground motions, using the lowest COV when randomizing gives the minimum RMSE. This means that if we use the base shear-wave profile and perform SRA the result should match the observation. There can be many reasons that the results fall on the lowest COVs and it seems that the uncertainties that exist in the shear-wave profile of this station are very low. This may be because that the shear-wave profile on this station

has been obtained using ground motion records or methods similar to that. The results on the other parameters are very similar to the results of $COV_{Profile}$ and it makes it hard to find the real uncertainties that exist in these parameters.

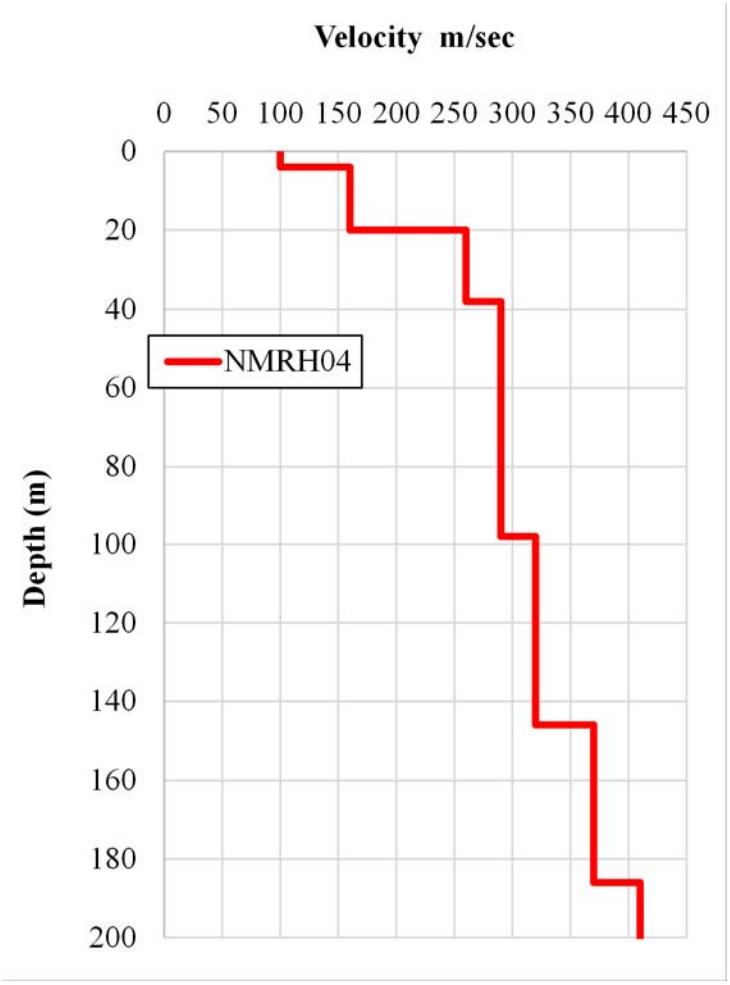

Figure 2-10. Seismic station NMR04 with site class E shear-wave profile.

Table 2-24. Frequency distribution of COV_{min} of 28 ground motions for the **shear-wave profile** randomization.

Bin	Bin	Period (seconds)															
Start	End	0.1	0.25	0.5	0.74	1	1.25	1.5	1.75	2	2.25	2.5	3	4	5	7.4	9.5
0.05	0.09	22	25	26	28	19	23	24	26	27	16	2	21	22	19	16	15
0.10	0.14	2	2	2	0	1	5	3	2	0	0	0	1	1	3	3	1
0.15	0.19	1	1	0	0	0	0	1	0	0	0	0	1	3	0	1	2
0.20	0.24	1	0	0	0	2	0	0	0	0	0	0	0	0	2	0	2
0.25	0.29	2	0	0	0	1	0	0	0	0	0	2	0	2	2	1	0
0.30	0.34	0	0	0	0	0	0	0	0	0	0	0	0	0	0	0	2
0.35	0.39	0	0	0	0	0	0	0	0	0	0	0	0	0	0	3	2
0.40	0.44	0	0	0	0	4	0	0	0	1	12	9	0	0	0	1	3
0.45	0.49	0	0	0	0	1	0	0	0	0	0	15	5	0	2	3	1

Table 2-25. Frequency distribution of COV_{min} of 28 ground motions for the **shear-wave velocity** randomization.

Bin	Bin	Period (seconds)															
Start	End	0.1	0.25	0.5	0.74	1	1.25	1.5	1.75	2	2.25	2.5	3	4	5	7.4	9.5
0.05	0.09	22	23	26	28	21	20	24	26	27	19	2	21	21	18	14	11
0.10	0.14	0	2	1	0	0	8	2	0	0	0	0	1	2	2	3	3
0.15	0.19	2	2	0	0	0	0	0	2	0	0	0	0	1	0	0	1
0.20	0.24	3	1	1	0	0	0	2	0	0	0	1	0	2	5	1	1
0.25	0.29	1	0	0	0	0	0	0	0	0	0	0	1	0	0	2	1
0.30	0.34	0	0	0	0	4	0	0	0	0	0	1	0	1	0	0	2
0.35	0.39	0	0	0	0	0	0	0	0	0	0	2	0	0	0	2	4
0.40	0.44	0	0	0	0	1	0	0	0	1	0	5	0	0	1	0	0
0.45	0.49	0	0	0	0	2	0	0	0	0	9	17	5	1	2	6	5

Table 2-26. Frequency distribution of COV_{min} of 28 ground motions for the **soil layers thickness** randomization.

Bin	Bin	Period (seconds)															
Start	End	0.1	0.25	0.5	0.74	1	1.25	1.5	1.75	2	2.25	2.5	3	4	5	7.4	9.5
0.05	0.09	7	11	25	23	18	15	16	19	26	23	0	23	19	16	13	12
0.10	0.14	3	9	1	5	0	5	6	6	1	0	1	2	2	3	2	1
0.15	0.19	3	0	0	0	1	4	1	0	0	0	1	1	1	1	2	2
0.20	0.24	2	0	0	0	0	4	3	2	1	0	0	0	0	0	1	1
0.25	0.29	4	1	1	0	0	0	1	0	0	0	0	0	2	0	2	2
0.30	0.34	4	0	1	0	2	0	0	0	0	0	0	0	2	0	1	3
0.35	0.39	4	6	0	0	0	0	0	0	0	0	0	1	0	5	0	1
0.40	0.44	0	1	0	0	3	0	0	0	0	5	10	1	1	1	0	1
0.45	0.49	1	0	0	0	4	0	1	1	0	0	16	0	1	2	7	5

Table 2-27. Frequency distribution of COV_{min} of 28 ground motions for the **shear modulus reduction (G/G_{max}) curve** randomization.

Bin	Bin	Period (seconds)															
Start	End	0.1	0.25	0.5	0.74	1	1.25	1.5	1.75	2	2.25	2.5	3	4	5	7.4	9.5
0.05	0.09	22	23	26	28	21	20	24	26	27	19	2	21	21	18	14	11
0.10	0.14	0	2	1	0	0	8	2	0	0	0	0	1	2	2	3	3
0.15	0.19	2	2	0	0	0	0	0	2	0	0	0	0	1	0	0	1
0.20	0.24	3	1	1	0	0	0	2	0	0	0	1	0	2	5	1	1
0.25	0.29	1	0	0	0	0	0	0	0	0	0	0	1	0	0	2	1
0.30	0.34	0	0	0	0	4	0	0	0	0	0	1	0	1	0	0	2
0.35	0.39	0	0	0	0	0	0	0	0	0	0	2	0	0	0	2	4
0.40	0.44	0	0	0	0	1	0	0	0	1	0	5	0	0	1	0	0
0.45	0.49	0	0	0	0	2	0	0	0	0	9	17	5	1	2	6	5

Table 2-28. Frequency distribution of COV_{min} of 28 ground motions for the **damping curves** randomization.

Bin	Bin	Period (seconds)															
Start	End	0.1	0.25	0.5	0.74	1	1.25	1.5	1.75	2	2.25	2.5	3	4	5	7.4	9.5
0.05	0.09	2	9	10	9	11	4	7	6	4	4	2	3	3	2	7	5
0.10	0.14	3	3	0	3	2	4	4	2	3	0	0	1	1	2	0	2
0.15	0.19	4	9	0	3	0	3	2	4	2	2	1	2	1	0	0	2
0.20	0.24	17	6	11	4	1	7	6	4	1	1	0	2	2	6	7	5
0.25	0.29	0	0	0	0	0	0	0	0	0	0	0	0	0	0	0	0
0.30	0.34	0	0	0	0	0	0	0	0	0	0	0	0	0	0	0	0
0.35	0.39	2	1	0	1	1	5	2	3	5	7	5	5	8	7	3	3
0.40	0.44	0	0	0	0	0	0	0	0	0	0	0	0	0	1	0	0
0.45	0.49	0	0	7	8	13	5	7	9	13	14	20	15	13	10	11	11

Table 2-29. Frequency distribution of COV_{min} of 28 ground motions for the **dynamic properties** randomization.

Bin	Bin	Period (seconds)															
Start	End	0.1	0.25	0.5	0.74	1	1.25	1.5	1.75	2	2.25	2.5	3	4	5	7.4	9.5
0.05	0.09	10	18	17	18	22	11	15	13	6	5	2	24	18	17	13	16
0.10	0.14	9	0	9	6	4	6	3	3	3	1	0	1	3	3	4	2
0.15	0.19	1	0	0	1	0	6	2	0	1	0	1	0	2	2	4	3
0.20	0.24	8	4	0	3	0	2	3	3	4	1	0	1	1	0	1	2
0.25	0.29	0	3	1	0	0	2	3	2	1	3	0	1	0	1	1	0
0.30	0.34	0	1	0	0	0	0	1	0	1	0	0	0	1	0	0	0
0.35	0.39	0	1	0	0	0	1	0	0	0	1	0	1	0	0	1	0
0.40	0.44	0	1	1	0	0	0	1	2	6	5	5	0	2	3	1	0
0.45	0.49	0	0	0	0	2	0	0	5	6	12	20	0	1	2	3	5

2.8. Summary

Through an exhaustive search we were able to investigate COV ranges to be used for soil properties randomization in SRA. Both aleatory and epistemic uncertainties of soil properties can be accounted in SRA results. We obtained COVs for input parameters such as shear-wave profile, shear modulus reduction G/G_{max}, and damping curves. The COVs are estimated for different site classes and various combinations of soil parameters. Four vertical arrays from the KIK-Net seismic network are used and each has a different site class. Vertical arrays give us a great opportunity to compare the real observed surface ground motions with ground motions obtained by site-specific response means. This is the main key that helped us to investigate COVs in each period based on comparing predicted and observed spectral accelerations. The comparison was performed based on calculating root mean square errors of the randomized spectra and the observed spectrum. The coefficient of variation that produces the minimum RMSE could be a good candidate to be used while performing randomization. In this research we show a procedure to be performed in any site when there are vertical arrays available for that site and there are not many soil property measurements. In this research $COV_{Profile}$ proposes values when the analyst wants to use the same COV to generate soil shear-wave velocity and layer thickness random cases. One can use more specific values for shear-wave velocity and soil thickness by using σ_{lnVs} and COV_{THK}, respectively. COV_{Dyn} proposes values when one wants to use one COV to generate dynamic soil properties (shear modulus reduction and damping curves) random cases. We can use more specific values for shear modulus reduction curve (G/G_{max}) and damping curve by using $COV_{G/Gmax}$ and COV_{Damp} respectively. Methods for generating random cases for different SRA input parameters are stated in the randomization procedures section. This study should be

improved by stronger statistically arguments to find the best coefficient of variation to use in randomization.

2.9. Recommendations for Future Studies

The study presented in this chapter of the dissertation can be considered as a methodology to find coefficient of variation for randomizing SRA input parameters when the soil property measurements of the site under study are not enough to develop a COV. This study can be improved by more studies in the future as follows: (1) perform the same procedure at other sites in different regions; (2) find the correlation between the earthquake characteristics and the COV_{min} values; (3) perform a thorough study to find the most suitable coefficient of variation corresponding to RMSE minimum when there are more than one minimum coefficient, (4) increase the number of randomizations for every ground motion; (5) use different SRA models and compare them to these results.

3. References

Aki, K. (1993). Local site effects on weak and strong ground motion. *Tectonophysics*, *218*(1–3), 93–111.

Andrade, J. E., and Borja, R. I. (2006). Quantifying sensitivity of local site response models to statistical variations in soil properties. *Acta Geotechnica*, *1*(1), 3–14.

Arsdale, R. V., & Cupples, W. (2013). Late Pliocene and Quaternary deformation of the Reelfoot rift. *Geosphere*, *9*(6), 1819-1831.

Assimaki, D., Li, W., Steidl, J., & Schmedes, J. (2008). Quantifying nonlinearity susceptibility via site-response modeling uncertainty at three sites in the Los Angeles Basin. *Bulletin of the Seismological Society of America*, *98*(5), 2364–2390.

Atkinson, G. M., and Mereu, R. F. (1992). The shape of ground motion attenuation curves in southeastern Canada. Bulletin of the Seismological Society of America, 82(5), 2014–2031.

Bazzurro, P., and Cornell, C. A. (2004). Ground-motion amplification in nonlinear soil sites with uncertain properties. *Bulletin of the Seismological Society of America*, *94*(6), 2090–2109.

Bodin, P., Smith, K., Horton, S., & Hwang, H. (2001). Microtremor observations of deep sediment resonance in metropolitan Memphis, Tennessee. *Engineering Geology*, *62*(1–3), 159–168.

Bonilla, L. F., Steidl, J. H., Gariel, J. C., and Archuleta, R. J. (2002). Borehole response studies at the Garner Valley downhole array, southern California. *Bulletin of the Seismological Society of America*, *92*(8), 3165–3179.

Bonilla, L. F., Steidl, J. H., Lindley, G. T., Tumarkin, A. G., & Archuleta, R. J. (1997). Site amplification in the San Fernando Valley, California: variability of site-effect estimation using the S-wave, coda, and H/V methods. *Bulletin of the Seismological Society of America*, *87*(3), 710–730.

Boore, D. M. (2007). Some thoughts on relating density to velocity. *Notes on personal web, not published*.

Boore, D. M., and Campbell, K. W. (2017). Adjusting central and Eastern North America ground motion intensity measures between sites with different reference-rock site conditions. *Bulletin of the Seismological Society of America*, *107*(1), 132–148.

Borcherdt, R. D. (1970). Effects of local geology on ground motion near San Francisco Bay. *Bulletin of the Seismological Society of America*, *60*(1), 29–61.

Building Seismic Safety Council [BSSC] (1998). NEHRP recommended provisions for seismic regulations for new buildings and other structures, 1997 edition, *FEMA 303 Report*, Federal Emergency Management Agency, Washington, D.C.

Cadet, H., Bard, P. Y., and Rodriguez-Marek, A. (2010). Defining a standard rock site: Propositions based on the KiK-net database. *Bulletin of the Seismological Society of America*, *100*(1), 172–195.

Cramer, C. H. (2003). Site-specific seismic-hazard analysis that is completely probabilistic. Bulletin *of the Seismological Society of America*, *93*(4), 1841–1846.

Csontos, R. M. (2007). Three-dimensional modeling of the Reelfoot rift and New Madrid seismic zone, Ph.D. Dissertation, Department of Earth Sciences, University of Memphis, Tennessee, 94 pp.

Darendeli, M. B. (2001). Development of a new family of normalized modulus reduction and material damping curves. (Ph.D. thesis). Austin, Texas: University of Texas at Austin 396 pp.

Dhar, M. S., & Cramer, C. H. (2017). Probabilistic seismic and liquefaction hazard analysis of the Mississippi embayment incorporating nonlinear effects. *Seismological Research Letters*, *89*(1), 253-267.

Electric Power Research Institute (EPRI) (1993). Guidelines for determining design basis ground motions, Final Report No. TR–102293, EPRI, Palo Alto, California.

Electric Power Research Institute (EPRI). (2012). Seismic Evaluation Guidance: Screening, Prioritization and Implementation Details (SPID) for the Resolution of Fukushima Near-Term Task Force Recommendation 2.1: Seismic. EPRI 1025287, Palo Alto, CA, Feb.

Electric Power Research Institute. (2012). Seismic evaluation guidance: Screening, prioritization and implementation details (SPID) for the resolution of Fukushima near-term task force recommendation 2.1: Seismic. ML 12333A170.

Erickson, D., McNamara, D. E., & Benz, H. M. (2004). Frequency-dependent Lg Q within the continental United States. *Bulletin of the Seismological Society of America*, *94*(5), 1630–1643.

Frankel, A., McGarr, A., Bicknell, J., Mori, J., Seeber, L., & Cranswick, E. (1990). Attenuation of high-frequency shear waves in the crust: Measurements from New York state, South Africa, and southern California. *Journal of Geophysical Research: Solid Earth*, *95*(B11), 17441–17457.

Goulet, C. A., Kishida, T., Ancheta, T. D., Cramer, C. H., Darragh, R. B., Silva, W. J., and Wooddell, K. E. (2014). PEER NGA-East Database, PEER Report 2014/17.

Green, R. A., Gibson, E., and Rodriguez-Marek, A. (2016). Treatment of Epistemic Uncertainty in Site Effects in Probabilistic Seismic Hazard Analyses. International Workshop on Earthquakes in North Iceland, 85.

Haley, B. R., Glick, E. E., Bush, W. V., Clardy, B. F., Stone, C. G., Woodward, M. B., and Zachry, D. L. (1976). Geologic map of Arkansas: *US Geol. Survey and Arkansas Geol. Comm., scale*, *1*(500,000).

Hart, R. M., Clark, B. R., and Bolyard, S. E. (2008). Digital surfaces and thicknesses of selected hydrogeologic units within the Mississippi Embayment regional aquifer study (MERAS) (No. 2008–5098). Geological Survey (US).

Hashash, Y. M. A., Groholski, D. R., Phillips, C. A., Park, D., and Musgrove, M. (2011). DEEPSOIL 5.0, user Manual and Tutorial. *University of Illinois, Urbana, IL, USA*.

Idriss, I. M., and Sun, J. I. (1992). User's Manual for SHAKE91. *Center for Geotechnical Modeling, Department of Civil Engineering, University of California, Davis*.

Kaklamanos, J., Baise, L. G., Thompson, E. M., and Dorfmann, L. (2015). Comparison of 1D linear, equivalent-linear, and nonlinear site response models at six KiK-Net validation sites. *Soil Dynamics and Earthquake Engineering*, *69*, 207–219.

Kramer, S. L. (1996). *Geotechnical Earthquake Engineering*, Prentice Hall, Upper Saddle River, New Jersey, 653 pp.

Lermo, J., & Chávez-García, F. J. (1993). Site effect evaluation using spectral ratios with only one station. *Bulletin of the seismological society of America*, *83*(5), 1574–1594.

Li, W., and Assimaki, D. (2010). Site-and motion-dependent parametric uncertainty of site-response analyses in earthquake simulations. *Bulletin of the Seismological Society of America*, *100*(3), 954–968.

Li, Z. (2014, July). Uncertainty of soil properties in earthquake ground-motion site response analyses. In *Tenth US National Conference on Earthquake Engineering Frontiers of Earthquake Engineering, Anchorage, Alaska, USA, July*.

Majenu, M. (2015). The Structural Analysis of Enola and Greenbrier, Arkansas Earthquake Swarms: Cause and Effect? (2015). *Theses and Dissertations*. 1358. University of Arkansas.

McNamara, D. E., Owens, T. J., and Walter, W. R. (1996). Propagation characteristics of Lg across the Tibetan Plateau. *Bulletin of the Seismological Society of America*, *86*(2), 457–469.

Nakamura, Y. (1989). A method for dynamic characteristics estimation of subsurface using microtremor on the ground surface, Quarterly Report of Railway Technical Institute (RTRI) 30, 25–33.

National Research Institute for Earth Science and Disaster Prevention [NIED] (2019). Strong-motion seismograph networks: KiK-net database, available at http://www.k-net.bosai.go.jp/ (last accessed May 2019).

Nelson, W. J. (2013). Surficial Geology of Carbondale Quadrangle, Jackson and Williamson Counties, Illinois. *IGQ Carbondale-SG*.

Petersen, M.D., Moschetti, M.P., Powers, P.M., Mueller, C.S., Haller, K.M., Frankel, A.D., Zeng, Yuehua, Rezaeian, Sanaz, Harmsen, S.C., Boyd, O.S., Field, Ned, Chen, Rui, Rukstales, K.S., Luco, Nico, Wheeler, R.L., Williams, R.A., and Olsen, A.H. (2014). Documentation for the 2014 update of the United States national seismic hazard maps: U.S. Geological Survey Open-File Report 2014–1091, 243 p.

Schnabel, P. B., Lysmer, J and Seed, H. B. (1972). SHAKE: A computer program for earthquake response analysis of horizontally layered sites, *Report UCB/EERC–72/12*, Earthquake Engineering Research Center, Univ. of California, Berkeley, 102 pp.

Schweig, E. S., VanArsdale, R. B., and Burroughs, R. K. (1991). Subsurface structure in the vicinity of an intraplate earthquake swarm, central Arkansas. *Tectonophysics*, *186*(1–2), 107-114.

Seed, H. B., Wong, R. T., Idriss, I. M., and Tokimatsu, K. (1986). Moduli and damping factors for dynamic analyses of cohesionless soils. *Journal of geotechnical engineering*, *112*(11), 1016–1032.

Steidl, J. H., Tumarkin, A. G., and Archuleta, R. J. (1996). What is a reference site? *Bulletin of the Seismological Society of America*, *86*(6), 1733–1748.

Toro, G. R. (1993). Probabilistic model of soil-profile variability, in Early Site Permit Demonstration Program: Guidelines for Determining Design Basis Ground Motions, J. F. Schneider (Editor), EPRI Project RP3302, Volume II, Appendix 6A, Electric Power Research Institute.

Toro, G. R., and Silva, W. J. (2001). Scenario Earthquakes for Saint Louis, MO, Memphis, TN, and Seismic Hazard Maps for the Central United States Region: Including the Effect of Site Conditions (p. 247). Boulder, CO: Risk Engineering.

Toro, G. R., Silva, W. J., McGuire, R. K., and Herrmann, R. B. (1992). Probabilistic seismic hazard mapping of the Mississippi Embayment. Seismological Research Letters, 63(3), 449–475.

Van Arsdale, R. B., and TenBrink, R. K. (2000). Late Cretaceous and Cenozoic geology of the New Madrid seismic zone. Bulletin of the Seismological Society of America, 90(2), 345–356.

Van Houtte, C., Ktenidou, O. J., Larkin, T., & Kaiser, A. (2012). Reference stations for Christchurch. *Bulletin of the New Zealand Society for Earthquake Engineering*, *45*(4), 184–195.

Zandieh, A., and Pezeshk, S. (2011). A study of horizontal-to-vertical component spectral ratio in the New Madrid seismic zone. *Bulletin of the Seismological Society of America*, *101*(1), 287–296.

Zhang, J., Andrus, R. D., and Juang, C. H. (2005). Normalized shear modulus and material damping ratio relationships. *Journal of Geotechnical and Geoenvironmental Engineering*, *131*(4), 453–464.

Zhao, L. F., Xie, X. B., He, J. K., Tian, X., and Yao, Z. X. (2013). Crustal flow pattern beneath the Tibetan Plateau constrained by regional Lg-wave Q tomography. Earth and Planetary Science Letters, 383, 113–122.